Experimental investigation of particle trajectory through an hydrocyclone using a Positron Emission Tomography (PET) scanner

Øystein Lee Aasen

Master Thesis in Multiphase Systems, Process Technology

Department of Physics and Technology

University of Bergen

31.08.2010

Acknowledgment

The present work is a master thesis which all graduate students from the master program process technology, at the University of Bergen (UoB), Department of Physics and Technology, have to submit as a part of their Master Science degree.

Many people have contributed and been a great help and inspiration throughout the completion of this thesis. First I want to thank my supervisors Professor Alex C. Hoffmann and Dr. Weiming Peng for help and good discussions throughout the work with this thesis. Their help and knowledge has been indispensable. Thanks to Ph.D. student Yu-Fen Chang for very good discussions and collaboration throughout our common work with these experiments. Thanks to Ph.D. Catalin G. Ilea that has always been very helpful, especially regarding computational challenges. Thanks to Leif Egil Sandnes at the Mechanical workshop at University of Bergen, who always were helpful and provided invaluable help for designing and building the experimental rig used in the experimental work. I would also thank the staff at the Centre for Nuclear Medicine/PET at Haukeland University Hospital for excellent assistance during our experiments there. Especially Chief Radiochemist, Ph.D. Tom Christian Holm Adamsen that in addition has proofreading parts of this thesis in his spare time.

I would also use this opportunity to thank my fellow master students at UoB.

Finally I would like to thank my parents Berit Aasen and Rune B. Aasen, for encouragement and financial support in hard times through the whole five year study period. And to Janne Clausen who has been of great support and kept up with me even though the hours at UoB in some periods have been longer than the hours at home.

Abstract

Hydrocyclones are much used in process technology and in many different industrial applications. In the oil and gas industry the hydrocyclones, both gas-solid and liquid-solid cyclones are widely used. Getting the sand out of the oil and gas production flow is critical for the production- and separation- equipment. Also for environmental and health concerns, efficient hydrocyclones are needed. Today the knowledge about the flow pattern inside the hydrocyclones is very limited. Many models are derived, both theoretical and experimental, the accuracy of which is less than satisfactory because of limited knowledge of the flowpatterns of liquid and particles.

The motivation in this present investigation has been to gain a better understanding of the trajectory of a particle. A better understanding of the particle trajectory, will represent a significant step in the direction of designing more efficient hydrocyclones.

The equipment used in this investigation is a Positron Emission Tomography (PET) scanner. The basis of the PET scanner is detection of radioactivity. A particle is put in a radioactive liquid and absorbs radioactivity for some time. PET scanner measures the actual position of the particle with an accuracy of less than 1 mm each millisecond.

The outcome of the experimental investigation is images of particle trajectories that never has been revealed before. Accuracy of the measured result are without comparison much better then the state of knowledge today. The results of the experiments show that when the particle moves downward the outer hydrocyclone wall, the particle turn and follows the inner upward flow, this repeats itself several times. Additional analysis has been carried out to attempt to find out the reason for this very interesting trajectory. The reasons considered for this reversal of axial flow direction are disturbances in the tangential velocity or the particle actually impacting on the wall. Additionally the particle residence time has been investigated. Because of lack of sufficient amount of experimental results at this time, no definite conclusions can be drawn on these issues.

In one experiment it might look like the particle hits the wall, but at this time in the investigation it seems more like the trajectory is random rather than specific.

Either way this research is a breakthrough in hydrocyclone development, and will give much information to designing better cyclones in the future. In addition to this the present investigation shows that PET generally is a great working tool also for high velocity particles. This will probably be much more appreciated and used in the future.

Contents

Chapter 1

Introduction

1.1 Relevance

The oil and gas industry have challenges toward getting sufficient oil and gas to a needing world. Therefore older reservoirs are often longer in production, many of them produce much sand, for instance on the Norwegian continental shelf. The sand can create many problems especially in the production equipment, but also in separation and processing. Therefore it is important to separate the sand from the liquid, much of the sand is further discharged to the sea. The sand disposal to sea is restricted by international agreements and national laws and regulations (OSPAR, EU restrictions, White Papers, Pollution Control Acts, etc). The limits for discharge are continuously becoming stricter. On the Norwegian continental shelf the Petroleum Safety Authority Norway (PSA) and Norwegian Pollution Control Authority (SFT) sets the limits for oil in sand discharge, today that is 10 g per one kg of dry mass. This means that sand and other solid particles must not be discharged to the sea unless the content of formation oil, other oil or other organic liquids is less than the limit [1].

The ability of a controlled and automated removal of sand from organic liquids has

many advantages. For instance sufficient washing of the sand so it can be disposed in good relation with the environment, prolonged equipment lifetime and reduced downtime. Additionally people nowadays have to be in contact with the polluted sand regarding manual removal when the hydrocyclone becomes clogged.

1.2 Technological background

Hydrocyclones are used for separation of flows with defined different densities, the separation occurs because of the centrifugal force. There are no moving parts, only the pressure from an external pump, further advantages are that it's cheap, compact and versatile. With a significant density difference hydrocyclones can effectively separate particles down to 2 μm in diameter.

This thesis is written as a part of an ongoing research project founded by the Norwegian Research Council, from the Petromaks Programme, "Environmental Technology for the Future". The main project is named, "Solid Separation from Highly Viscous Liquids by Cyclone Technology" (CLEANSAND). The focus in the research project is generating and applying basic knowledge about the separation of sand from liquids. The point of view in this thesis is experimental particle tracking through the hydrocyclone by using a Positron Emission Tomography camera. The CLEANSAND project is a co-operation between Aker Kværner Process Systems (AKPS) and University of Bergen (UoB). The existing knowledge of sand separation by cyclone technology in the oil and gas industry is mainly limited to separation from pure water.

The environmental concerns related to the discharge of sand are leading to stricter limitations. This is in contrast to the challenges regarding aging wells were the separation and purification is becoming more difficult. Problems because of the sand will only be a increasing problem in the years to come, as the wells are getting older and the produced water and sand rates are increasing.

In addition to the environmental problems, the sand creates many problems for the equipment, for instance:

- The solids interfere with control and instruments, reducing safety and reliability of the system significantly.
- Erosion reduces the lifetime of the equipment. Substantial risk is faced if combined corrosion-erosion problems occur.
- Valves are clogged, reducing the operational capability, safety and reliability.
- Separation tanks are filled with sand, reducing firstly the retention time for the separation eventually resulting in a shut-down of the separators for manual sand removal.
- Sand can create problems for injection wells and injection pumps.

Also economically it is an advantage with better cyclones, the reason is the possibility for higher production rate because of larger amount of sand into the production train.

Current sand washing system can wash the sand in produced water with approximately 2000 ppm oil in water to the required purity. Today a common practice regarding testing and calculating sand separation performance, is to neglect the oil content in the liquid and only regard separation from pure water. This limits the liquids which sand separation can be achieved, to only regard water with small oil concentrations and light oils. The challenges for the future are related to heavy oils and non-standard particles. The heavy oil gives poor oil-water separation, and therefore the sand has to be able to be removed from a liquid phase with a considerable content of heavy oil. The affect this heavy oil content has on the cyclone performance is not comprehended or theoretical explained. The different concentrations, types and sizes of sand, other corrosion products and scale will be investigated in CLEANSAND project.

Positron Emission Tomography - PET

The CLEANSAND project will also try to reveal the actual particle trajectory in a liquid-solid hydrocyclone. This will be the first time this is revealed. It will be done by tracing an individual radioactive tracer particle, in the cyclone in a positron emission tomography (PET) camera. Haukeland University Hospital with their new PET facility makes this possible. Professor Alex C. Hoffmann has worked at the Department of Chemical Engineering, University of Groningen, The Netherlands, that worked on fluidized bed in PET. It was revealed that the position of the tracer particle could be determined to within one mm^3 once per ms [2] in a modern PET camera.

1.2.1 Approaches, hypotheses and choice of method

The project is divided in two experimental setups at the University of Bergen, one part is a full-scale hydrocyclone 1.5" (inch) with abilities to measure velocity, pressure, particle size of inlet flow, underflow and overflow, this will be referred to as the UiB-rig. Here there will be taken samples at the inlets for sedimentation and direct measuring size and efficiency. The other application is a simpler rig, named "PET rig", with the main objective to find the particle trajectory through the hydrocyclone. On the PET rig it will be possible to do measurements of pressure and velocity. The design of both experimental setup's will be done in the beginning of this thesis. This PET - part will be further investigated in this thesis. The experiments are done in collaboration with Haukeland University Hospital (HUH) and their Centre of Nuclear Medicine / PET, Dept. of Radiology. There it is possible to make radioactive tracer particles by using a cyclotron. The results from the UoB and PET rig's will be compeered at a later time.

1.3 PET main objectives

The main objectives for this thesis are to:

a) Design and construct apparatus for hydrocyclone testing

b) Use positron emission tomography to decide the trajectory of one particle inside a hydrocyclone

1.4 PET - Medical application

Positron emission tomography (PET) is mainly used in medicine. The advantage with PET is that PET combines nuclear medicine procedure and biochemical analysis. Positron emission tomography measures biochemical processes in vivo. It is used on patients with brain or heart conditions, but mostly cancer. As explained by [3], the difference between PET and conventional nuclear medicine is that PET helps to visualize the biochemical processes taking place inside the body, and can be quantitatively measured. This is mostly done by looking at metabolism, the process by which cells convert food into energy after food is digested and absorbed into the blood. Where other nuclear medicine examinations only detect the amount of radioactivity inside an organ or specific location for tissue function, PET gives quantitative answers by measuring the cellular metabolism. In PET a patient is most commonly injected with a tiny amount of a radioactive substance, called a radiopharmaceutical (radioactive tracer). The most commonly used radiopharmaceutical is [^{18}F] FDG, glucose. The substance makes it possible to examine the metabolism of a particular organ or tissue, both the physiology (functionality), as well as its biochemical properties.

The combination of these makes PET able to see the onset of a disease process before anatomical changes within the same disease takes place. Anatomical change is what is viewed in other imaging processes such as computed tomography (CT) and magnetic

Figure 1.1: Siemens Biograph 40 Truepoint PET-CT scanner.

resonance imaging (MRI). The last decade PET started to be used in conjunction with CT. The use of PET/CT enables the visualization of both anatomy and physiology. In a few years, multimodal platforms such as PET/MR will probably provide even greater insight. Especially in neurology combined with functional Magnetic Resonans Imaging (fMRI).

1.5 History

PET history

Positron emission tomography (PET) has through the years been driven forward by the medical industry, helped by advances in practical physics. Additionally many great scientist, physicians, and businessmen, have dedicated their entire lives to this technology. The history of Positron emission from radioactive nuclei is outlined by Dale Bailey in Positron Emission Tomography - Basic Sciences [4] and starts with discovering by Thibaud and Joliot in 1933 [5, 6]. In 1973 Michael E. Phelps built the first PET tomograph, known as PETT 1, at Washington University. This was unsuccessful in producing

proper reconstruction images because they used lead collimators, limited sampling, and did not provide for attenuation correction. This tomograph did in fact use a proper Fourier-based image reconstruction algorithm [7].

Since the scanner that is used in this thesis is a Siemens Biograph 40 PET-CT a brief look at Siemens newest improvements have been made [8].

- In 2002 the first 16-slice PET/CT scanner, further introduced with 4 mm resolution. A whole-body PET/CT scan in less then 15 minutes.
- In 2006 they introduced Biograph TruePoint PET/CT.
- In 2007 HD-PET were introduced. They had 2 mm uniform resolution throughout the field of view, and doubled the improvement in signal-to-noise.

Hydrocyclone history

The history of hydrocyclone is over 100 years old. The use of centrifugal acceleration for separation purposes was first patent in 1885, for removing dust from air streams. The patent were granted for such a device in the United States and Germany to the Knickerbocker Company, USA [9, 10].

Bretney [11] patented the application of the air cyclone to liquid streams in 1891. The first recorded use of a hydrocyclone was by an American phosphate company in 1914 [12]. It was first after the Second World War that the industry started using the hydrocyclone for full. It was first used in mining and mineral processing. After that they have been used and appreciated by a much larger part of the industry, for instance: chemical, textile, petrochemical, power generation and metal working.

1.6 Usefulness in industry

Hydrocyclone in industry

Hydrocyclones are widely used in industry for many different application of two-phase separation, mostly for clarification and thickening, combined with the low cost and simplicity. The ability to thicken the flow to a coarser material is useful for instance for pre-treatment before filtration. In addition to the oil- and gas- industry, a common place where hydrocyclones are used is in grinding mill classification. When used in wet grinding circuits the hydrocyclone works as a classifier, where the underflow is recycled back to the mill, i.e. closed-circuit grinding. Additional application in the mineral industry is the ability for hydrocyclones to de-slim, that means divide fine particles from larger ones when they are loosely attached. More places and industries see the interest of using hydrocyclones, because of the lack of moving parts and relative cheapness.

PET in industry

Chemical engineering investigations using radiotracer methods are according to Stegowski and Nowak [13], not widely used. The usefulness and benefits of positron emission tomography looks to be not sufficiently understood in the industry. The accessibility to PET scanner are in many places a disadvantage. The International Atomic Energy Agency (IAEA) have seen the interest and the usefulness for the industry to use radiotracer application and given out a book,"RADIOTRACER APPLICATIONS IN INDUSTRY - A GUIDEBOOK" [14], which gives information for design and use. This is because the advantage of using tracer particles inside the equipment, for better knowledge about the processes. Choosing a suitable radiotracer, the process of interest will not be interfered.

Chapter 2

Theory

The essence of this theoretical investigation is to give an understanding of the important phenomena inside the hydrocyclone, how it physically works. This is done for the design purposes of the hydrocyclone, but also for better understanding and interpreting the results from the positron emission scanner. There is also given a wide theoretical explanation of how the positron emission tomography scanner works, and the physics and technology behind this revolutionary equipment.

Hydrocyclone

Hydrocyclone is a separation device, based on the effect of centrifugal forces. Hydrocyclones have the ability to separate liquid-liquid, gas-liquid, liquid-solid and gas-solid with only minor adjustments. The most important separation consideration is the finite density difference between two phases.

2.1 Principle of hydrocyclone

The principle of a hydrocyclone is shown in Figure 2.1. A hydrocyclone has three main applications, an inlet for the fluid, an underflow and an overflow. There is no moving

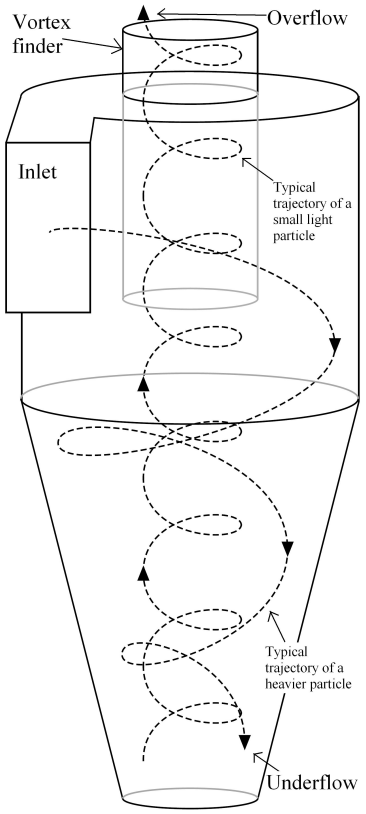

Figure 2.1: Principle of hydrocyclone.

or rotating parts inside the hydrocyclone. The vortex is produced by pumping the fluid tangentially into the cylindrical section of the cyclone. The cylindrical part has a top cover with a hole in the center, this hole is a pipe where the overflow exits. The overflow piping is called a *vortex finder*. The vortex finder enters through the cover and continues some distance down the center of the cylindrical section. The cylindrical section is connected in the bottom with a conical part, in both sections the vortex is centrifuged outwards. In the bottom of the conical part there is an apex where most of the dens particles or fluid are leaving the cyclone. The lighter fluid is turning in the bottom of the cyclone and follows the upward vortex around the center of the cyclone. The upward

vortex goes through the vortex finder and out, as a separated fluid. Some of the inlet flow "short-circuits" the vortex by leaking directly from the inlet and into the vortex finder. Which is some of the reason for the unclassified material, to reduce this, it is important with a good vortex finder design.

The diameters of cyclones can range from 10 mm to 2.5 m. The separated particles cut size for most solids range from 5 to 250 μm. Further can the capacity of the flow for one single cyclone vary from 0.1 to 7200 cubic metres per hour. The operating pressure drop can vary from 0.34 to 6 bar, the smaller units operating the highest pressure differences [15].

2.2 Arrangements, Types and Designs

In hydrocyclone arrangement a small particle separation size is often desirable, which is given in a hydrocyclone with small diameter. A small diameter gives challenges regarding the volume flow through the cyclone. Hydrocyclones is therefore in the industry often gathered in multiple installations with many units operating in parallel. This may also interfere with the grade efficiency curve, see section 2.3.4. The grade efficiency curve has originally a fairly shallow slope, but can obtain a "sharp" cut when several hydrocyclones are employed in series, or working with other classifiers.

Examples of hydrocyclone are shown in Figure 2.2, where two hydrocyclones that are often used are displayed. As reviewed in this thesis, the one with a long cone for thicker underflow, and the other shorter for a sharper cut. Hydrocyclones can differ a great deal from the design shown in Figure 2.2, for instance hydrocyclones used for separation of oil dispersed in water. This design was lead by the use computational fluid dynamics, and it has been well documented by Coleman & Thew [17]. Another interesting design used in oil/water separation, and also mineral flotation is using porous walls which air passes through and into the hydrocyclone body. This is described as the air-sparged

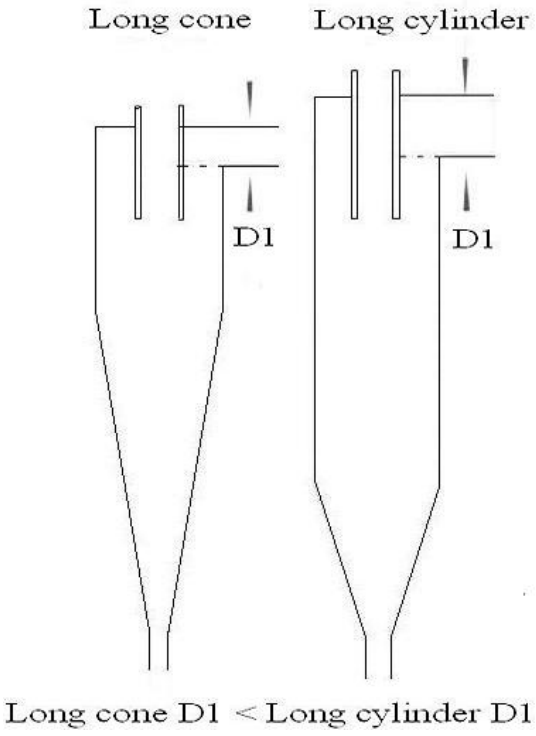

Figure 2.2: Hydrocyclone designs. Reference: [16]

hydrocyclone [18].

2.3 Basic terminology

The technology in hydrocyclones is widely appreciated, in this chapter a rapid review of their basic terminology and important effects will be given.

The solid leaves with the underflow, and the dilute liquid goes with the overflow. But with both the overflow and the underflow some of the opposite quality follows the fluid. To be able to compare different hydrocyclones the quality of the separation have to measured. The usual way to do this is to look separately at the solid and liquid, in two independent factors. The first is the mass fraction of the solids recovered, and

the second is moisture content, or the concentration of the recovered solids. The mass fraction of the solids recovered is often called the separation efficiency or solids retention. That is only the measurement of the solids and do not take the liquid into account. A good way to express this is a graph, separation efficiency versus particle size. The reason for this is the high particle size dependency in separation, for hydrocyclones this graph is known as grade efficiency curve. The hydrocyclone has an advantage, the curve is fixed at some operation conditions and do not interfere with the size distribution of the feed. Figure 2.3 represent grade efficiency curves for several types of separators. A second method of measuring separation efficiency, the moisture content, is a measure of the imperfection in the separation of the liquid. This is how much "misplaced" liquid that follows with the solid through the underflow. It is often measured with the mass or volume concentration of the solids in the underflow. Neither way the dryness of the separated solids are important, this is often a neglected issue in scale-up. Referring to Svarovsky [15] both methods are best to leave separate.

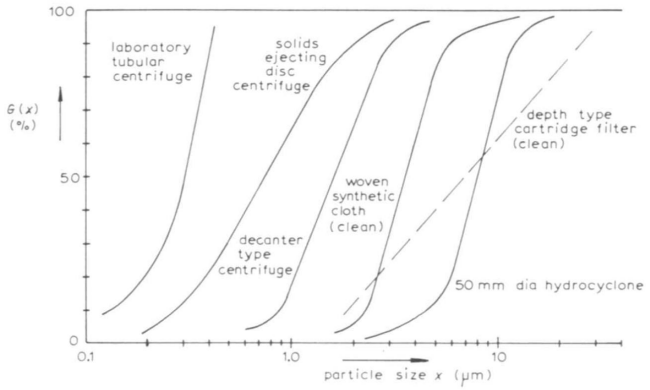

Figure 2.3: Examples of grade efficiency curves of several types of separators. Reference: [15]

2.3.1 Total efficiency

The separation efficiency is often first calculated, it is the total mass recovery as a function of the feed mass flow rate.

$$E_T = \frac{M_c}{M} \tag{2.1}$$

E_T is total efficiency, M_c is total mass recovery and M is feed mass flow rate. It is no accumulation in the hydrocyclones of solids, an overall mass balance must apply. The total efficiency can therefore be calculated by knowing two of the three flows, feed, underflow and overflow. This gives three combination of efficiency testing, and if all conditions are equal. Such as accessibility and accuracy of sampling, it can be shown from Svarovsky [19] that the most accurate estimate of total efficiency is the combination of the two outgoing, underflow and overflow. By using this procedure there is a disadvantage, it is not a general criterion of separation efficiency, this is because it usually depends on the size distribution or other properties of the feed solids. A value of the total efficiency always has to be accompanied by a full characterization of the solids of the feed and test conditions used.

2.3.2 Reduced total efficiency

In 2.3.1 there is included the effect of flow splitting, called "dead flux". This means that when calculating the total efficiency the only concern is the amount of each outflow, not the material characteristic in the flow. This gives a "guaranteed" efficiency, it is because any separator divides the flow in two, the solids included. The solids are at least divided in the same ratio as in the underflow-to-thoughput ratio (U/Q), see Equation 2.3. A method to take this into account and consider the separation effect alone is the reduced total efficiency E'_T. [20, 21].

$$E'_T = \frac{E_T - R_f}{1 - R_f} \tag{2.2}$$

where R_f is the underflow-to-throughput ratio defined as:

$$R_f = \frac{U}{Q} \tag{2.3}$$

Where U is the underflow volumetric flowrate and Q is the feed volumetric flowrate.

Equation 2.2 satisfies the basic requirements for an efficiency definition [22] in that it becomes zero when no separation takes place ($E_T = R_f$) or unity for complete separation [15].

2.3.3 The degree of separation

To magnify the top end of the efficiency scale it is possible to use the ratio of the total efficiency to the penetration i.e:

$$\beta = \frac{E_T}{1 - E_T} \tag{2.4}$$

this is referred to as the "degree of separation" [15].

2.3.4 Grade efficiency

The grade efficiency curve is as shown in Figure 2.3 a continuous function of particle size x. The curve is hard to derive and express, because it can rarely be approximated by analytical expression or derived from first principles. The way of obtaining the curve is by either feeding the separator with mono-sized particles in several batches, or by few batches of poly-dispersed particles in the required size range. Regardless the total efficiency has to be measured, in the poly-dispersed testing the size distribution from two

of the material streams has to be analysed. The concept of grade efficiency is widely used in hydrocyclone because their performance does not change with time under steady-state conditions. By compeering hydrocyclones against each other, or with operating variables the curve is not so easily used, here the *cut size* is used.

2.3.5 Reduced grade efficiency

As explained in 2.3.2 the flow splitting, or "dead flux" contributes to challenge in grade efficiency also. In hydrocyclones it makes the performance of the cyclone better than it really is. This is shown in Figure 2.4, where both the typically grade efficiency curve and the reduced grade efficiency curve to a hydrocyclone is plotted.

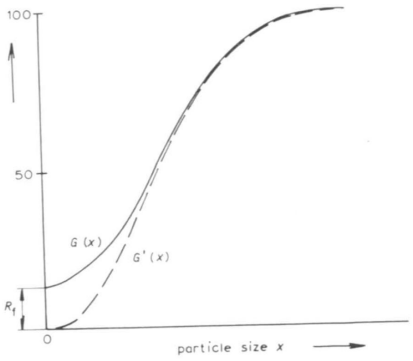

Figure 2.4: A typical grade efficiency curve for a hydrocyclone (full line) and the reduced grade efficiency (dashed line). Reference: [15]

The curve for the typically grade efficiency do not start in the origin, like it would do for inertial separation. This higher starting point is usually equal to the underflow-to-throughput ratio (Rf). The reason for this is the very fine particles, which simply follows the flow and split in the same manner as the fluid. This is regarded in the reduced grade efficiency curve, which makes different equipment much more comparable. The slope of the curve itself can give information, the less steep the grade efficiency curve is, the

grater the amount of misplaced particles will be.

2.3.6 The cut size

The cut size is the particle size, as shown in Figure 2.3. It can be the x-axis on a strongly size dependent separation process in the grade efficiency curve. It is from this curve the best definition of the cut size is made. The general definition of the cut size is the 50% line in the grade efficiency curve, also called "equiprobable size" x_{50}. Where the particle separation efficiency is 50%, that means that the particles have a 50% chance of entering the overflow or the underflow. Cut size, is very useful in scale-up of hydrocyclones because it is referred to the grade efficiency curve and therefore independent of the feed solids.

2.4 Centrifugal Separation

One of the main mechanism in hydrocyclone separation is related to the velocity distribution. Centrifugal separation utilizes an enhanced field force, over that provided by gravity, to cause separation of different densities. Centrifuges used for separation are often divided into two main categories, a sedimentation principle and a filtration principle. Hydrocyclones are much like sedimenting centrifuges, but the energy to get the flow to rotate, comes from the flow itself and not from a mechanical device. These three separation equipment have some basic particle mechanics in common [16].

2.4.1 Angular velocity and acceleration

Consider a limited body in circular motion around a point O with an angular velocity ω, as shown in Figure 2.5. As derived in Rushton, Ward & Holdich [16] if the velocity changes from point A to point B, there is a acceleration occurring. The centrifugal acceleration follows equation 2.5.

As derived in Appendix A, the centrifugal acceleration is:

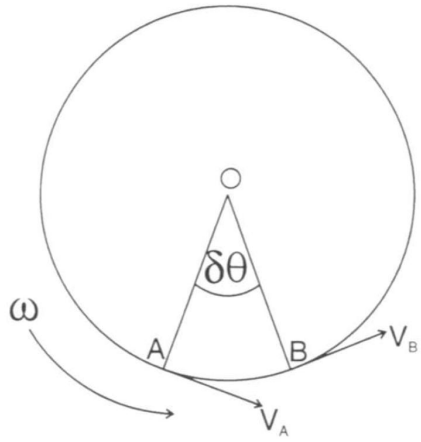

Figure 2.5: An illustration of angular velocity during rotation. Reference: [16]

$$a_c = r(\omega)^2 \tag{2.5}$$

Which acts toward the center of a circle for a restrained object.

2.4.2 Particle velocity in a Centrifugal Field Force

Stokes law in equation 2.6, defined for spherical particles is often used for calculation of separation. In this case it gives a good explanation of what happens. This simple equation is the one that is used in theory [16], by manufacturer [23, 24] and the operators [25] of separation equipment.

$$v_s = (\frac{d^2_{solid}}{18\mu_l})(\rho_{solid} - \rho_l)g \tag{2.6}$$

Stokes'law.

As shown the separation velocity, v_s, is decided by the solid particle size, d_{solid}, gravitation g, density difference between solid and liquid $(\rho_{solid} - \rho_l)$, and viscosity to the liquid the solid particle sinks in, μ_l. The Stokes equation is working ideally with

a droplet that sinks or rises in a non-moving fluid only influenced by the gravitational forces, it is normal to use Stokes law as an approximation of fluids in motion. There are two considerations that has to be taken when using the Stokes law. At first there is the concentration, which has to be so low that the settling of particle will not be interfered by the neighbour particle. The second consideration is that the Reynolds number should be less than 0.2 [16]. If those assumptions are valid the settling is called "free settling".

In Equation 2.6 the Stokes settling velocity of a small particle was derived, by neglecting all forces other than the gravitational field force and the liquid drag. It is possible to derive a similar equation for velocity in a centrifugal field force by following the same procedure. By setting the product of mass and acceleration (centrifugal field force) equal to the liquid drag and assuming the particle to be spherical:

$$\frac{\pi}{6}x^3(\rho_{solid} - \rho_l)r(\omega)^2 = 3\pi\mu x\frac{dr}{dt} \tag{2.7}$$

Where x is the particle diameter. The particle mass has been replaced by the product of volume and density, accounting also for the buoyancy effect. The particle velocity outwards is dependent on the radial distance from that centre; as the term r appears in the acceleration expression, unlike in gravity settling where the acceleration is constant. As Rushton, Ward & Holdich derived in [16], the velocity must be written in the differential form rather than a constant. The equation can be rearranged to provide the following equation analogous to gravity settling:

$$\frac{dr}{dt} = \frac{x^2}{18\mu_l}(\rho_{solid} - \rho_l)r(\omega)^2 \tag{2.8}$$

Referring to centrifugal acceleration derived in section 2.4.1, when Stokes equation is used in accelerating systems like hydrocyclones, the acceleration as in equation 2.5 will be put in for g in equation 2.6.

The flow through a hydrocyclone is often so complicated that simple equations from

Stokes law as shown in equation 2.6 can not be use. That is because it will only give an estimated calculation and understanding of the separation process. Today it is impossible to fully describe a hydrocyclone with theoretical equations because of two-phase flow, complex velocity- and pressure-distribution.

2.5 Hydrocyclone velocity

The design of the hydrocyclone is very important, their non-axisymmetric flow provides the means of separation. To understand how a hydrocyclone works, it is essential to know the three types of velocities working inside, and regarding the off centre flow pattern. In the following discussion reproduced from Rushton, Ward et al. [16], some distinction between the solid and liquid velocity has to be drawn. For obvious reasons the liquid has to concentrate in the overflow and solids in the underflow. Therefore the solids and liquids velocities have to differ in at least one direction. It is especially important to understand the lack of symmetry when working with numerical solutions. If it is not taken into consideration there will only be a trivial solution to the continuity (mass balance) equation, and that gives no information about the fluid flow.

2.5.1 Tangential velocity

The tangential velocity is very important in the hydrocyclone, it is the reason for the centrifugal force that works on the solids. This is because of drag force on the solids as they follow the liquid. The tangential velocity of the solids and liquid will be similar at the entry. It is assumed that this is also the case at all points with a radius smaller than the entry. The linear velocity at the inlet of the hydrocyclone v_f as seen in equation 2.9 is related to the volume throughput Q and area of inlet A_I.

$$v_f = \frac{Q}{A_l} \tag{2.9}$$

Equation 2.9 gives additionally a value of the tangential velocity at the outer radius of the hydrocyclone. At smaller radii a estimate can be made from principles of conservation of angular momentum, under frictionless conditions:

$$v_t r_i = constant \tag{2.10}$$

Where v_t is the tangential velocity at the radius of rotation r_i. In real applications energy is lost, and angular momentum will be less, this equation 2.11 accounts for.

$$v_t (r_i)^n = constant \tag{2.11}$$

n is between 0 and 1, depending on the different liquids and flow criteria.

According to Rushton, Ward & Holdich [16] experimental measurements of the tangential velocity has shown that it varies as shown in Figure 2.6.

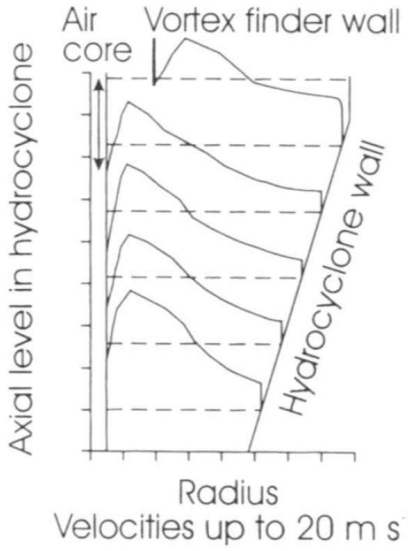

Figure 2.6: An illustration of tangential velocity during rotation. Reference: [16]

2.5.2 Radial velocity

The solid - liquid radial velocity have to vary much if there should be an effect in separation, an illustration is given in Figure 2.7. Normally the radial velocity components are hard to measure accurately, and they are much smaller than the tangential and axial velocity components. The net liquid velocity inwards can be estimated from knowing the net flow into the overflow, and further the dimension of the surface of assumed uniform flow inward, more outlined in "Equilibrium orbit theory" in section 3.1. The net liquid velocity outwards in the hydrocyclone can be estimated at each point by means of a force balance between the centrifugal field and the liquid drag forces. As explained by Rushton, Ward & Holdich [16] both liquid and solid maximum velocity is found at the wall of the hydrocyclone, diminishing to zero at the air core. Experimental measurements has shown that radial liquid velocity is negligible in the cylindrical section of the hydrocyclone.

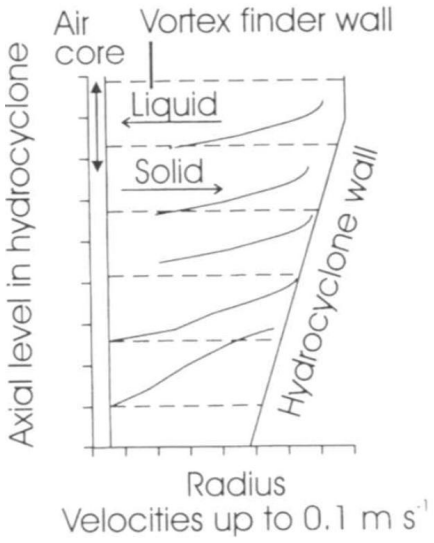

Figure 2.7: An illustration of radial velocity during rotation. Reference: [16]

2.5.3 Axial velocity

As in the tangential velocity the net solid and liquid flows are in the same direction. But there are two distinct regions inside the hydrocyclone with net velocities in different directions. The secondary vortex flow upwards and into the vortex finder, and the primary vortex net flow is downwards at the outer walls and out through the underflow.

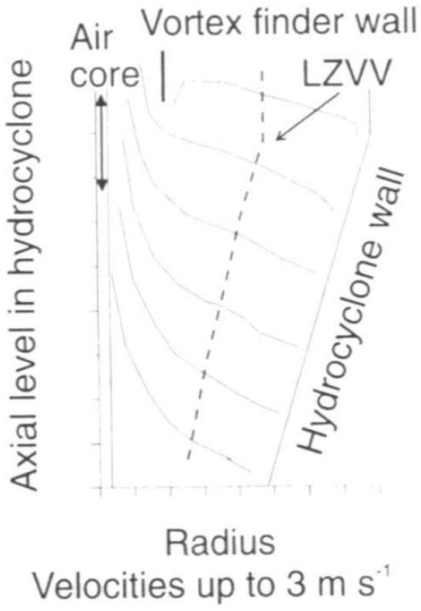

Figure 2.8: An illustration of axial velocity during rotation. Reference: [16]

The axial velocity becomes upward at radii between the cyclone wall and the vortex finder. Because of wall-induced flow which runs inward along the top of the cyclone, the area around the vortex finder may observe strong downward flow [26]. An important consequence regarding these opposing velocity directions, is that there must be a position of no net vertical movement which acts as the boundary between these two regions. This three dimensional rotating surface down through the cylindrical and conical part, as shown in Figure 2.8, are expressed as a locus of zero vertical velocity (LZVV). The point where the locus changes from cylinder to cone is subject to some debate, but will not be

taken into consideration in this thesis.

2.6 Residence time

Residence time is the actual time a particle spends inside different systems, the time from it enters to it is out of the system. Residence time is a well used expression in process technology and many other scientific fields, it is often used to characterize the mixing and flow within a reactor. It is also used to compare models with real reactors. The amount of substance in the system will have a direct impact on the measured time. A larger amount of substance in to the system gives a longer residence time, a average residence time is often calculated for specific systems. In hydrocyclone research the residence time is a important parameter, that is because if the residence time is high that means that the particle stays inside the hydrocyclone for a long time. With additional a high amount of particles inside the hydrocyclone at the same time, there will be an increased chance of clogging. Huang, An and Wu [27] has worked on the impact of different angles of the conical section to optimize the solid liquid separation, with respect to tangential velocity and residence time. According to [27], the total separation efficiency decreases with an increasing cone angle, and further increased residence time. The cone angle expression used by Huang, An and Wu, is the angle of the conical walls seen from the lower end of the cyclone.

2.7 The effect of particle concentration

As Svarovsky [28] wrote, "The flow patterns in a hydrocyclone are complex enough with a clean liquid, before we even put any particles in the flow." Since particle-particle interaction and additional presence of particles in swirling, turbulent flow are highly complicated, and our knowledge is inadequate. Most theories only apply for dilute systems,

both for analytical and numerical solutions. Dilute systems are only used for clarification concerns and they are rare in industry.

Some bulk models utilizes the effect of particle concentration in a clean flow model by using the feed concentration as a variable. The slurry density and viscosity are also based on the feed concentration of solids, but this has two unfortunate sides. First, in average the most particles (by mass) go to the wall rapidly after the inlet because they are coarse, that means that the concentration in the flow will be reduced quickly. Secondly, because of radial settling and ongoing radial dilution, this also leads to steep reduction in particle concentration along the fluid flow. The result shows that it is more realistic to use a clean liquid density and viscosity than that of feed solid concentration. Both the pressure drop and separation efficiency depends strongly on the cumulative effect of the density and viscosity distribution in the flow.

Low solid concentration

In hydrocyclones with low solid concentration, the flow pattern is unaffected by the presence of particles. Referring to Svarovsky [15] particle-particle interaction is negligible. Under these conditions only a few particles follows the underflow, and the underflow-to-throughput ratio (R_f) is low. This can further be assumed to have no effect on the cut size x_{50}.

High solid concentration

In cyclones with a higher input concentration some changes have to be made, the underflow-to-throughput ratio (R_f) has to be increased. It means that the underflow needs to be more opened so the increased volume of separated solids can be discharged.

2.8 Physics and Instrumentation in PET

In 1928 the young Englishman Paul AM Dirac postulated that a subatomic particle existed, this was equivalent in mass of an electron but carried a positive charge. He used the newly discovered quantum theory combined with Einstein‘s theory of relativity.

Dirac then found out that every particle had a corresponding antiparticle, a twin, each with the same mass and spin, but with the opposite electrical charge. Four years later Carl Anderson proved Dirac‘s postulate experimentally in cosmic ray research using cloud chambers. He photographed the track of a cosmic ray particle in a cloud chamber. [29] The track had an unusual curvature, and he deduced that it could only be produced by a particle *"carrying a positive charge but having a mass of the same order of magnitude as that normally possessed by a free negative electron"* [30]. He called this positively-charged electron a positron - the first identified antiparticle. For both their accomplishments, Paul AM Dirch and Carl Anderson received the Nobel Prize in Physics in 1933 and 1936, respectively. After Anderson's experiments it was shown that when positrons interact with matter two photons were simultaneously sent out in almost exactly opposed direction. These developments have strings to much of the important advances in physics in the first 50 years of the twentieth century. Today positron-emitting radionuclides are produced under controlled laboratory conditions in particle accelerators. There are these positron emissions (β^+ -decay) that are exploited in PET.

2.8.1 Mass and energy

The molecules are held together by their chemical bonds among its atoms. These bonds are formed by the force of electrical attraction between oppositely charged parts of the molecules. The atom is often represented by the planetary model created by Ernest Rutherford as illustrated in Figure 2.9. The planetary model is a representation of the protons, neutrons and electrons.

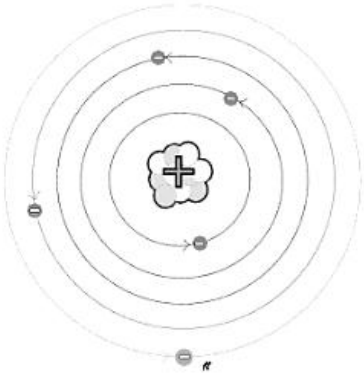

Figure 2.9: Flat atom. The standard two-dimensional drawing of atomic structure. Reference: [31]

This electrical force is named the Coulomb force, after the physicist who characterized it, Charles A. de Coulomb. This force is involved in chemical reaction ie. combining hydrogen and oxygen to form water. The electrons of the atom are held in place by the electrical force between them and the positive nucleus. Nucleus is held together by - nuclear force - which is involved in the release of atomic energy. Nuclear forces are of greater magnitudes than electrical forces.

Electron shells

The actual distance each orbit has from the centre is not so important, but the difference in energy between each shell is. The closer an electron is to the nucleus, the more tightly it is held by the positive charge of nucleus. That means that it requires more energy to remove a inner-shell electron than a outer one. The energy that has to be put into the atom to separate an electron is called the *electron binding energy.* It is usually expressed in *electron volts (eV).* The electron binding energy varies for inner-shell electrons from a few thousand electron volts (keV), to just a few electron volts (eV) for less tightly bound

outer-shell electrons.

Nucleus

The nucleus consist of a simple but useful model which is a tightly bound cluster of protons and neutrons. Protons are positively charged and will naturally repel each other; however, there is powerful binding force named the *nuclear force* that holds the nucleons together very tightly. The work (energy) required to overcome the nuclear force, is called the *nuclear binding energy*. It is the same amount of work that is required to remove a nucleon from the nucleus. The binding energy is typically in the rage of 6 million to 9 million electron volts (eV), this is approximately one thousand to one million times the electron binding force.

The energy (E) to electromagnetic radiation was demonstrated by Max Planck in 1900. The electromagnetic radiation is related to the frequency of radiation (υ) by the Planck's constant (h), this is derived in (Valk, Bailey at. el 2005) [32]:

$$E = h\upsilon \tag{2.12}$$

The energy of each photon is the integer multiple of hυ. The energy of a photon with a wavelength(λ) of for instance 450 nm is:

$$E = h\upsilon \ = \frac{hc}{\lambda} = \frac{6.63 \times 10^{-34} Js \times 3 \times 10^{8} m.s^{-1}}{450 \times 10^{-9} m} = 4.42 \times 10^{-19} J \tag{2.13}$$

The energy has the unit joule (J). The wavelength of 450 nm can seen in Figure 2.10, it is in the ultraviolet part of the visible light. Energies in joules can be converted into electron volt (eV), electron volt are the measurement when a unit charge is moved through a potential difference of one volt. $1eV = 1.6 \times 10^{-19} joules(J)$. For the wavelength of 450 nm the energy in eV would then be:

$$E = 4.42 \times 10^{-19} J = \frac{4.42 \times 10^{-19} J}{1.6 \times 10^{-19} J.eV^{-1}} = 2.76eV \tag{2.14}$$

X-rays and γ- rays contain energies of thousands to millions of electron volts per photon. Using Einstein's Special Theory of Relativity, $E = mc^2$, *rest-mass equivalent energy* of a particle is shown. This is the energy that would be liberated if all the mass of the particle would be converted to energy. *Rest-mass* are calculated when the particle is at rest, and has no kinetic energy. Looking at the electron, which has a rest mass $[m_o]$ of 9.11×10^{-31} kg, from this the amount of energy this mass can form can be calculated:

$$\begin{aligned} E &= m_o c^2 \\ &= 9.11 \times 10^{-31} kg \times (3 \times 10^8 m.s^{-1})^2 \\ &= 8.2 \times 10^{-14} J \\ &= \frac{8.2 \times 10^{-14} J}{1.6 \times 10^{-19} J.eV^{-1}} \\ &= 511keV \end{aligned} \tag{2.15}$$

c is the speed of light. This amount of energy will be recognized in the coming sections, it is the same amount of energy the photons emits in positron-electron annihilation.

2.9 Radiation

Radiation can be classified into electromagnetic or particulate radiation. First the electromagnetic radiation will be introduced. As shown in Figure 2.10 radiation is distributed across the electromagnetic spectrum. It is classified into *non-ionising* radiation, and *ionising* radiation. Ionising radiation is radiation with high energy; and has sufficient energy to remove electrons from atoms. This will further cause ionisation. This can take place with high-energy electromagnetic radiation (X-ray and γ radiation) and charged particles (α, β^-,β^+). Examples of non-ionising electromagnetic radiation include light-, radio-,

and microwaves. The focus will be on ionising radiation since that is of greatest interest in this present work.

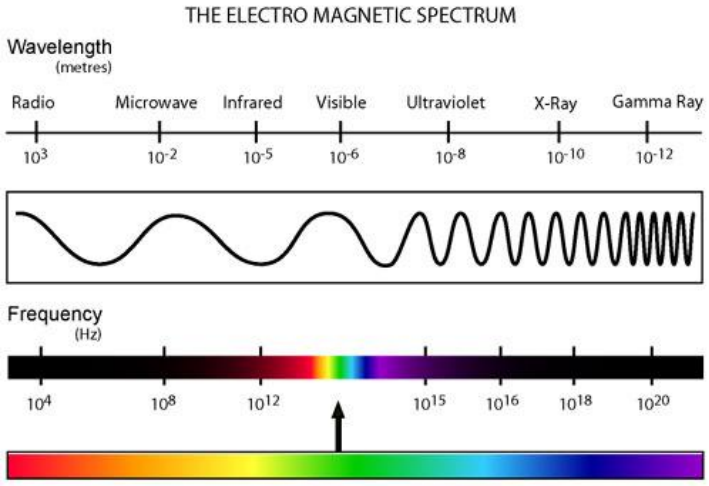

Figure 2.10: The Electromagnetic Spectrum. Reference: [33]

2.9.1 Electromagnetic radiation

Electromagnetic radiation is pure energy. The amount of energy associated with each quantum is determined by the wavelength (λ) of the radiation. Humans are capable of detecting a few types electromagnetic radiation. Those are thermal radiation, or heat, with a wavelength of about 10^{-5} m, and visible light with a wavelength of about 10^{-6} m. This is indicated in Figure 2.10. The energy of radiation can be absorbed, and stopped, partly or totally by different materials. For instance light can be stopped by a paper, while lead is needed to stop γ with shorter wavelengths. Electromagnetic radiation may be X-rays, which is produced within an atom, but outside of the nucleus. Characteristic X rays are produced when orbital electrons drops down and fill up a vacancy in an inner shell of an atom. In this process the electron gives off energy, this energy is the characteristic X-ray. The energy of the X ray is determined by the difference in binding

energy between the levels. X-rays normally has energy in the range of $\sim$ 1 - 100 keV.

Annihilation radiation

Annihilation radiation is also electromagnetic radiation, in the same manner as X- and γ- rays. It may be the energy of a positron-electron annihilation process. Which is the rest-mass energy discussed in section 2.8.1. Annihilation radiation is produced outside the nucleus and often also outside of the positron emitting atom. From each positron decay and further annihilation there are produced two photons. Each photon has energy of 511 keV, and the photons are given off close to 180° from each other. This is the element that is exploited in positron emission tomography (PET), and will be derive more in detail later. A representation of this is shown in Figure 2.11

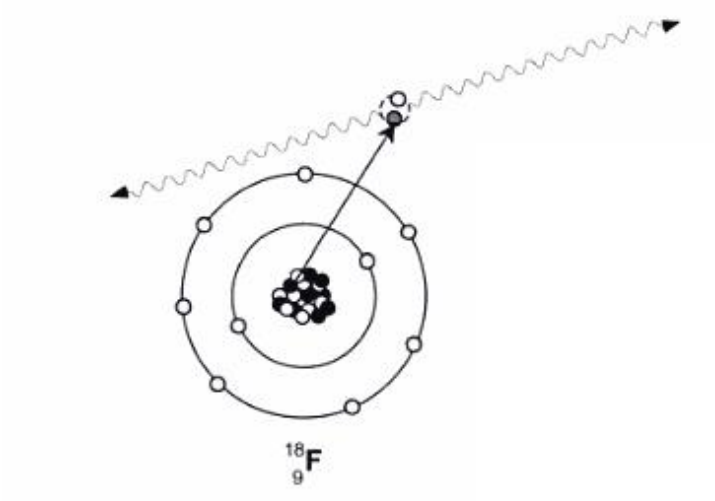

Figure 2.11: Annihilation radiation. Reference: [32]

2.9.2 Particulate radiation

Particle emission from natural radioactive decay was the first observation of radioactivity. In 1895 Wilhelm Rontgen produced electromagnetic radiation in the form of X-rays. One year later, in 1896, Henri Becquerel showed that naturally occurring uranium produced radiation spontaneously. They first believed that uranium radiation was similar to the X-ray, but Rutherford showed that some types of radiation were more penetrating than others. The name he gave the radiation were after how penetrating they were, lightest alpha (α) rays, then the more penetrating ones beta (β) rays. It was soon after shown that a magnetic field could deflect these kinds of radiation. This meant that these radiations had to carry charge, and were not electromagnetic rays, but in fact particles.

2.9.3 Unstable Nucleus and Radioactive Decay

An unstable nucleus will adjust itself until it is in stable state ether by ejecting portions of its nucleus or by emitting energy in the form of photons *(gamma rays)*. This process is called *radioactive decay*. The most common types of decay can be; alpha, beta or gamma.

Alpha decay

Alpha particle has a large mass, and this gives reason for a deposition of large amounts of energy in a very small area. This is the further reason for the great radiation hazard if ingested or inhaled. Alpha particles inside the body can cause any or all of the symptoms of radiation poisoning. "It is estimated that chromosome damage from alpha particles is about 100 times greater than that caused by an equivalent amount of other radiation."[14] But on the other side, their short distance makes them relatively easy to shield and further stopping.

Too many Protons: Positron Decay and Electron Capture

In the same way as excess of neutrons, an unstable nucleus with too many protons can undergo a decay that will convert a proton into a neutron. This can occur in two ways: positron decay and electron capture.

Positron decay

A proton can be converted into a neutron and a positron.

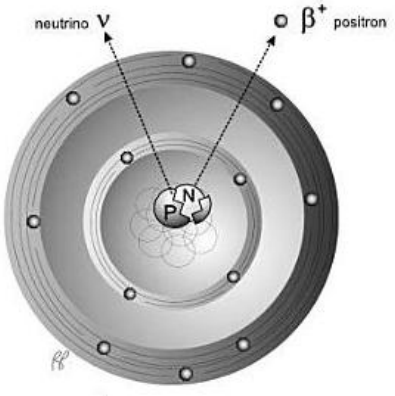

Figure 2.12: β^+ (positron) decay. Reference: [31]

The positron emitted survives only a brief moment compared to the electron. Positron quickly encounters an electron, and both are *annihilated*, see Figure 2.11. Annihilation occurs when two antiparticles such as electron and positron react with each other. The energy of the combined antiparticles is converted into two photons with equivalent energy to the rest mass, 511 keV.

The reason for the reaction between the positron and electron is that after emission from the nucleus, the positron loses kinetic energy by interactions with the surrounding matter. As described in "Positron Emission Tomography - Basic Sciences" [32], the positron interacts with other nuclei as it is deflected from its original path by one of four

types of interaction:

- *Inelastic collisions* with atomic electrons, which is the predominant mechanism of loss of kinetic energy
- *Elastic scattering* with atomic electrons, where the positron is deflected but energy and momentum are conserved
- *Inelastic scattering* with a nucleus, with deflection of the positron and often with the corresponding emission of Bremsstrahlung radiation
- *Elastic scattering* with a nucleus where the positron is deflected but does not radiate any energy or transfer any energy to the nucleus

When the positron passes through matter it losses energy, it happens either in ionisation events with other atoms or by radiation after an inelastic scattering. The result will be a deflection in positron path, which again may send the positron on a tortuous passage through matter. This is way it is so difficult to estimate the range of positrons based on their energy alone. Empirical measurements are usually made to determine the mean positron range in a specific material.

Eventually the positron combines with an electron when they are both at rest. A metastable intermediate species called *positronium* may be formed by the positron and the electron combining. Positronium is a non-nuclear, hydrogen-like element, with a mean life of around 10^{-7} seconds. The positronium behaves as expected much alike hydrogen atom with respect to spectral lines, but because of positroniums smaller mass ratio the frequency is about half. In water and human tissue formation occurs in about one-third of the cases, direct annihilation of the electron and the positron is more favourable. Subsequent annihilation means that the positron-producing event (the annihilation) occurs outside the radioactive nucleus.

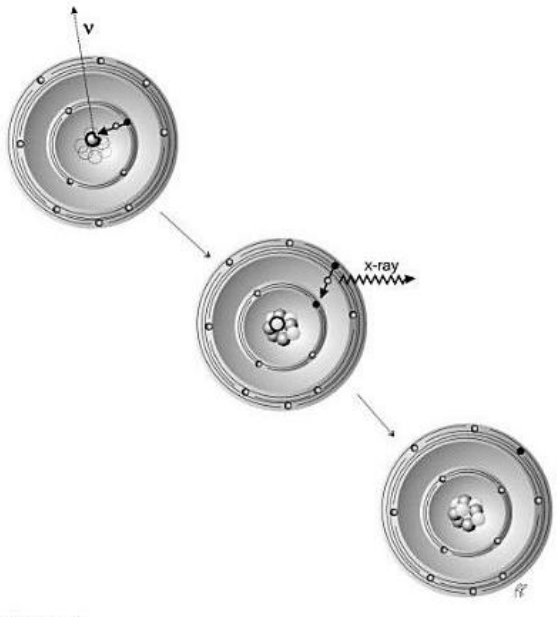

Figure 2.13: Electron capture. Reference: [31]

Electron capture

Electron capture is a process that competes with positron decay. The nucleus can combine with one of its inner orbital electrons and then achieve to convert a proton in the nucleus into a neutron. Then an outer-shell electron fills the inner shell vacancy left by the captured electron. The energy given out by an outer-shell electron "falling" in to an inner shell as shown in Figure 2.13 is emitted as an x-ray. The probability for electron capture increases with the atomic number, Z.

2.9.4 Half-life

A very important part of the nuclear radiation is the half-life. The half-life is the time it takes for half of an amount of radioactive atoms to decay. It is not possible to determine which nucleus will decay, because it is a stochastic process. The half-life is predicted by

the average behaviour of a radioactive sample containing billions of atoms. The scientific notation is $T_{\frac{1}{2}}$. The time it takes for the next half of the remaining atoms to decay is also $T_{\frac{1}{2}}$. This will as shown in Figure 2.14, carry on until the radiation is almost zero and the process is considered complete. The rate of decay at any particular instance in time is referred to as the activity of the radionuclide. The curve in Figure 2.14 is the average behaviour of the sample of radioactivity, it can be described by the decay equation:

$$A(t) = A(0)e^{-0.693t/T_{\frac{1}{2}}} \tag{2.16}$$

where $A(0)$ is the initial number of radioactive atoms. t is the time from the initial start. In theory $T_{\frac{1}{2}}$ will never go entirely to zero when $t \to \infty$.

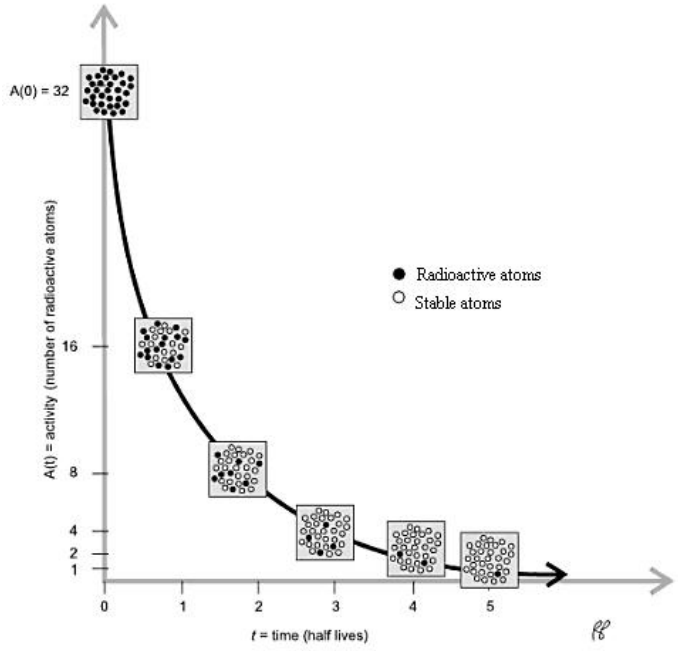

Figure 2.14: Decay curve. Reference: [31]

The SI unit of activity is Becquerel (Bq), after the nuclear pioneer, Henri Becquerel. One Becquerel is defined as one radioactive disintegration (or decay) per second. This will

give a very small unit, so it is common to work with MBq (Mega Becquerel), GBq (Giga Becquerel) and also TBq (Tera Becquerel). An example of calculating the radioactivity of a 200 MBq sample of ^{18}F where $T_{\frac{1}{2}} = 109.5$ minutes, 90 minutes after calibration.

$$\begin{aligned} \lambda &= 0.693/109.5 = 6.330 \times 10^{-3} min^{-1} \\ A_t &= 200 \times e^{(-6.330 \times 10^{-3} \times 90)} \\ &= 113.14 MBq \end{aligned} \tag{2.17}$$

The activity after 90 minutes is 113.14 MBq.

An older much used unit, still in use in the US, is the Curie (Ci), after Marie Curie. One curie (Ci) is defined as 3.7×10^{10} decays per second. Another useful term related to radioactivity is *specific activity*. It is the ratio of radioactivity to total mass of the species present. The term of the specific activity is outlined from the ratio of radioactivity (Bq or Ci) and the total mass of compound, this can be Bq/kg or for instance GBq/μmol. 63000 GBq/μmol is the maximum specific activity to ^{18}F, with a half-life of 109.7min [34]. This specific activity is important in medical application in PET work, because of quantification purposes.

2.10 Interaction of Radiation with Matter

When high-energy radiation strikes matter, energy can be transferred to the material. A range of effects may happen, for instance transfer of radioactive energy to the atoms and molecules. Further heating the matter and even modifying the structure. Commonly is the ionisation or excitation of the atoms in the absorbing material. Large particles such as alpha particles with a relatively short range in matter, makes the chance greater for them to be absorbed by the material. Larger mass gives larger chance of absorption. Beta particles are lighter and more penetrating. The neutrino with there extremely small

mass and no charge interacts poorly with material. This again means that it is very hard to stop or detect. High energy photons, which are massless, are also obviously highly penetrating.

Interaction of Photons with Matter

There are several mechanisms when high-energy photons interact with matter; they are dependent on the energy of the electromagnetic radiation and also the material. The three main mechanisms that dominate are, (i) the photoelectric effect, (ii) the Compton effect / Compton scattering, and (iii) pair production.

2.10.1 Photoelectric Effect

In the theory of radiation, the photoelectric effect is dedicated a special place. In 1899 Philipp Lenard demonstrated that light caused the metal to emit electrons, and this was called the photoelectric effect. As Figure 2.15 shows, the photoelectric effect is an interaction of photons with orbital electrons in an atom.

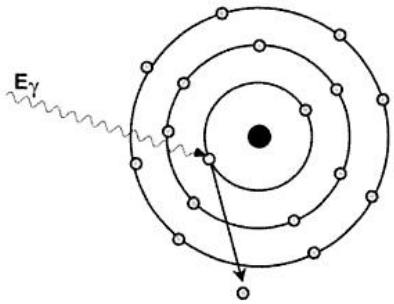

Figure 2.15: The photoelectric effect involves all of the energy from a photon being transferred to an inner shell electron, causing ionisation of the atom. Reference: [32]

The inner shell electron carries on all the energy from the photon. Parts of the energy is used to release the electron from the binding energy, the remaining energy is transferred

as kinetic energy to the electron. This is characterized by,

$$E_{photoelectron} = E_{photon} - E_{binding} \tag{2.18}$$

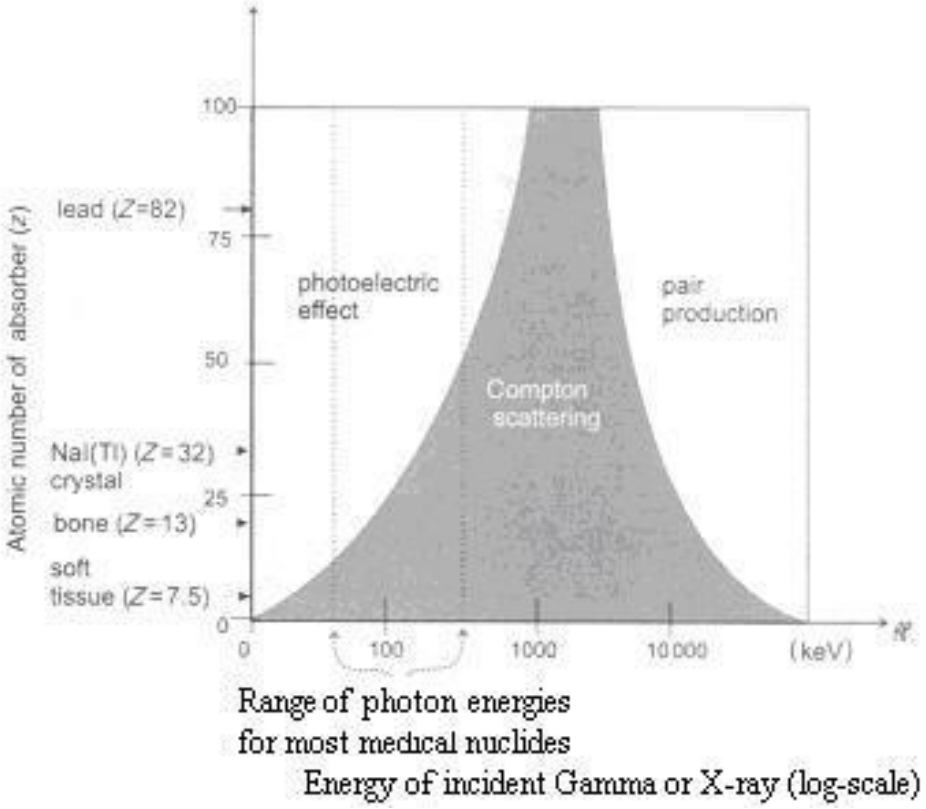

Figure 2.16: Predominant type of interaction for various combinations of incident photons and absorber atomic numbers. Reference: [31]

As the electron is ejected, another more loosely bound outer orbital electron drops down to occupy the vacancy. This will then send out a characteristic X-ray. The atom may emit a second electron to remove the energy, this is named an Auger electron. The emitted electron is known as a photoelectron.

The photoelectric effect is as Figure 2.16 shows the dominant material interaction

in higher atomic numbers such as lead (Z = 82), combined with range of energy. The human tissue has a much lower atomic number (Z = 7.5). In the use of PET scan the photoelectric effect has little impact on the annihilation radiation. This is because the annihilation radiation is 511 keV, but in the use of PET/CT scan it is important for the attenuation correction in the CT.

2.10.2 Compton Scattering

Compton scattering is the interaction between a photon and a loosely bound orbital electron, the electron is so loosely bound that it can be considered as "free". This is as shown in Figure 2.16 the main challenge around all energies that are of concern in PET research. The energy of the photon can be much higher than the binding potential between the electron and the atom. That means that the binding potential in some cases can be neglected in the calculation, otherwise it follows eq. 2.18. After the interaction as shown in Figure 2.17, the electron is ejected from the atom, and the photon changes direction. The lost energy of the photon is divided into two parts, the small binding energy, and the kinetic energy given to the Compton recoil electron. The energy transfer does not depend on the properties of material or its electron density.

The energy of the photon after interaction with respect to Compton scattering, can be calculated from the Compton equation:

$$E'_{\gamma} = \frac{E_{\gamma}}{1 + \frac{E_{\gamma}}{m_0 c^2}(1 - \cos(\theta_c))} \tag{2.19}$$

m_o and c are the electrons rest mass and speed of light, respectively. θ_c is the recoil direction. E_γ is the initial energy.

The energy to an annihilation photon after a single scatter of 60°.

E_γ = 511 keV

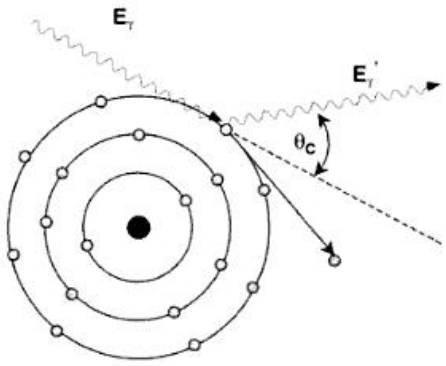

Figure 2.17: In compton scattering, part of the energy of the incoming photon is transferred to an atomic electron. This electron is known as the recoil electron. The photon is deflected through an angle proportional to the amount of energy lost. Reference: [32]

$\theta_c = 60°$; $\cos[\theta_c] = 0.5$

$m_0c^2 = 9.11 \times 10^{-31}kg \times (3.0 \times 10^8 m.s^{-1})^2$

$\equiv 511$ keV

$$E'_\gamma = \frac{511}{1 + \frac{511}{511}(1 - 0.5))} = 341keV \tag{2.20}$$

The energy after interaction is 341 keV. By examining the Compton equation it is found out that the maximum energy lost is when the photon is back-scattered, scattering angle is 180 ° (cos(180) = -1). A back-scattered photon, with an initial energy of 511 keV, will have energy of 170 keV afterwards. The probability of Compton scattering is not equal at all energies or scattering angles.

In Figure 2.18 the result is shown as a function from 0 - 180°. According to Powsner & Powsner [31] Monte Carlo computer simulations has shown that the vast majority (>80%) of scattering events in tissue-equivalent material used in PET, has only under-

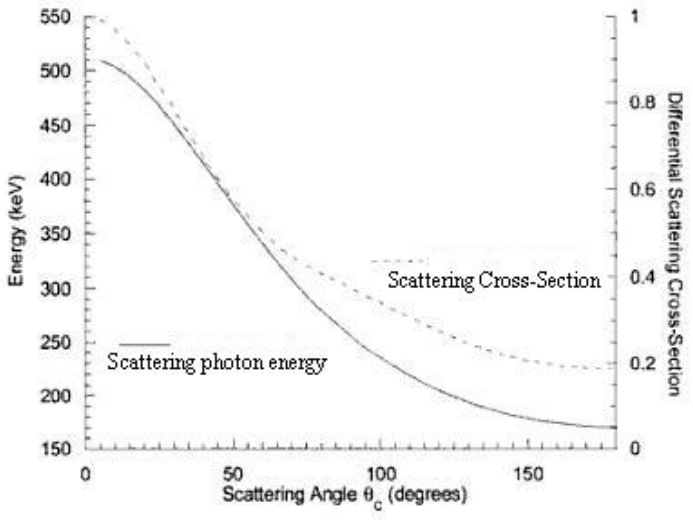

Figure 2.18: The angular probability distribution (broken line - differential scattering cross-section) and resultant energy (solid line) for Compton-scattered annihilation photons anr shown. Reference: [32]

gone one single scattering interaction.

2.10.3 Pair production

Pair production is the final main mechanism in photon interaction with matter. Photons with a total energy grater than 1.022 MeV that is passing in the vicinity of a nucleus, may split into two electrons with opposed signs to conserve charge. This is the dominate interaction mechanism at high energies in the Coulomb field of a nucleus. This will not be further detailed since the only concern is energies around 0.511 MeV. An illustration is given underneath in Figure 2.19.

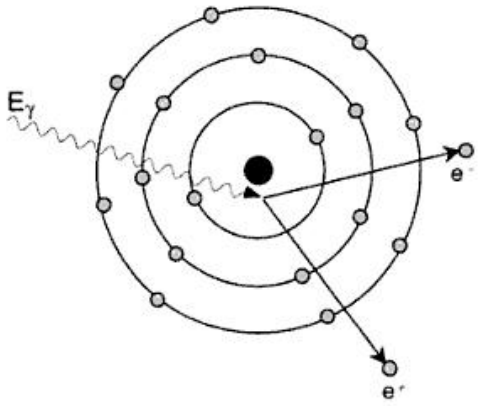

Figure 2.19: The pair-production. As a photon passes in the vicinity of a nucleus spontaneous formation of positive and negatively charged electrons can occur, at a threshold energy of 1.022 MeV. Reference: [32]

2.10.4 Scattering of photons

Scattering of photons is one of the main challenges in positron emission tomography. As outlined earlier it is the Compton interaction that is the most important for photon interaction with soft matter in energies around 0.511 MeV. The result of this interaction is that the primary photon changes direction and loses energy. Further, the atom where the scatter occurs is ionized. Looking more closely on the PET detection, it is based on coincidence detection. The line-of-sight ascribed to an event is determined by the paths taken by both annihilation photons. This means that the events can be outside of the object with respect to lines of response. This is illustrated in Figure 2.20.

In Figure 2.21 it is showed that the count rate observed in an object only depends on the total thickness, D, of the object. Further showing that the count rate observed is independent of the position of the source inside the object. If the count rate from one single photon emitting count source of radioactivity at a depth, a, in a attenuating medium of total thickness, D, is considered. The following section is a review of Valk,

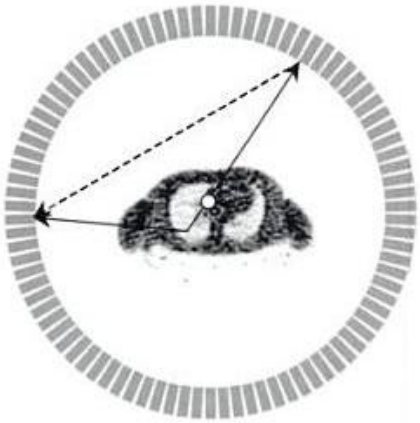

Figure 2.20: Scattering of photons. Reference: [32]

Bailey et al. [32].

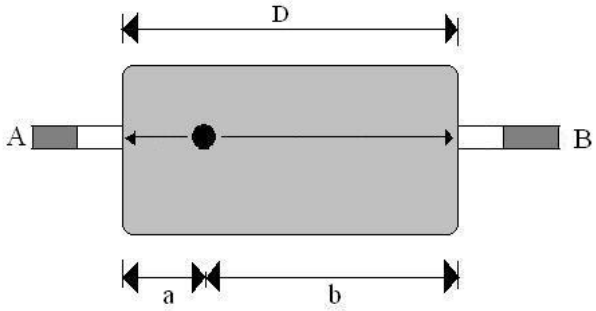

Figure 2.21: Scattering of photons. Redrawn from: [32]

The count rate C observed by an external detector A would be,

$$C_a = C_0 e^{-\mu a} \tag{2.21}$$

Where C_0 represents the unattenuatted count rate from the source, and μ is the attenuation coefficient of the medium (assumed to be a constant here). The count rate

changes with the depth α. The count rate from detector B, if they are measuring the source 180° opposed from A would then be:

$$C_b = C_0 e^{-\mu(D-a)} \tag{2.22}$$

where the depth b is given by $(D-a)$. The count rate would then be equivalent in the detector when $a = b$. The same case would be considered for positron emitting sources. There detectors A and B measure the coincident photons. The count rate is given by the product of the probability of counting both photons and will be:

$$\begin{aligned} C &= (C_0 e^{-\mu a}) \times (C_0 e^{-\mu(D-a)}) \\ &= C_0 (e^{-\mu a} \times e^{-\mu(D-a)}) \\ &= C_0 e^{-\mu(a+(D-a))} \\ &= C_0 e^{-\mu D} \end{aligned} \tag{2.23}$$

So to correct for attenuation of coincidence detection from annihilation radiation it is only one measurement, the total attenuation path length (-μ D), is all that is required [32].

2.11 Challenges in PET

In PET-scanning physics there are several different challenges with regard to the signals and resolution. The main challenges are timing resolution, coincidence detection, energy resolution, scatter and sensitivity and depth of interaction, they will be briefly explained underneath. All this interference influences the reliability of the measurements.

2.11.1 Timing Resolution and Coincidence Detection

Timing resolution in PET detectors describes the event by event uncertainty in the timing characteristics with regard to statistical fluctuation. The timing resolution is important because of its ability to bind two lines of response (LOR) together. It also has to be accounted for detecting coincident events. Figure 2.22 gives a schematic overview of the detection of two coincident photons being emitted.

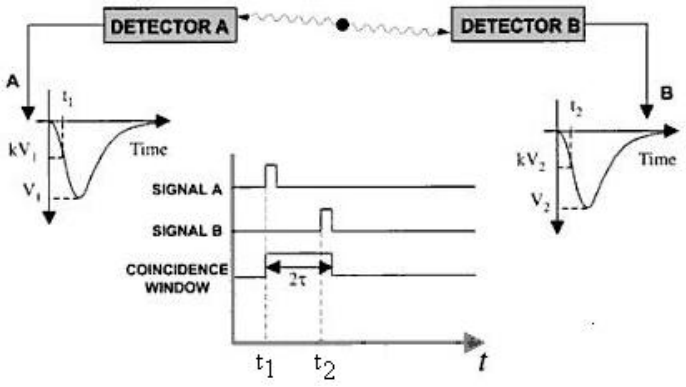

Figure 2.22: Schematic representation of detecting coincidence events in two detectors. Signal A results in a trigger pulse 1 which marks the start of the coincidence window of width Δt. Similarly, signal B results in a trigger pulse 2. A coincidence circuit then checks for coincidence between pulse 2 and the coincidence window. Reference: [32]

The following is referred from Valk, Bailey et al. [32]. When the signals sent out from the two detectors, V_1 and V_2, passes a certain fraction of their amplitudes a narrow trigger pulse is sent out. The amplitude of the pulse may differ for incomplete deposition of energy or varying gains of the two photo-detectors. At time t_1, signal A trigger pulse 1 that will register and further produce a coincident time window of a predetermined width of 2τ. Signal B, will trigger at a later time, t_2, this depends on the timing resolution to the camera. The difference t_2 - t_1, may or may not overlap the coincidence window. For detectors with poor energy resolution a larger value for 2τ needs to be used for detecting

most of the valid coincident events. The distances the photons travels before interaction with the detector is dependent on were in the scanner field of view (FOV) the emission occurs. The timing resolution must have such a large 2τ, that it takes into consideration an emission in the edge of FOV.

Random coincidences

Random coincidences have the opposite requirements. It occur when two unrelated photons are emitted and entering the opposite detector inside the same timing window. In these events the scanner gives out false line of response (LOR). A large timing window will give an increased number of unreal LOR. For reducing the number of random coincidences in PET imaging a fast scintillator is desirable.

2.11.2 Energy Resolution and Scatter

In scintillation detectors the energy resolution is a function of the combination between the relative light output of the scintillator, as well as its intrinsic energy resolution. The intrinsic energy resolution accounts for other non-statistical effects that arise in the energy measurement process. To achieve good image contrast and reduce background counts in PET, good energy resolution is necessary, especially in 3D volume image mode. There are as mentioned three types of coincident events in PET scanners; true, random, and scattering coincidences. Random coincidence as already discussed, are incidental detection of two unrelated LOR, that is falsely believed to relate in the same timing window. The random coincidence adds to the image background and will therefore reduce its contrast. The last coincidence that will worsen the image contrast is the Compton scattering. This is single annihilated event, were one or both of the photons undergo Compton scattering inside the FOV. This will then lead to mispositioned LOR, and therefore misrepresent the true activity distribution. Since scattering involves loss of

energy, the scattering not around the photopeak in the energy spectrum can be rejected. This can be done by good energy resolution in the detectors. To further remove these false lines from the image and improve image contrast, additional scatter-correction techniques which estimate the distribution of scattered radiation are used.

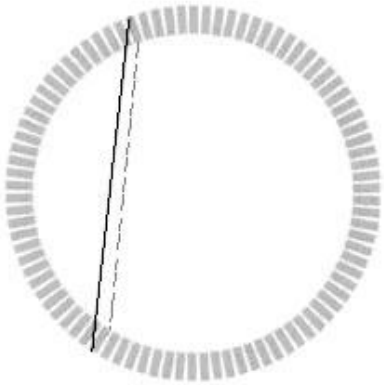

Figure 2.23: A schematic representation of parallax error introduced in the measured position due to the unknown depth-of-interaction of the photons within the detectors. Reference: [32]

2.11.3 Sensitivity and Depth of Interaction

The last main momentum regarding the uncertainty of the PET scanner; is about the sensitivity and depth of interaction inside the detector. The sensitivity is determined by two parameters of scanner design, its geometry and stopping efficiency for 511 keV photons. The geometry for high-sensitive scanners is ideally small diameter and large axial FOV. The stopping efficiency in PET depends on the type of detectors being used. Regarding the stopping power the photons travels a short distance into the detectors before it depositing its energy. This is typically not measured in PET, today it is assumed that this happens on the surface and is illustrated in Figure 2.23. This is a problem

scientists are working on, because it creates deviations from the real position. This is because the photons may enter the detector at oblique angles, and this can lead to deviation, blurring of the reconstructed image. This "parallax" blurring typically happens with annihilations that happen in large radial distances from the scanner's central. For a BGO whole-body scanner, measurements show that the spatial resolution worsen from 4.5 mm near the centre of the scanner to about 8.9 mm at a radial distance of 20 cm [35].

2.11.4 Uncertainty from annihilation

Some uncertainty of the location of the nucleus in positron emission tomography is made because of the annihilation. Because of the distance the positron travels after emission and before it annihilates. The uncertainty due to positron range is a function that increases with increasing initial energy of the positron. For high energy positrons such as ^{82}Rb (E_{max} = 3.4 MeV), the mean range in water is around 5.9 mm. Table 2.1 shows some commonly used positron emitting nucleus and associated properties. ^{18}F has a mean range in water of about 0.6 mm.

2.11.5 The way ahead for PET

The positron emission tomography technology has trough the last decades developed enormously, and are still advancing. Both detectors and instrumentation developments have brought PET in as a sophisticated clinical tool. Now a whole industry is interested in developing higher- sensitivity and -resolution devices. The scintillator may expand further especially with regards to time-of-flight. Another improvement is Light-collection technology which may move from photomultiplier tubes to more solid-state devices like Avalanche photo diode (APD). This will further improve coupling and increase the bandwidth for data collection and processing by reducing the multiplexing of the signals. The

Nuclide	E_max	E_mode	$t_{1/2}$	Range in Water	(mm)	Use in PET
	MeV	(MeV)	$(mins)$	Max	Mean	
^{11}C	0.959	0.326	20.4	4.1	1.1	Labelling of organic molecules
^{13}N	1.197	0.432	9.96	5.1	1.5	$^{13}NH_3$
^{15}O	1.738	0.696	2.03	7.3	2.5	$^{1}5O_2, H_2^{15}O, C^{15}O, C^{15}O_2$
^{18}F	0.633	0.202	109.8	2.4	0.6	$[^{18}F] - DG, ^{18}F^-$
^{68}Ga	1.898	0.783	68.3	8.2	2.9	$[^{68}Ga] - EDTA, [^{68}Ga] - PTSm$
^{82}Rb	3.40	1.385	1.25	14.1	5.9	Generator-produced perfusion tracer
^{94m}Tc	2.44	*	52	**	**	β^+-emitting version of ^{99m}Tc
^{124}I	2.13	*	6.0×10^3	**	**	Iodinated molecules

* Many-positron decay scheme hence no E_{mode} value given. ** Not reported to date.

Table 2.1: Properties of some positron-emitting nuclides of interest in PET compiled from variety of sources. Reproduced from [32]

scanner design will also probably continue to evolve. This may again provide challenges in terms of photon detection, discrimination, and performance. Further developments in basic physics will support many of these enhancements.

Chapter 3

Literature survey

The way of designing and construct efficient hydrocyclones today is done by using models, which can for instance be empirical, analytical or computational. Section 3.1 is a review of general models and the background for them. The models give a good understanding of the complexity of the hydrocyclones. In section 3.2 an extensive theoretically investigation has been performed for finding which models and methods that are used to make state-of-the-art hydrocyclones today. Most of the methods explained in section 3.2 have its origin in the general methods from section 3.1.

3.1 Review of general hydrocyclone models

Ladislav Svarovsky made in 1996 a critical review of hydrocyclone models. Models have for many years been the method used to calculate cyclones. As early as in 1952 Kelsall [36] made the first effort in modeling the velocity distribution in a hydrocyclone. He measured the tangential and axial velocity in the equipment finding that the tangential velocity was independent of the z coordinate [28]. His work has later been developed by many researchers. The utilization of models has several reasons, the main are prediction of the performance under given operation condition. It is important to have as correct

models as possible. The models have two main criteria, flow capacity (i.e. pressure drop - flowrate relationship) and separation efficiency. Other considerations can also be figured out, for instance sharpness of cut. Hydrocyclones are generally often only modelled for particles in pure liquids, and often only verified for water. The seven most used specific models for hydrocyclone are formulated underneath, reviewed by Svarovsky [28].

1. Simple fundamental theories which take no or little account of the effect of the flow ratio (or the size of the underflow orifice), of the feed concentration or of the feed size distribution. The simple fundamental theories give a correlation of the cut size and the pressure drop to a hydrocyclone, but only by few dimensions. The theories fall into two groups: the equilibrium orbit theory or the residence time theory.

    - The principle behind the equilibrium orbit theory is the concept of the equilibrium radius. This means that the liquid drag on a particle, caused by radial flow of liquid into the centre of the hydrocyclone are equate by the centrifugal field force on the particle in one specific radius [16]. If the two forces are equal, then the particle will not move, nor inwards or outwards. It will follow an orbit around the hydrocyclone with a appropriate tangential velocity. If this radial orbit is the locus of zero vertical velocity (LZVV) then the particle will not have any preferences in following the overflow or underflow. The dependent is the diameter of a particle that orbits at LZVV, this will be the hydrocyclone separation size x_{50}. Equilibrium orbit theory may be used to correlate and explain the relation between flow rate and hydrocyclone cut size. The usefulness as a predictive tool is limited, because of tests that must be conducted to determine several parameters required in the model: the flow split and exponent on the radius. According to Rushton, Ward et al. [16], it does not provide any information on the required pressure drop to perform the separation, or on the sharpness of the cut.

The hydrocyclone with LZVV is shown in Figure 3.1.

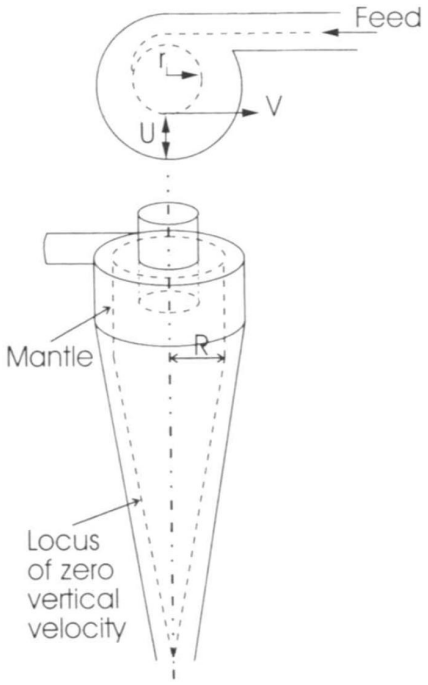

Figure 3.1: An illustration of the equilibrium orbit theory, a hydrocyclone with LZVV. Reference: [16]

- The residence time theory, has been reviewed several times since Tengbergen & Rietema [22] first proposed it. The residence time theory despite many different procedures leads to results that are very similar to those from the equilibrium orbit theories. The disadvantage of the theory is that it takes no consideration to the radial fluid flow, the hindered settling at higher concentrations and assumes no influence of turbulence. The Holland-Batt [37] so called "bulk-model", does take the radial fluid flow into consideration, and also uses a hindrance factor for settling concerns [38].

2. A more sophisticated, two-phase flow theory which includes the effects of feed

concentration and the mean particle size in the feed. The turbulent two-phase flow theory takes the challenges in the tangential velocity into concern. The turbulent two-phase flow theory allows the effect of the feed solids on the separation in a hydrocyclone. "The theory points to small cone angles and curved feed inlets for clarification duties where high mass recoveries are required" [28].

3. The crowding theory which explains the strong effect of the size of the underflow orifice on cyclone performance. The crowding theory only concern very specific cases, and will not be further derived in this thesis.

4. The all-embracing empirical models, based mostly on regression analysis of the measured data, applicable only to the specific system tested (e.g. copper ore in Krebs cyclone etc). The regression model is so-called mathematical models, but is really almost only regression analysis of test data. The results in the model are equations that are purely empirical and dimensionally inconsistent, requiring empirical constants with a dimension, and specified units to be used for each variable.

5. The chemical engineering approach based on dimensionless groups, combining 1,2,3 and 4 above. The dimensionless group model gives much more reliable performance predictions, than the once mentioned above. The dimensionless group model is used in chemical engineering model for hydrocyclone scale-up. The model concerns around three dimensionless equations which fully describe the function of a hydrocyclone. If the cut size and underflow concentration is known, the three equations will give, cyclone diameter, the number of cyclones to be used in parallel and the size of the underflow orifice which will produce the required performance and capacity (under the given pressure drop) [28]. There are developed tables for several commercial hydrocyclones, with constants for prediction of cut size and pressure drop, without doing any laboratory test. This approach gives more information

than the equilibrium orbit theory and does not need any preliminary testing. But testing can be useful in the dimensionless group model, especially concerning the accuracy of scale-up constants.

6. The analytical mathematical models are modelling the flow patterns inside the hydrocyclone. Analytical flow models are based on mathematical solutions of the basic flow mechanism. Possible models would be of the particle trajectories, including the boundary layer flow, the short circuit flow and the internal eddies but at low feed concentrations only.

7. Numerical simulation. The usual way to design and predict the performance of a hydrocyclone today is by computational fluid dynamics (CFD). Many commercial software packages are available for mapping the streamlines inside the hydrocyclone. In CFD simulations the hydrocyclone are discretised with many different grid points which represents positions inside it. The governing differential equations are solved by a finite difference or element model. In modelling the flow through the hydrocyclone the continuity equation are used on the fluid, solid and momentum, whereas the fluid motion is described by the Navier-Stokes equation for incompressible flow. The programs input requirements are cyclone geometry and the inlet feed conditions. Simulation can predict the pressure drop, cut size, grade efficiency or flows into each discharge port. Other advantages by using CFD are that it is easy to change and investigate the inlet conditions or cyclone geometry. Referring to Rushton, Ward et al. [16] the usual way to numerical model a hydrocyclone is to assume symmetry around the axis, which considerably simplifies the computational requirement. For a true representation of the hydrocyclone all three velocities in time and space has to be possible to vary, this because of turbulent liquid flow inside and further large number of solid phases to represent a size-distribution. All this is an enormous amount of computational information,

and some simplifications are often made. According to Rushton, Ward et al. [16] some numerical studies considers the flow to be laminar, axis symmetric and even with only an overflow [39]. As more assumptions or constrains are made, the less reliable the result will be. As reviewed, CFD simulations has many advantages, but also its limitations, for instance turbulence modelling in highly swirling confined flows is very difficult, there are also many challenges regarding high solid concentrations when particle-particle interactions and possible non-Newtonian effects are present. Many of the phenomena in cyclones (for instance end of vortex simulations), which may be crucial for the operation, can not be modelled with a steady-state simulation but requires a transient one. Therefore also when using CFD, practical testing is necessary for validation of the model. Regarding CFD of cyclone the state-of-the-art today is the work done in Delft by Derksen and coworkers [40–42] using Large Eddy Simulation (LES) for the turbulence modelling.

3.2 Experimental investigation of cyclone models

There has been done a lot of research during the years to find out more about the flow pattern in a hydrocyclone. Some of the challenges have already been explained earlier in this paper. Some of the newest and most interesting research is gathered underneath, among them some of the papers accepted for the Hydrocyclone '96 conference. The actual theoretical models derived in Hydrocyclone '96, will not be outlined in this thesis, only the results from the work.

Svarovsky once said "The easily designed hydrocyclone, with its structural and operational simplicity, hides the high complexity in the classification mechanism." In the development of hydrocyclone flow pattern, two types of models has according to Concha, Barrientos et al. [43] been outlined, empirical and phenomenological models. The empirical models are looking on the experimental observation, together with statistical

correlation of numerous data. This is done with different approaches, in some cases simple conceptual models are used to interpret the results, while in others the equipment are considered a black box. The best known empirical models are those of Lynch and Rao [44–46] , and of Plitt [47]. Referring to Medronho & Svarovsky [48], experience has shown that these models has serious limitations, the reason is that they have to be used only in a small neighborhood of the conditions for which their parameters have been determined. The empirical models can not be used for optimization of the design, because it does not understand the reason for the equipment behavior.

Phenomenological models are based on the physical phenomena which are the reason for the classification of particles. These studies started in the early 1950's, but describing the flow in the equipment has taken time, because of the demanding task of solving the set of non-linear differential equation. According to Concha, Barrientos et al. [43] two approaches have been used to tackle this problem. One is to simplify the field equations, by making suitable assumptions, and then proceed to solve the resultant equation that usually is still very complicated [36,49–58]. The second approach is to solve the complete set of differential equations numerically by CFD in a powerful computer [59, 60]. This procedure gives opportunity to instantly evaluate geometrical details.

3.2.1 Forces

A short introduction to the forces that have effects inside the hydrocyclone flow pattern are given by Stegowski & Nowak [13] and reviewed in this thesis. The forces are the reason for the flow splitting, and the high number of high density output from the underflow and lower density from the overflow. Regarding the solid phase, the centrifugal forces are moving the solid grains out to the walls of the hydrocyclone. The centrifugal force has counteracts in the drag forces, the volume of the drag forces depends on the size and shape of the particles and the turbulent intensity of the flows. Small particles

will not be influenced by the centrifugal force, because of repealing from drag force and turbulent diffusion [13]. These small particles will follow the flow of the water, so that the overflow to underflow ratio is the same as for water. Larger particles will be affected by the centrifugal force, and follows out to the wall and down the underflow. The selectivity and classification curves are the basic selection characteristic of the solid particles in a hydrocyclone referring to section 2.3.4, Frachon & Cilliers [61] and Kraipech, Chen et al. [62]. The selectivity and classification curves contribute to the major parameter for the hydrocyclone classification process description, the cut size.

The last decade has given solid-liquid mixture flow pattern in hydrocyclone a significant development. There are two reasons for this development, first, several new experimental methods for evaluation of the velocity distribution and the solid phase distribution. These are: Laser Doppler velocimetry [63–65], electrical tomography [66, 67] and ultrasound tomography [68]. The second reason for this great development is the use of CFD codes for flow pattern simulation [69–73].

3.2.2 Flow pattern

"A phenomenological model of a hydrocyclone", by Concha, Barrientos et al. [43] The flow pattern in a hydrocylone, with boundary layer flow around the walls and an exterior inviscid flow between the boundary layers and the air core, leads to a non conventional definition of classification. The work is based on the experimental observations of Hsieh & Rajamani [60] and the work of Bloor & Ingham [52]. The model simulates the performance of a conventional hydrocyclone with a wide range of designs and operating conditions. The model is validated with use of pilot and industrial data. The conclusion is given regarding the hydrocyclone divided into six zones, see Figure 3.2. Each of the zones is outlined by equations, from solving the boundary layer equation and the exterior flow in the equipment.

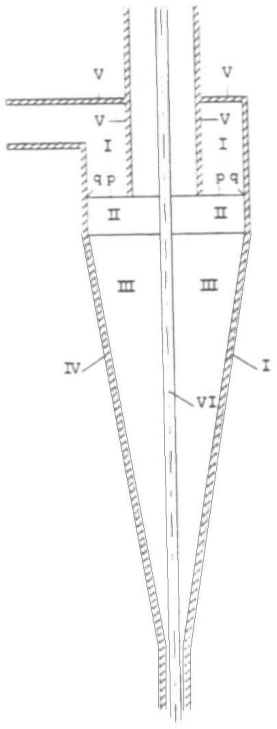

Figure 3.2: The six zones the hydrocyclone is divided into. Reference: [43]

According to Concha, Barrientos et al. [43], these give the local velocity distributions. Secondly, a momentum balance calculates the trajectories of the particles that enter the hydrocyclone. From the trajectories the classification values and the characteristic separation size may be obtained. Third, from the volume flow in the lateral boundary layers the short circuits to the underflow can be calculated, while from the volume flow in the boundary layer at the top of the equipment the leakage to the overflow can be estimated. Fourth, the selectivity values are than obtained from the short circuits and leakage and the classification values. Fifth, the capacity is calculated from a modified Plitt's empirical model. A last remark regarding the conclusion is to the validity of the model, a complete mass balance around a hydrocyclone is needed together with detailed information on the geometry of the equipment.

Further theoretical approach is derived by: "An analytical model for the prediction of solid-liquid hydrocyclone performance", by Vavro, Hodur & Dizianik [74].

The work is derived to relate separation performance and split ratio to various parameters:

- Geometric proportions and wall roughness.
- Presence of a gas core.
- Ratio of outlet precisions at overflow and underflow.
- Inclination of hydrocyclone axis to the vertical.
- Inlet velocity of the feed .

The predictions are compared with experimental results from a Rietema Hydrocyclone of 44 mm diameter, with suspended chalk in water, and additional results from other researches.

The conclusion from this paper is that the theoretical model appears to be applicable for preliminary estimates of hydrocylone of various shapes over a range of feed conditions. Further the model has highlighted some known uncertainties in knowledge e.g. wall friction coefficients and the influence of particles on them, and particle - particle interaction. Experimental results from Medronho [75] on the same ø-44 mm Rietema, suspended water - chalk hydrocyclone are compared moderately well with predictions given in the model. Additionally the model had difficulty to predict the effect of hydrocyclone angle and variation in overflow - underflow outlet pressure value, in spite ratio and separation performance.

Another interesting practical investigation of the flow pattern in a industrial hydrocyclone is done by Stegowski & Nowak [13]. They used a radiotracer experiment and

compeered the results with computational fluid dynamics (CFD). In their experiment they used nine solid phases of different grain size and water in an ø-500mm hydrocyclone.

The models are based on the analysis of experimental data given from Nageswararao, Wiseman et al. [76] and Frachon & Cilliers [61]. The FLUENT CFD software was used for the simulations. The mission of the industrial radiotracer experiment is injecting a radioactive tracer into the input of the system, and further analysing the gamma-radiation intensity distribution (system response) at the outputs. The advantage of using radioactive tracer is that the injection does not disturb the process, and the measurements are done outside the process.

The experiments were executed in the following manner, injecting labelled Cu-64 (Copper-64) isotope on different copper ore grain size, which emits gamma rays of 511 keV energy. The amount of one sample of copper ore traces was about 100 g and activity was about 2 GBq. Gamma-ray detectors, the scintillation probes, were placed at the inlet, underflow - and overflow outlet. The probes and experiment control were done by a computer. A full description of the radiotracer experiments and other parameters were published in Stegowski & Leclerc [77]. The point is the detection of the radiation, it is done by measuring the gamma-ray intensity which is proportional to the radiotracer activity. This depends on the measurement point geometry and gamma-ray absorption. Experiments have given the calibration coefficients for recalculation of intensity to radiotracer activity. This was done by injecting known activities of the radiotracer to the underflow measurement point and measured the gamma-ray intensity. The same was done for the inlet measurement point.

The equivalent radiotracer method for particle trace measurement is outlined in Bhusarapu, Al-Dahhan et al. [78]. There they traced one radioactive particle through a circulating fluidized bed (CFB).

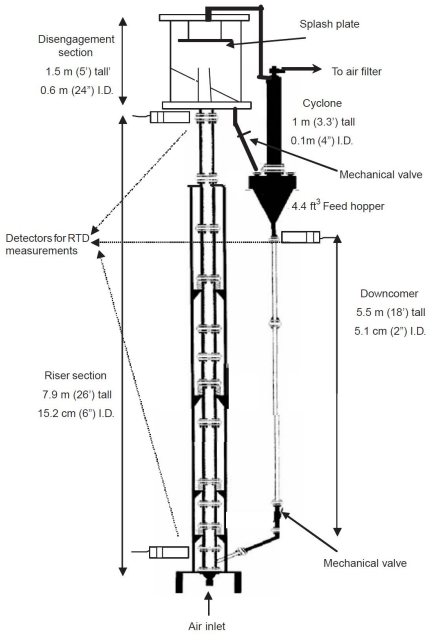

Figure 3.3: A schematic diagram of the CFB setup. Reference: [78]

An illustration of the setup Bhusarapu, Al-Dahhan et al. [78] used is shown in Figure 3.3, the principle is the same as used in Stegowski & Leclerc [77]. Three detectors are used, each detecting when the radioactive particle is passing. Bhusarapu, Al-Dahhan et al. used this for measuring the residence time, exact how long time the particle uses between the detectors.

Stegowski & Nowak's CFD experiments was executed with a k-ϵ turbulence flow and 220 thousand mesh grid for the hydrocyclone, this made it possible to simulate water-solid mixture flow for nine phases of solid particles.

The experimental results of solid particle tracks and the hydrocyclone selection process, are valuable for the assumed model and the computational validation of results.

As to the conclusion referring to the CFD work, the complex physical process is also theoretical complicated to describe, and therefore also complicated computationally. Al-

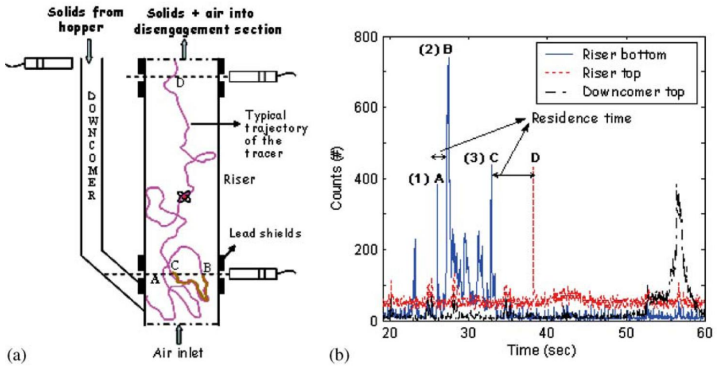

Figure 3.4: Figure (a) shows the believed flow to the particle inside the CFB. The peeks at Figure (b) show when the particle is crossing the detectors. That means that peek, 1 in (b) refers to the first crossing in A in Figure (a) and so one. The time between point C and D in Figure (a) can be exactly read out from Figure (b). Reference: [78]

most every model has theoretical or computational limitations, because some physical effects are difficult for mathematical modeling and then also for computational calculation. For mathematical modeling of the turbulent mixture flow, some experimental relations and parameters are used [77].

3.2.3 PET in process technology

The PET use in process technology is in the literature referred to as PEPT, positron emission particle tracking. The PEPT research in process technology until today has mostly been about tracking individual particles in low velocity systems. Process equipment like Fluidized Bed has been experimentally investigated [2,79,80]. Much pioneering work has been done at the University of Birmingham. There they have done more industrial research against other products as investigation of the flow in food cans, for better determining process time and further product quality [81, 82]. The use of PEPT for "in-container" flow following has proved highly effective and clearly demonstrates the

potential for exploring complex flow patterns within real situations. Additional experiments have been executed regarding equipment used for agglomeration [83] and mixer granulator [84].

3.3 Conclusion literature survey

There are as derived above many ways to estimate the flow inside a hydrocyclone. In all experiments and models mentioned above there are disadvantages and challenges that can not be numerical explained.

The use of computational fluid dynamics application is widely explained. Several numerical models have also been reviewed. The use of other experimental methods for instance radiotracer particles using gamma-gamma applications has been outlined. The principle used by Stegowski & Leclerc has many advantages, but regarding deciding the actual trajectory it is not accurate enough. The extensive and different work mention above has showed many good methods of designing hydrocyclones. But the need for better knowing what really happens inside a hydrocyclone and the definite trajectory of the particle is just increasingly showed. The literature survey has not retrieved any information that has the same accuracy as the position emission tomography scanner technique.

Chapter 4

PET related experimental apparatus and procedures

4.1 Radiation detection

One of the greatest draw-backs of high energy radiation is the human inability to detect it. But ionising radiation interacts with matter in a way that makes detection of radiation possible by utilizing specialized equipment. It exist many different types of equipment to measure radiation, e.g. Henri Becquerel used photographic film. The usual way for detection and measurement is to use some kind of substance or material that responds to radiation. Today many radiation detectors convert the deposited energy into a measurable electrical signal or charge. It is often the integral of this signal that is proportional to the total energy deposited in the detector by the radiation. The magnitude of the radiation will for several reasons of course vary, so will the detection equipment also. For instance in PET, with initial 511 keV photons, some will undergo one or several scatterings. The photons will deposit a portion of the energy each time, and then exit to the detector. With multiple Compton scattering it may be deposited almost the

entire energy of the photon before entering the detector. In this thesis different radiation detectors will be used, these are: proportional (gasfilled) chambers, film badge, and scintillation detectors.

4.1.1 Gas-Filled Detectors

The principle of the proportional chamber is working on the detection of the ionisation produced by radiation through a gas chamber. The ionisation electrons are accelerated by the high electric field inside the chamber. At the same time these highly energetic electrons collide with the gas atom, mostly used argon, and this result in secondary ionisation. The gas-filled detectors have both a positive and a negative electrode, anode and cathode respectively. The potential difference between them is maintained by a battery, and measured by a current meter as shown in Figure 4.1. The positive and negative ions are attracted to the opposite electrode. The positive ions are eventually gathered at the cathode after some energy deposition by the incident radiation. The movement of ions is an electric current, and can be detected by a sensitive current meter.

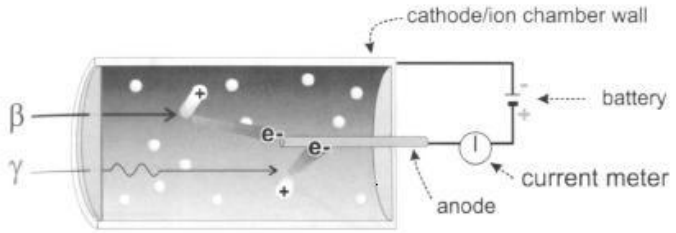

Figure 4.1: The presence of ionising radiation is detected by deflection of the current meter. Reference: [31]

Each type of gas-filled detectors depending on the nature and state of the gas used inside has its own favourable applications. The gas-filled detectors are usually used to measure strongly ionized charged particles such as the alpha and beta radiation.

This is because of the large distance between the molecules in the gas, and then strong ionization is favourable. But with a good design a gas-filled detector can also be used to measure photon radiation. The gas-filled detectors are typically proportional up to a given counting rate.

Applications

In the above explanation the current has been measured, some of the gas-filled detectors are instead counting the individual pulses produced as each individual charged particle or photon enters the gas. One of the types of these gas-filled detectors is Geiger-Mueller (G-M) counter.

Another application of gas-filled detectors is a dose calibrator, referred to as well-counter in this thesis. This is usually used to confirm the correct amount of activity in nuclear medicine department. The radioactivity is measured in amount of current, how is proportional to the primary ionization in the chamber. The dose calibrator is only able to measure the activity, in Becquerel or Curie, not the type of radiation or radiopharmaceutical. The accuracy of the measurements is affected by factors like the type of dose container, its proper placement in the chamber, and the calibration and regular recalibration of the instruments itself. The rules for using and calibrating the dose calibrator are very strict, this is because of the importance of giving the correct amount of activity to patient.

Sensitivity

The sensitivity of the ionisation chamber is determined by the meter used to measure the current and its sensitivity. For low- and moderate - energy photons (10 keV to 1 MeV) it has a sensitivity down to $<$ 1 mR (roentgen) in standard equipment [31].

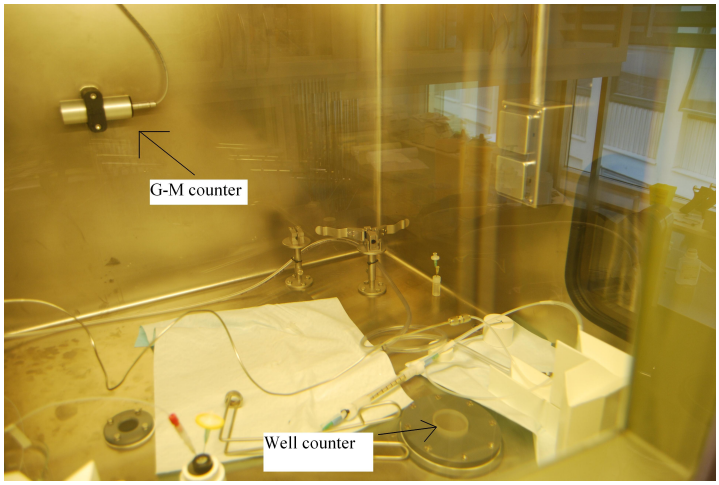

Figure 4.2: Inside the hot-cell, both a G-M counter on the wall and a well counter.

4.1.2 Film badge

Film badge detector is a plastic card witch contains a radiosensitive film. In the card there is strips like indicated in Figure 4.3, the strips have different densities (such as aluminium, cadmium, and lead).

The film is influenced by the type and energy of the radiation (alpha, beta, gamma or x-ray), and the density of the absorber. Some estimation of type and energy of the radiation can be read out by the amount of exposure of film behind each strip, compared with an uncovered area. Reading out the information from the film must be read out from an external laboratory.

4.1.3 Scintillation Detector

Scintillation detectors are used in positron emission tomography scanners. The scintillation detectors consist of crystal detectors and photo-detectors. The photo-detectors are called Photomultiplier Tubes (PMTs). The detectors consist of an inorganic crystal (scintillator), the most widely used crystals are made of sodium iodide (NaI) or the

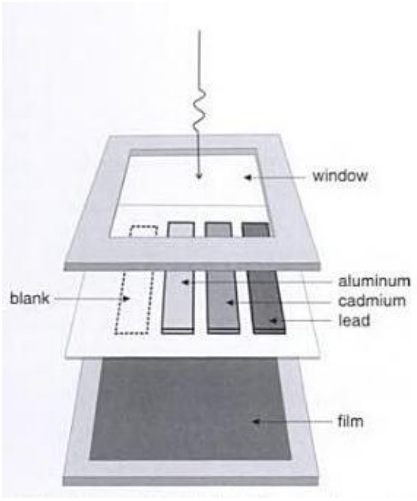

Figure 4.3: Film badge. The absorbers assist in estimating the type and energy of radiation exposure. Reference: [31]

newer bismuth germanate (BGO) and lutetium oxyorthosilicate (LSO). The faster LSO scintillator doped with cerium, has through the last years significantly improved clinical imaging in PET. The LSO has a much shorter decay time, that that again reduces system deadtime and improves count rate performance, especially at high activity levels. More important are the faster scintillators potential to decrease the coincidence timing window, and thereby reducing the random coincidence rate. Further improvements are better energy resolution, position accuracy that makes it possible to cut the crystal blocks into finer pieces that again gives better spatial resolution. The process of converting and finally measuring gamma radiation is very complex. A short summary of radiation conversion, is that the energy in the radiation is absorbed in the crystal, and leaves the electrons in an excited state. The radiation transfers the energy in one or more Compton or photoelectric interaction in the crystal. As the crystals return to their original state, some of the energy is released as light photons. In the scintillators the radiation is converted to visible (scintillation) light photons. The scintillation photons that are

emitted are detected and measured by the photo-detector. The energy deposited inside the crystal is generally proportional the number of scintillation photons (or intensity of light). "For each kiloelectronvolt (keV) of gamma ray energy absorbed by the crystal, approximately forty light photons are emitted" [31].

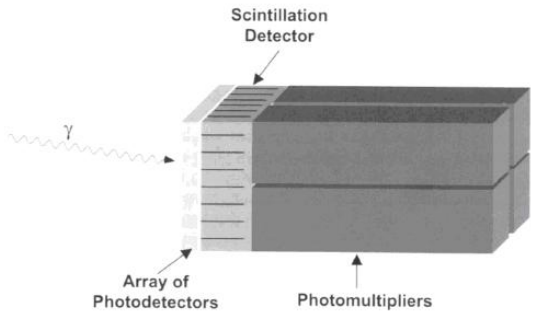

Figure 4.4: A single channel of one layer detector for DOI determination through the use of two photo-detectors at the crystal ends. Reference: [32]

In PET the scintialltion detector are commonly used because of the combination of high stopping efficiency and good energy resolution are most important. The detector materials high atomic number (Z), which again gives a high stopping efficiency for 511 keV photons, for instance I (Iodine) has Z = 53.

Photo-detector design in PET

An illustration of a photomultiplier tube is Figure 4.5 , the tube is placed adjacent to the crystal. The photomultiplier tube is a vacuum tube with a photocathode on the end. A photocathode is a clear photosensitive glass surface, which is coupled to the surface of the crystal. The coupling is done with a light-conductive transparent gel, this has the same refractive index as the crystal and the PMT window. When the light strikes the photocathode, it emits electrons, called photoelectrons. Four to six light photons strikes in average the photocathode before one photoelectron is produced. The number

of electrons produced inside the PMT is greatly enhanced because of the electrons striking the tube's dynodes. The dynodes are metal electrodes, which has a higher positive charge than the previous. That means that when the electron strikes the dynode, it knocks out more electrons. Generally two to four new electrons joins the progressively larger pulse of electrons after each dynode, and at last hits the anode in the end of the tube. This means that for each electron that enters the first dynode, and there are for instance three dynodes in total in the PMT, there will be between 2^3 and 4^3 electrons leaving the last. If the electron is cascading against ten dynodes, it will yield between 2^{10} and 4^{10} electrons.

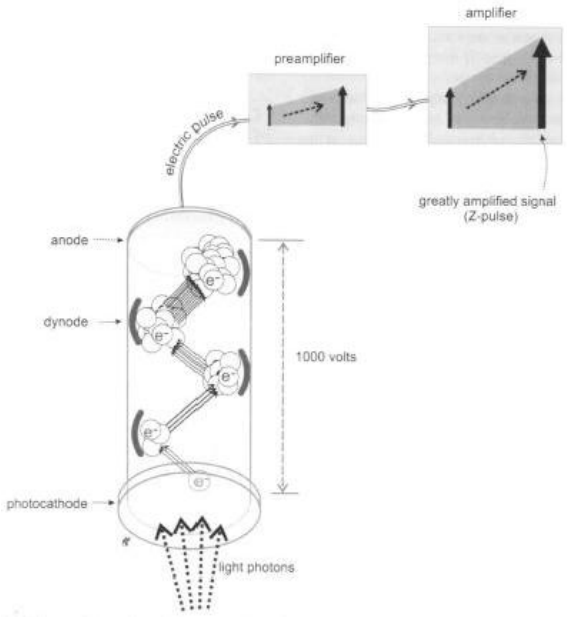

Figure 4.5: A photomultiplier tube and its preamplifier and amplifier. Reference: [31]

Preamplifiers and Amplifiers

Before processed and counted, the current produced by the PMT must be amplified. This amplification must take place despite the earlier multiplications of electrons in the PMT. Often this amplification is a two stage process. The first amplifier is positioned close to

the anode, and increases the number of charges. This increased current is transmitted through a cable to a main amplifier, here the current of electrical pulses can be increased in thousand-fold.

4.1.4 Detector structure

The PET scanner that is used in the experiments in this thesis is a Siemens Biograph 40 Truepoint PET-CT. This is equipped with hi-resolution LSO crystals, which is divided into 13 $\times$ 13 crystals in each detector, advanced from the earlier 8 $\times$ 8 crystals. This gives more crystal elements, $>$ 24,000, which again enhance spatial resolution from conventional 6.3 mm to 4.6 mm. The crystal size in reduced to 4.0 $\times$ 4.0 mm [85]. The scanner has three rings of detectors, each ring has 48 detectors, 144 detectors in total. Each detector is divided into four PMT. The physical properties of the scanner are 70 cm in diameter and depth of 15.6 cm FOV.

4.2 ALARA - Radiation protection

The essence in radiation protection is to reduce the exposure of radiation to a minimum. This is done for instance by monitoring the individuals contact with radiation, and taking corrective steps to reduce exposure. All work with ionising radiation is done following the ALARA-principle, which sets the system of recommended dose limitation, referring to ICRP - International Commission on Radiological Protection. To quote from United States 56 Federal Register No. 98: *"ALARA (acronym for "As Low As Reasonable Achievable") means making every reasonable effort to maintain exposures to radiation as far below the dose limits ... as is practical consistent with the purpose for which the licensed activity is undertaken."*

4.2.1 Risk

Radiation exposure has shown through history an increasing risk of certain cancer types, for instance after the bombing of Hiroshima. Radiation may increase the risk of cancer in, head, neck, pharyngeal, thyroid, breast, lung and also leukaemia. The risk and range of radiation for α , β and γ are shown in Table 4.1. The risk can be calculated for the individual if the exposure history is known. The absorbed dose can be multiplied with the *risk factor*. The risk factor referred in this thesis is the current risk factor used by the U.S. Nuclear Regulatory Commission. For cancer induction for the adult working population exposed to low dose [31], the dose rate radiation is 4 $\times 10^{-2}$ cases of cancer per sievert [Sv]. The rate for the general population, including the young, is somewhat higher at 5 $\times 10^{-2}$ cases of cancer per sievert [31].

To give an example, a radiation dose of 2.5 mSv / year, in 20 years. The lifetime dose will then be, 2.5 $\times 10^{-3}$ Sv /year $\times$ 20 years = 5 $\times 10^{-2}$ Sv. The chance of cancer is then 4 $\times 10^{-2}$ cases/Sv $\times$ 5$\times 10^{-2}$ Sv = 0.002. That means an individual increased risk of 0.2% for cancer. In comparison the natural incidence of fatal cancer is about 20% [31].

4.2.2 Dose limits

The dose limits is divided into several branches, firstly internal exposure and external exposure. This is as the name says, radioactive sources that have been taken into the body, and radiation from outside the body, respectively. For instance x-ray machine or particle radiation, are external. Further the dose limits are divided into occupational workers, pregnant and the general public.

The radiation dose is measured in Sievert (Sv), while the radiation itself is measured in Becquerel (Bq) or Curie (Ci). One more important aspect on the radiation is what

	Alpha (α)	Beta (β^+ or β^-	Gamma (γ) -/ X-ray
Energy of radiation	$\approx 4 - 8MeV$	$\approx 0.02 - 4.8MeV$	$\approx 10keV - 3MeV(\gamma - ray)$ $\approx 10eV - 120keV(X - ray)$
Range of radiation	$\approx mm - 8cm$ in air ≈ 0.04 mm in water/body	$\approx 0.015 - 6minair$ ≈ 0.013 - 8 mm in water/body	$\approx m - \infty invacuum$ $\approx$ cm - dm in water/body
Health risk	- Does not penetrate the skin - Stopped by a thin paper of clothing - Very dangerous if ingested/inhaled	- Usually stopped by clothing and glasses - Usually stopped by plastic (perspex) (low density) - Can harm skin and eyes	- Stopped by lead (high density) - Can harm internal tissue and organ

Table 4.1: Radiation hazards. Reproduced from course in radiation protection UoB 2010

kind of radiation it is. Alpha radiation leaves energy that can interfere biologically inside the body. Gamma radiation can pass straight through the body without leaving any energy. Since there is not left any energy, it is equivalent whit that one has not been exposed for any radiation dose, and therefore no increased health risk.

The Norwegian Radiation Protection Authority has set the dose limits for professional workers to 20 mSv a year in average (during a 5-year periode). For pregnant the radiation to the foetus shall not exceed the limit of 1 mSv for the rest of the pregnancy. For the general public the limit is 1 mSv a year [86]. Exposure from background whole body radiation, at sea level, is approximately 3.6 mSv/year, including 2.0 mSv/year from radon [31].

4.2.3 Internal exposure

Protection techniques are oriented mainly toward preventing the radioactive material from entering the body. The most common entrance is by inhalation, this risk can be reduced by good laboratory design. Ingestion can be avoided with good hygiene, such as wearing protection gloves and hospital coats when preparing doses or handling body fluids from a radioactive patient. It is also strongly recommended that hands be washed after removal of gloves. This is for reducing the risk for inadvertent ingestion of radioactivity, eating, drinking and smoking in radiation areas is strictly prohibited [31].

4.2.4 Limiting exposure

There are three methods of reducing external exposure from radiation: time, distance and shielding [31].

Time

Minimize the time spent in the vicinity of a source of radiation. Work efficiently, and plan your experiments with regards to exposure time.

Distance

Maintain as large a distance from the source as practical possible. The radiation dose decreases with the inverse square of the distance (r) from the source ($1/\mathrm{r}^2$). At a distance r, the entire dose is spread over a sphere with a surface area of $4\pi r^2$. At twice the distance, 2r, the dose is spread over a sphere with four times the area, $16\pi r^2$. This means that at twice the distance the radiation dose is decreased to one fourth. So when handling radioactive doses, tools such as tongs can effectively reduce exposure to hands and forearms.

Shielding

When time and distance alone are not sufficient in preventing radiation to reach the body, shielding is usually used. Shields will differ a great deal for witch kind of radiation one is working with. Shielding can be; lead aprons, syringe shields, vial shields, countertop shields (often with leaded glass), fixed and portable (on casters) lead barriers, but also thinner shield as plastic that may be used for beta-emitting and low-energy gamma-emitting sources.

4.2.5 Regulations

The Norwegian Radiation Protection Authority is the government specialist environment in radiation - and atomic safety. The Norwegian Radiation Protection Authority founded under The Ministry of Health and Care Services and has the overall responsibility for government policy on health and care services in Norway. The Norwegian Radiation

Protection Authority has the administration - and supervision responsibility for all use of radiation-sources in medicine, industry and research. It has further responsibility of monitoring natural and artificial radiation in environment and professional situations.

4.2.6 Hot-cell

The labelling of particles is done in a hot-cell, shown inside in Figure 4.2 and outside in Figure 5.8. This is a lead container with a door and two openings for the hands that is possible to open. Additional it is a large glass / leadglass window to look through. The box is constructed with 7.5 cm tick lead walls, door and opening lid for hands, the window is leadglass witch is equivalent to 7.5 cm lead. The door is used if larger equipment is put into the hot-cell, otherwise only the openings for the hands are in use. Inside the hot-cell there is a Geiger-Mueller detector on the wall, which works as a rate counter. This will give a warning when the activity is inside the hot-cell and estimate the amount of activity. The exact amount of radioactivity is measured when the sample of radioactive liquid is lowered down into a dose calibrator called a well counter. The openings for the hands are for safety reasons closed as much as possible. The well counter in the hot-cell is calibrated every day. This is done by a using a Caesium-137 (Cs-137) source that has a half-life of 30 years.

4.2.7 Cyclotron

The core of the positron emission tomography scan is the radioactive tracer. The tracers used in human scans have a short half-life, so they will decay relatively fast. The same tracers as often is used in many human scan, fluoride - 18 (^{18}F), is used in these experiments. The tracers with the short half-life has to be made almost at the same perimeter as the PET-scanner. There are three basic types of equipment for making medical radio nuclides: generators, nuclear reactors and the one use in the present work, cyclotrons.

Cyclotron is a device invented by E. O. Lawrence and M. S. Livingston in the 1930's that is used to accelerate charged particles by means of a magnetic field. Cyclotron is a circular accelerator where charged particles such as protons and alpha particles are accelerated to high velocities. This is done in a spiral path within a vacuum, and by a power supply that provides rapidly alternating voltage across the "dees", see Figure 4.6. The "dees" are the two D shaped dipole magnets placed back-to-back with the straight side. They are parallel but slightly separated. This alternating voltage is defined by the radio frequency (RF) - field. This produces a rapidly alternating electric field that passes vertically through the dees and accelerates the particle. The particles are injected near the centre of the magnetic field, the acceleration occur only when they passes through the gap between the dees. The magnetic field combined with the increasing energy of the particles forces the particles to travel in a spiral path. At a certain radius in the field, the particle has a certain amount of energy. When the particle has reached the sufficient velocity it will be deflected and hits a target. The target contains a chamber of stabile atomic nuclei. Some of the particles and kinetic energy hitting the target are incorporated into the nuclei of the atom, and creates excited unstable nuclei. In PET positron emitters are needed, for instance Fluoride-18 (^{18}F), this is produced by bombardment with 16 MeV protons on (^{18}O) oxygen bound in water. A nuclear reaction will then occur and the proton enters the nucleus, a new element with a higher atomic number is produced. At the same time a neutron is discharged.

4.2.8 Positron emitting radionuclides

The radionuclides ^{11}C, ^{13}N, ^{15}O and ^{18}F are widely used in PET studies and as positron emitting radiopharmaceuticals. The advantage of using radionuclides as ^{11}C, ^{13}N, ^{15}O in a molecule, is that they don't change the pharmacological properties of the radioactive

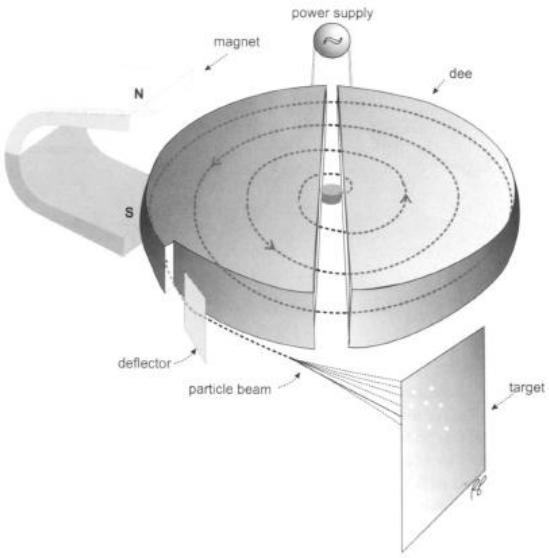

Figure 4.6: Cyclotron, image from ref. [31]

ligand compared with the stable compound. The disadvantage of these three radionuclides is their short half-life, which complicates the ability of chemical synthesis and makes prolonged scanning studies impossible. The bromine isotopes ^{75}Br and ^{76}Br also seen in Table 4.2 have a rather unfavourable decay characteristic, and are rarely used for clinical application nowadays [87]. The reason the ^{18}F was chosen for our experiments, is its relatively long half-life. Additionally advantage is the ability to produce ^{18}F in high yields and with high specific activity. The ^{18}F does not emit any γ-rays other than the 511 keV annihilation photons, thus giving a high accuracy of detected locations.

4.2.9 Fluoride-18 (^{18}F)

As discussed above, the cyclotron produces the radionuclide ^{18}F. 96.9% of the ^{18}F decay emission is positrons (β^+) and neutrino (ν) [34]. The reason for the emission is the transformation in the nucleus of a proton into a neutron. The nuclide which is formed is

isotope	$t_{1/2}$	E_{max} (MeV)	β^+(%)
^{11}C	20.3	0.96	100
^{13}N	10.0	1.19	100
^{15}O	2.0	1.72	100
^{18}F	109.7	0.63	97
^{75}Br	95.5	1.74	76
^{76}Br	16.1	3.98	57

Table 4.2: Positron emitting isotopes for PET. Reproduced from [34]

oxygen-18. The remaining 3.1% of ^{18}F decays by electron capture.

$$^{18}F \rightarrow ^{18} O + \beta^+ + \nu \tag{4.1}$$

The Fluoride-18 has very favourable properties for high-resolution PET imaging [88], the maximum energy from the positron decay is 0.633 MeV, with a mean range of 0.6 mm, ref. Table 2.1 .

Chapter 5

Design and commisioning of the experimental rig

A significant part of this thesis has been to choose the right particles for the experiments. The most critical was to get sufficiently high amount of activity on the particle surface used in the experiments. It was also important for the fluid dynamic that the particle is as near-identical the bulk studied as possible, and additional does not react chemically with the other fluid. One of the major concern before starting with experiments were leakage of activity from the particle surface to the surrounding liquid. Finding a good labeling technique was important for the success of the experiments.

5.1 Labeling of particles

Two particle labeling alternatives were found which are outlined in Fan, Parker & Smith [89], direct activation and ion-exchange technique. Direct activation process, is direct bombardment of the particles placed in an aluminium-back plate with drilled holes according to particle size. The front is sealed with aluminium foil, and the back cooled by means of water. The bombardment is done using a 33 MeV ^{3}He beam. Then a few

of the oxygen atoms in the particle are converted into ^{18}F radioisotope. Practically this technique can be applied for particles in the size range of 1 to 10 mm, the material of the particle must also be able to resist high temperature. The other labeling technique found were the ion-exchange technique, which can label resin particles in the size range of 60 to 1000 μm. The parameters for controlling the radioactivity labeling process is resin material, anion's present in the radioactive water and processing time.

In Parker & Fan [90] it has been executed experiments for positron emission particle tracing (PEPT) following up to three particles. A requirement for tracking several particles are significant different in individual activity. Several challenges are in relation with detecting and reading out the precise particle. So overall it is only recommended to use several particles when tracing one single particle can not give sufficient information.

In the experiments presented in this present work the ion-exchange technique has been used. When ^{18}F is available as a positron emitter as it is on Haukeland University Hospital a strong-base anion exchange resin was used. The Amberlyst A26 hydroxide form from the "Rohm and Haas/Ion Exchange Resins" was found to have the needed property's. The product data sheet is attached in Appendix B. According to Parker & Fan [90], it is also possible, but not recommended to use a weak-base anion exchange resin, this is strongly controlled by pH. Parker & Fan has the ^{18}F produced from purified water, under a direct bombardment of a 16 MeV Proton beam from a cyclotron. The specific activity to the water is about 10 GBq ^{18}F after 15-min bombardment. The resin beads are then added into the radioactive water and shaken for some time. The activity of a resin bead particle can according to Fan, Parker & Smith [89], be as high as 1000 μCi with a size of 250 μm particle, by using the ion-exchange technique under optimum conditions.

The radioactivity in a single bead is dependent on the ^{18}F concentration and the contact time. Fan, Parker & Smith [89] did labeling experiments there they derived that when the contact time exceeded 20 min, the decay rate was greater than ^{18}F exchange rate, and the radioactivity starts to decrease. In [89] they also discovered that to get a smooth tracking, the radioactivity in a tracer should surpass 300 μCi.

Then the labelling process starts used in this present work is the same as Fan, Parker & Smith [89] used. The radioactive liquid is filled into a vial, and the particle is put into it. The vial is stirred for some time, and then washed several times with water. This is done by taking out as much radioactive liquid as possible from the vial by using a syringe. Then injecting water and stirring it again, taking out the water and repeat the procedure. The radioactivity that is left is stuck in or on the surface of the particle.

The Amberlyst A26 Hydroxide Form used had sizes from 400 to 700 μm. The mixture is shaken for about 10 min for radioactivity uptake. By this procedure the activities of the resin beads reached 450-1440 μCi depending on the amount of initial radioactivity in the liquid. During the labeling no considerably leakage to the water was detected.

5.2 Abstract design

The strong vortex flow and the flow pattern inside the hydrocyclone has been studied by many researchers and occupational workers earlier. Regarding the design and the use of hydrocyclones, four consideration has been made by Svarovsky in a "Handbook of powder technology" [15].

- Most important, for separation of solid particles by use of centrifugal forces, there has to be a finite density difference between the solid and the liquid.
- The flow must be steady, free of any disturbances or fluctuations.

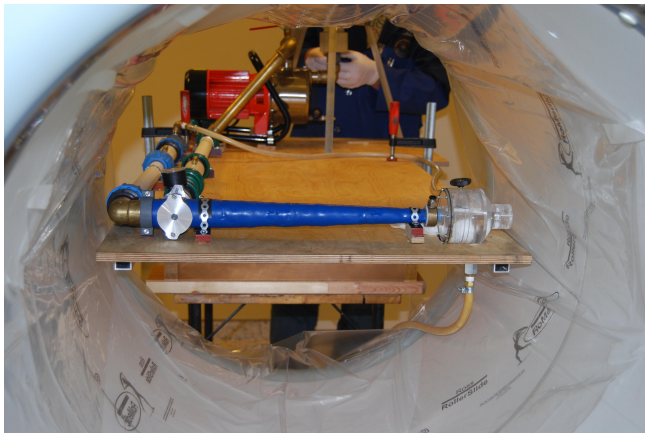

Figure 5.1: Hydrocyclone inside PET scanner.

- The vortex has a depression in the center and any dispersed and dissolved gas in the feed tends to migrate to the center and form a gas core. This is quite a desirable phenomenon as long as the gas core is straight. It will be distorted by sharp bends immediately above the vortex finder and this has to be avoided.

- There is a very steep velocity profile in the flow, thus leading to high shearing forces which tend to break loose any flocks, agglomerates or droplets in the flow. Therefore any flocculants to improve the separation performance of the hydrocyclones is a waste. In fact, in classification duties, this is a positive advantage because the classification is then according to the size of the individual particles and not the agglomerates.

Another important element is that the discharge of the separated particles into the underflow orifice is due to the flow itself. The flow pushes the particles layer at the wall down into the apex. Gravity does not significantly affect the separation, the exception is in very large cyclones which also tends to be used for separation of large particles. From this it is know that hydrocyclones do not necessarily have to be operated in a vertical

position, it can be inclined or even inverted if necessary [15].

The hydrocyclones can be made in many different materials depending on its applications. The most common are steel (rubber or ceramic-lined if necessary), ceramics, polyurethane and other plastics. Further design features is that it will be a slight advantage in making the inlet rectangular, with the longest side parallel to the cylindrical wall. Instead of a simple circular hole. There are published allot of work about the dimensions on the hydrocyclone versus the effect of separation and pressure drop. Referring to Svarovsky [15], there is a rule according to which every measure which increases resistance to flow improves separation efficiency and vice versa. This applies to all the proportions of the cyclone body, within certain reasonable limits, except for the length of the cyclone. It has been done many studies of the behaviour of optimum cyclones and further recommended designs published.

There is only one dimension of the hydrocyclone that has be possible to change, the underflow. The reason for this is that with the known technology it can not be predicted accurate enough, and adjusting the size of the opening of the underflow during operation is necessary. For optimal operation the best way is to adjust the opening after the start-up, or after changes in operation conditions. For the adjustment of the opening there is made several application. For instance, replaceable nozzles, mechanically adjustable orifices, pneumatically operated adjustable orifices or even self-adjusting devices, which maintain a constant underflow density or concentration. In designing a good hydrocyclone there is many aspects to consider, but the two most important are the operating pressure drop and the feed concentration. The resistance and pressure drop over the cyclone influence the efficiency of separation. Higher pressure drop gives higher efficiency of separation, but the law of diminishing returns applies here. An increase in pressure drop over 5 to 6 bars has little effect, the usual operating pressure is between 1 and 2 bar [15]. Another important point regarding separation with hydrocyclones is the feed

concentration, by increasing this it results in a rapid reduction in separation efficiency. That means that when high total mass recovery is wanted, hydrocyclones are operated with dilute feeds. When changing size and scaling up hydrocyclones, the only dependent is the cut size, because of geometrically similar relation inside a cyclone family, referring to grade efficiency curve.

5.3 Criteria

The rig was designed in regard to the following criteria given from Aker Kværner Process Systems, table 5.1.

Parameter	Unit	
Required Separation Performance	μm	20
Max Particle Size	mm	20
Smallest Opening	mm	4
Max Sand Concentration	Vol%	6
Max Pressure Drop	Bar	10
Min Pressure Drop	Bar	$7^{(1)}$

(1) Recommended, given by design pressure of line (10 bar).

Table 5.1: Design criteria for hydrocyclone.

5.4 Design process

The design of the equipment started in January 2009, with designing of the UoB-rig. Through the whole spring semester different applications and possibilities about the

setup was discussed. The critical parameters were the feeding of particles into the liquid stream, position of the flow measurement, and use of online measurement of the particles. In the beginning of August 2009 a decision on a specific plan on the whole setup for the UoB-rig was made, Figure 5.2. Then a much simpler setup for the PET rig project was designed, Figure 5.3.

The reason for the simpler configuration than the original UoB-rig, is because in this thesis it will be the trajectory of the particle through the hydrocyclone that is of interest. As far as the investigation of theory has revealed, there has never been done similar experiments in liquid-solid high velocity hydrocyclone. Because of this it is important to minimize the risk of failure, leakage and downtime, this is done with a simple setup. A leakage inside the PET scanner may have critical outcome.

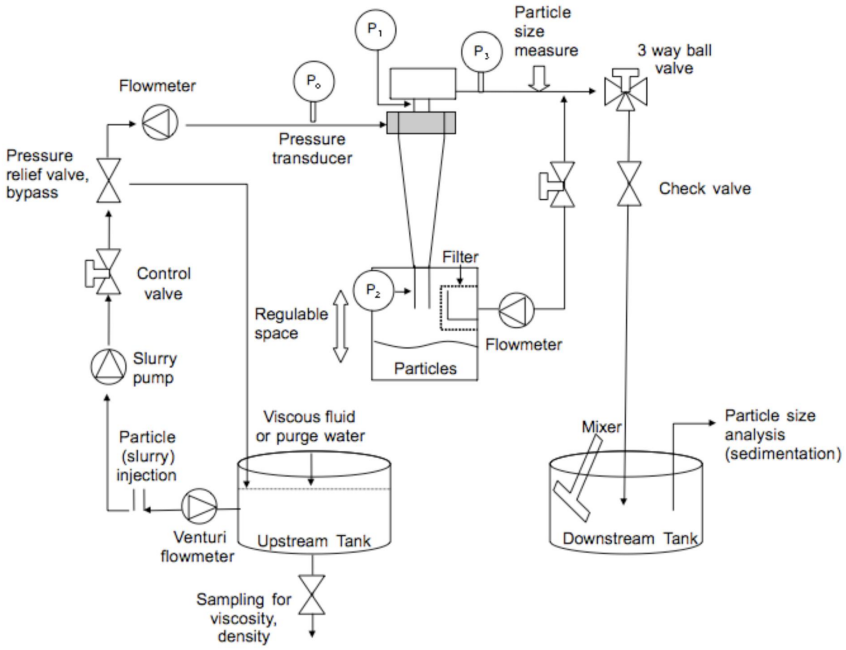

Figure 5.2: A schematic presentation of the UoB-rig.

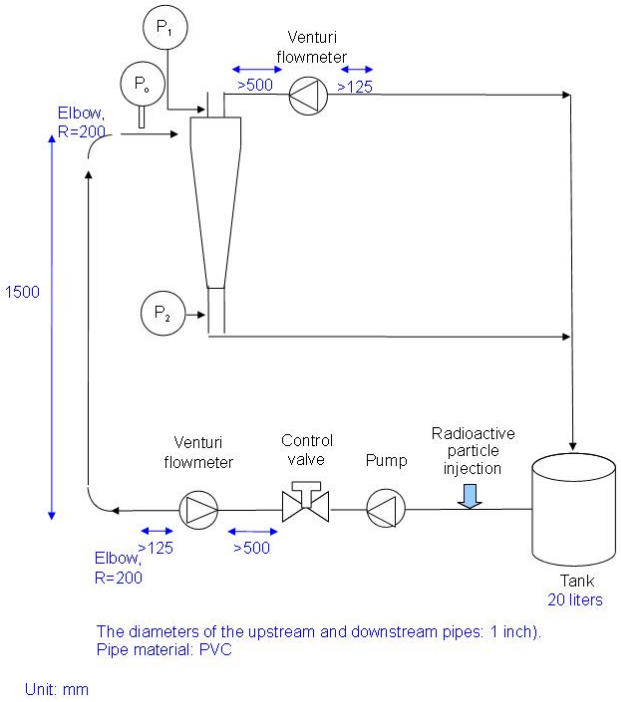

Figure 5.3: A schematic presentation of the PET rig.

5.4.1 Specification

Referring to the PET rig in Figure 5.3.

Tank: The size was decided from a view of continuous operation, also with respect to the "back-flow" after the hydrocyclone. The volume of the piping in the rig is about two liters, see estimate in Appendix C. Because of the moving of parts and challenges with moving large equipment, supplement to the risk of volume if leaking, a tank on 20 l were used.

Pump: The pump dimension was given from the needed pressure. The needed pressure was found to be 3 bar. A Cotech pump from Clas Ohlson satisfied the specifications it had ability to create 4.6 bar and a capacity of 65 l/min, or 3.9 m3/h. The inlet and outlet was 1".

Figure 5.4: A picture of the PET rig.

Pipe: The pipe was the same size as the pump inlet and outlet 1", the material is PWC.

Particle injection: There are two different ways of injecting particles, directly into the fluid tank, or injected into the pipe on the low pressure side of the pump. The last method was used during the experiments. The advantage of the pipe injection method is that the radioactive particle will go straight into the pump after injection, and further on into the hydrocyclone.

Venturi: On the rig it has been designed two venturi flow meters to measure the flow. In front of the venturi a straight section on 500 mm is needed to achieve laminar flow, after the venturi a straight section of 125 mm, to avoid getting any influence into the venturi. The venturi flow meter is a commonly used application in process equipment. It is a simple design, a constricted section of a pipe, with pressure tapping before and in the narrow area. The principle is that a lower speed in the narrow venturi section gives a higher velocity. This can be derived by the Bernoulli equation combined with the equation of continuity. Only taking incompressible fluids into consideration, the theoretical pressure drop $(p_1 - p_2)$ will be: $(\rho/2)((v_2)^2 - (v_1)^2)$.

$$(\rho_1 - \rho_2) = \frac{\rho}{2} * ((v_2)^2 - (v_1)^2) \tag{5.1}$$

Subscript 1, indicate the wide area with low fluid velocity, subscript 2, describe the narrow area with high velocity, ρ is the density of the fluid, see Figure 5.5. The volumetric flow rate (Q) can be calculated since:

$$Q = v_1 * A_1 = v_2 * A_2 \tag{5.2}$$

Equation 5.1 and 5.2 gives:

$$Q = A_1 * \sqrt{\frac{2(p_1 - p_2)}{\rho * ((\frac{A_1}{A_2})^2 - 1)}} = A_2 * \sqrt{\frac{2(p_1 - p_2)}{\rho * (1 - (\frac{A_2}{A_1})^2)}} \tag{5.3}$$

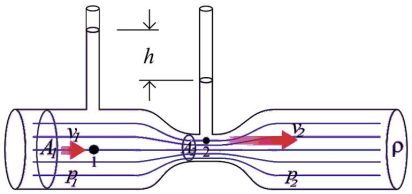

Figure 5.5: Venturi principle.

Hydrocyclone: General information about hydrocyclone is outlined in section 1.2.1. The main dimensions is similar to the UoB-rig, for later comparison. The design is done with respect to the Stairmand HE design. The Stairmand cyclone with a particular geometric shape is considered as the most optimized design, where the velocity profile is well maintained similar all over the axial stations and the collection efficiency is very high [91]. The hydrocyclone is made of glas-fiber material, with the following size characteristic in Figure 5.6 and Table 5.2.

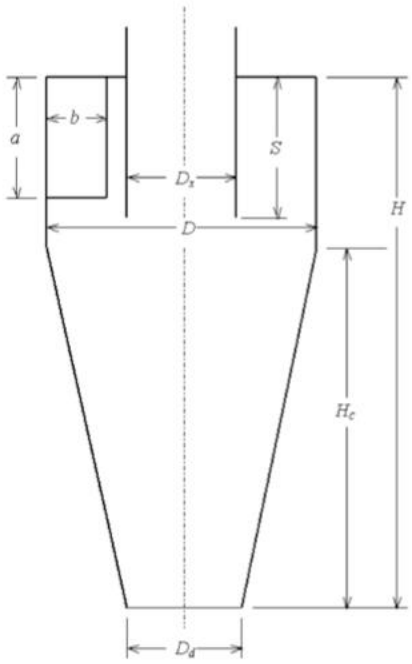

Figure 5.6: Measurements of hydrocyclone

General: The general design of the setup has some limitations because of the size of PET-scanner itself. Therefore the dimension of the vortex-finder tube and the solid-finder-box and the straight section between the box and the hydrocyclone, had to set in relation to PET scanner physical diameter. According to Svarovsky [15] a straight section after the vortex finder is needed.

Symbols	D	D_X	S	H	H-H_c	H_c	a	b	D_d
Cyclone [mm]	40	20	30	414	60	354	29	9	10

Table 5.2: Size of the hydrocyclone

The size of the PET scanner is also the reason for the horizontal operation condition. Because the "table" shown in Figure 1.1 is need inside the PET scanner during operation. The equipment and then the height will be insufficiently low if operated vertically. Physically it will not make any differ for the hydrocyclone if it is operated horizontally. Referring to Svarovsky [15], this is because of the magnitude of the centrifugal forces.

5.4.2 Experimental

The experiments is done by using the above derived equipment, all experiments and tests are done according to the strictest safety regulations. The following procedure is used for labelling of particles, first the radioactive liquid is produced in the cyclotron. This liquid is transported from the cyclotron by tubes to the hot-cell. The hot-cell as shown in Figure 5.8 is the working place for radioactivity, it is here all the work with the radioactive tracers is done. The surroundings are shielded from the radioactive source. When the laboratory personnel are working with their hands inside, they are equipped with finger dosimeter to measure finger radiation. Tongs for increasing the distance from the radioactive source is used if possible. Figure 5.1 show the inside of the hot-cell. The well counter is used for measuring the exact activity of the liquid when it arrives from the cyclotron. After the particle labeling the vial and the particle are once again put into the well counter, assuming that the activity measured is only from the particle. After the radioactive particle has gone through the labeling process, it is taken out from the

hot-cell, in a lead-box. Additional, all personnel in contact with the particle or with ability to be exposed to radiation wears a film badge. Additionally everyone in contact with the particle wears gloves, coat and glasses. The particle is brought to the PET scanner where the PET rig is set. The radioactive particle is then injected into the PET rig by a needle and the testing of the hydrocyclone can start.

5.4.3 Execution of experiments

As shown in Figure 5.3 and Figure 5.4 the setup of the PET rig is a circulating system. It works by filling the tank with sufficient amount of water, and starting the pump. The flow will be regulated by the valve after the pump, inside the hydrocyclone the flow will split depending on the opening of the underflow valve. The underflow is shown in Figure 5.2, where the transparent hose is connected back to the overflow from the vortex finder. The valve on Figure 5.7 is the one used to regulate the underflow. The other hole seen in the bottom of the particle box in Figure 5.7, is used to drain the system for radioactive particles between each experiment.

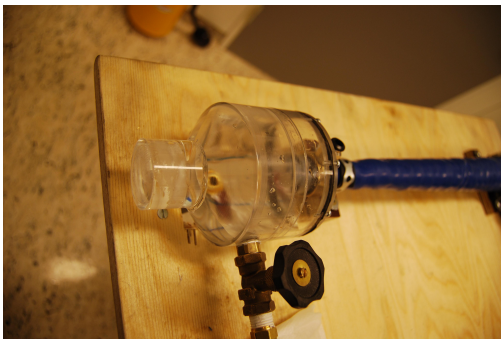

Figure 5.7: Image of the particle box, the blue is the lower end of the hydrocyclone, and valve for controlling underflow. Bottom hole is for draining of particle box.

All the preparation to the experiments are done in a laboratory dedicated for the University of Bergen, at the same floor as the PET-centre. Before moving the rig to the

PET-scanner facility, the system is filled with water, pressurized and checked for leakages. Then it was moved with a table on wheels to the PET-scanner. The hydrocyclone setup stands on the table and is not in contact with the PET-scanner during the experiments. In the UoB lab each radioactive particle is taken from a vial and into a syringe. Then the syringes are transported in lead boxes to the PET-scanner. In all experiments the particles are injected into the hydrocyclone system after the water tank and before the pump, referring to Figure 5.9. Then there is more control over the particle and knowledge about when it enters the pump. In all experiments the particle has followed the underflow out and stayed in the particle box. The particle is not always easy so the see, so the position of the particle after each experiment was finished, was measured with a portable G-M counter. Then the table had to be taken out from the scanner and the particle box drained until the particle was out. This is because that the algorithm used in the present work only considers one radioactive source inside the field of view at the time. Then the table was rolled back into the scanner and a new particle can be injected.

Figure 5.8: The front of the hot cell. With lead window and circular holes for the hands.

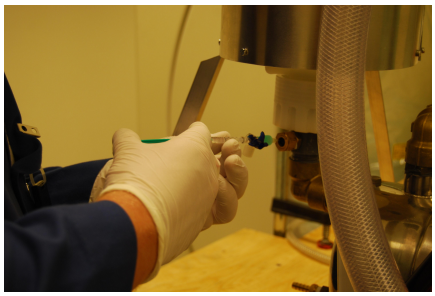

Figure 5.9: Injection of a particle.

Chapter 6

Results

The results section is divided in two parts. The first section contain the work that is done to make it possible to do experiments with the PET scanner. The second section is the final results with the output from the PET scanner. The first part include:

- Design of the rig used for the experiments.
- Following up the manufacturing process.
- Choosing the right particles for the experiments, regarding size, weight and with the ability to absorb sufficient amount of radioactivity.
- Find out how the list-mode-files (LMF) from PET was organized and extracted.

Experiments with different amount of radioactivity has been carried out.

Simultaneously as experiments were done with the particles, an investigation on how the the data from PET could be read out was started. At first it was tried to figure out the structure of the output, by using the method described by Hoffmann, Dechsiri et al. [2]. Then there was done several experiments for trying to figure out and deciding the structure. Several lines of investigation was pursued to decipher the information in the

binary output from the camera. One experiment was to shield a radioactive point source in all directions with blocks of lead, except two sides. This was done to try to recognize patterns in the binary output specific for the few sensors receiving signals with this setup. It was not recognize any such patterns, and it was later found out that the 32-bit output that was studied at that time, was a condensed summary of the information from several decay events. This was therefore not suitable for the event-by-event analysis that was required in this present work.

After some time contact was established with the LMF developers in the SIEMENS organisation. After a lot of communication and many experiments it was a breakthrough, a software modification had to be done before starting the scan. Additionally enough information was gathered to comprehend the way to read out the files as 64 bits binary words and understand the structure of them.

There has been done experiments two times when the scanner ran with the right approach and software. The first experiment was conducted 6. May 2010. The experiment was to figure out if the way of performing, reading and understanding the output was correct. The experiments were executed in the following manner; using single radioactive particles positioned at fixed points in the scanner's field of view (FOV). The particle was positioned at different specific places that was measured, to compare with the data output.

A FORTRAN program were made that redefined binary form to positions in a coordinate system. When this was successful, a second experiment using the hydrocyclone rig were done the 26. May 2010.

Everything worked as planned, six experiments were conducted, two with the underflow closed, and four with the underflow open. It was very important that it was only one particle inside the FOV at the time. The reason is because the averaging calculation in the FORTRAN program only takes one particle into consideration at the time. If there

was two particles inside the FOV the averaging would take a position between them.

6.1 Investigation of results

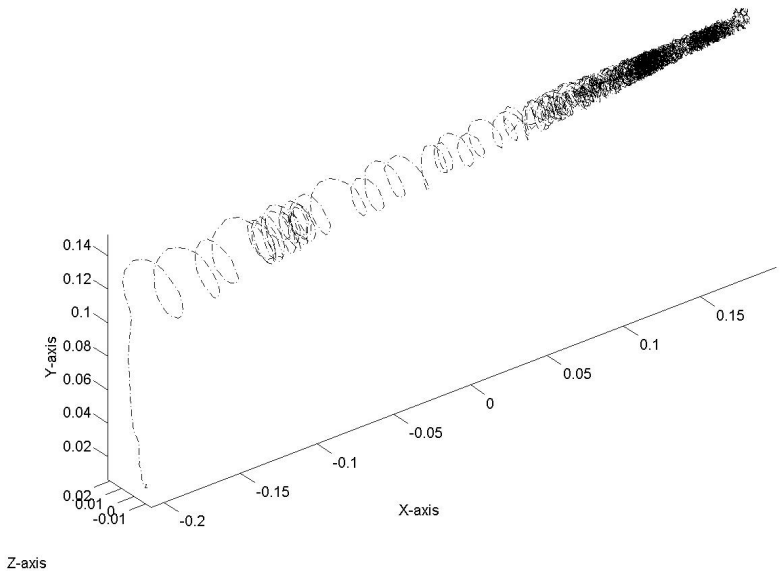

Figure 6.1: The trajectory of a particle through a hydrocyclone with open underflow.

Figure 6.1 is a plot of the actual trajectory of a particle as it moves from left to right through the hydrocyclone. This trajectory of a particle in a liquid hydrocyclone has never been presented before. An interesting observation that can be made directly from these experimental data, is that in some points down the hydrocyclone, the downward flow of the particle turns and follow the core of the cyclone upwards flow. Then the particle follows this upward flow before it turns at one point again and starts going downwards. Figure 6.1 shows a 3D plot of the particle trajectory from the inlet and until the particle is out of the hydrocyclone. By explaining Figure 6.1 in more detail, the first part of the hydrocyclone has a fine downwards trajectory. It is not that easy to see in a "still

picture" 3D plot, but at some distance down the hydrocyclone it looks like the particle tracks accumulate, this is not the case. What happen is that the particle goes in a fine downwards path past the first point where the tracks appear to accumulate, then it turns, goes upwards for some distance and turns again, following the primary downwards flow. This repeats itself at several occasions during the trajectory of the particle from inlet to outlet. In the lower part of the hydrocyclone the phenomena occures many times.

Some points of interest in the experimental results are:

- How accurate is the measurements?
- Is this trajectory specific or random?
  - Is it at some specific positions that the particle turns?
  - Is it some correlation regarding the tangential velocity and the turning position?
- How long is the residence time of the particle?

6.2 Details from PET experiments

When executed the experiments in the PET scanner, another software than usually used for standard medical PET had to be used. This is because the ordinary output from the scanner is 3D-pictures of radioactive pulses in patients, requiring image reconstruction algorithms and support from the CT part of the scanner. The output from the PET scanner as is needed in the present work is list-mode-files in 64 bits binary word format. The content of this 64-bits list-mode output is the position of the lines of response (LOR) in event words, divided by additional timing words every millisecond [ms]. The LOR's can be seen in Figure 6.2, here it is possible to see the lines of response crossing mostly in the center where the particle is. Each LOR reflects to one annihilation. Some points

will not be correct, as described in section 2.10. The number of event words between every timing word varies from tens to tens of thousands. All event words between each timing word are used to narrow in to one average position per millisecond.

The general reading of the results is done by taking all of the LOR's in event words, and finding the cutpoints between the lines. The cutpoint is the interesting part, since that gives the position. First all the cutpoints are found, then the average from all the cutpoints are calculated. Then one point is set. As seen in Figure 6.2, there will always be some deviation around the particle. After the first averaging of the total area of results, the area of the average is narrowed in and a new average point is calculated. This is done ten times, average and narrowing, so the average position is getting closer and closer to the actual position. The last average is made out of up to 30 000 positions inside a very narrow area. The accuracy of the measurements is very good. In the results in the present work, positions with timing words with smaller amount of remaining cutpoints, after the elimination then 300 are not taken into consideration.

The 64 bits event word which gives one LOR has a certain structure. It was very time consuming work to figure out the structure. The structure of the word itself will for reasons of confidentiality not be revealed here.

6.3 Calculation of results

In the investigation of the experimental results in this thesis, only the experiments with the underflow open has been taken into consideration. There are several reasons for this, it is the most realistic regarding that a hydrocyclone in operation is always ran with the underflow open, otherwise it will not split the flow. Another reason was that most of the experiments were done with open underflow, and then it was a better foundation for comparing.

After running the Fortran code the particles specific positions inside a coordinate

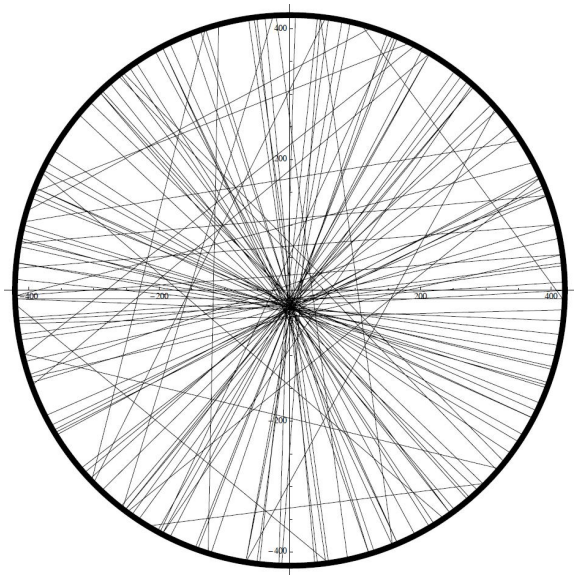

Figure 6.2: Lines of response.

system was determined. Excel was used to process the data further. The output from the Fortran code was pretty straight forward, each position is determined in x, y and z coordinate at one specific time. A table of the output for some positions can be seen in Appendix D. The x, y and z positions are in unit meter [m], and the time is in millisecond [ms]. Figure 6.3 gives a quick introduction of the data output. The particle inlet is where the line starts on the left hand side of Figure 6.3, while the hydrocyclone is narrower down the conical section, when the particle goes wider out to the side, it is inside of the particle box.

All calculations of the results are done in the following coordinate system, x - the axial position down the hydrocyclone, y- the "height" and z - "inwards", see Figure 6.1. A 3D plot as seen in Figure 6.1, gives good visual and understandable plots, but it was found easier to state specific positions in 2D. In the following it will mostly be used x-y plot, as see in Figure 6.3 and some z-y plot, see Figure 6.4.

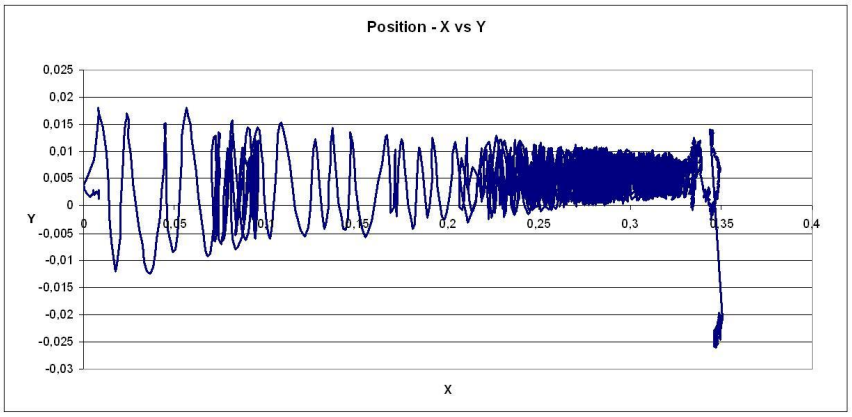

Figure 6.3: A x-y plot of the trajectory of the particle in a experiment.

6.4 Standard deviation

The first experiments the 6. May were done with a none moving particle, the results from these experiments were used to calculate the standard deviation to the final millisecond measurements. Figure 6.5 and Figure 6.6 represent the position of one stationary particle the first 100 ms, in the x-y direction and z-y direction respectively. Visually it can be seen that the standard deviation is larger in z direction than in x.

For giving an estimation of the accuracy the standard deviation is calculated in x, y and z direction in Table 6.1. The changes in standard deviation with respect to time are also calculated there.

The actual position of the different particles inside the PET scanner during measurements can be seen in the x-y direction in Figure 6.7 and z-x direction in Figure 6.8. V4 is in the center depth of the FOV, while the others are more on the edge, especially V1. An accuracy of about 0.24 mm in x direction, 0.32 in y and 0.3 in z direction in the middle of the scanner is regarded as very good. The reason for this higher standard deviation in z than x direction is because that in z direction there are not continues detectors, such as there are in x direction. In x direction there is a ring, and more radiation is detected.

Time [ms]	1-100	1-1000	1-10000
V1 - x	5.46E-04	6.08E-04	5.97E-04
V1 - y	8.39E-04	8.12E-04	8.08E-04
V1 - z	9.29E-04	8.85E-04	8.94E-04
V2 - x	6.85E-04	6.46E-04	6.37E-04
V2 - y	8.56E-04	8.71E-04	8.57E-04
V2 - z	7.53E-04	8.60E-04	9.16E-04
V3 - x	3.44E-04	3.74E-04	3.69E-04
V3 - y	4.81E-04	4.71E-04	4.67E-04
V3 - z	4.83E-04	4.83E-04	4.75E-04
V4 - x	2.41E-04	2.48E-04	2.45E-04
V4 - y	3.04E-04	3.21E-04	3.19E-04
V4 - x	2.97E-04	2.98E-04	2.99E-04

Table 6.1: Standard deviation against time.

Figure 6.4: A z-y plot of the trajectory of the particle in a experiment.

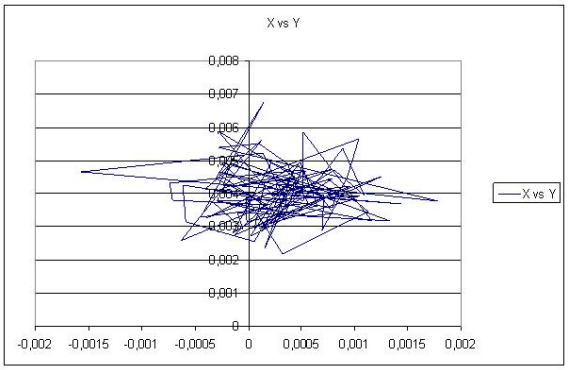

Figure 6.5: A x-y plot of a stationary particle in a experiment.

This is also some of the reason why the hydrocyclone was positioned in the x direction. The position the particle has inside of field of view, how near the edge the particle is positioned makes also a difference, referring to Table 6.1 and Figure 6.8. The standard deviation between point V4 in the center and V2 at the edge is sever. Because of this the hydrocyclone during experiments were positioned as near the center of the FOV as possible.

In Figure 6.7, x vs y shows the difference in height and axial position seen from the front. In Figure 6.8, z vs x shows the difference in direction seen from above. The reason

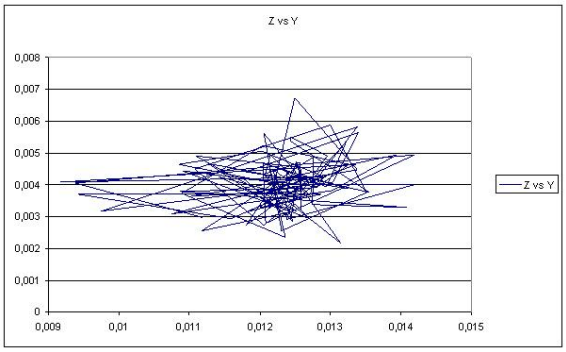

Figure 6.6: A z-y plot of a stationary particle in a experiment.

why V1 (black colour) is not shown in Figure 6.8, is because it is positioned in the exact same position as V2 (red colour).

Results from the hydrocyclone experiment

A second set of experiments was carried out after improvements had been made to the particle box.

The way the experiments were executed was by positioning the table with the rig in the center of the scanner. The hydrocyclone was positioned as straight and in the middle as visually possible. Then the pump was started, a signal was given to the HUH staff that started the scan, and then the particle was injected. Six scans over 120 seconds was carried out, the two first was with the underflow closed and the four last was with open underflow.

The two first scans have only been analyzed by visual inspection, for reasons already explained. Figure 6.9 is a 3D plot of one of the experiments with closed underflow. Comparing Figure 6.1, a hydrocyclone with open underflow and Figure 6.9 a hydrocyclone with closed underflow, it is visually easy to see the differences in trajectory. When the underflow is closed the particle have a much more turbulent trajectory and turns to flow

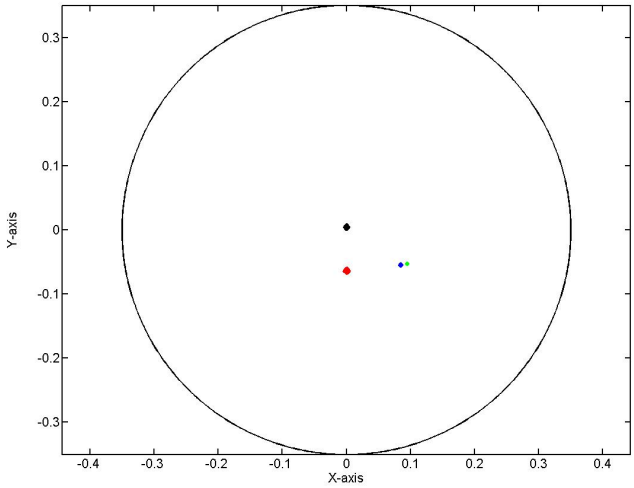

Figure 6.7: A x-y position of the particle when calculating standard deviation in PET. Black is V1, Red - V2, Blue - V3 and Green - V4.

upward several times more, than if the underflow is open. The reason for this has to be further investigated, but is probably related with more fluid going upwars again, giving more friction and lower velocity.

Every dot in the plot in Figure 6.9 corresponds to the position at each millisecond.

After visually investigating each of the experiments and revealing the extremely interesting turning of the particle, the reason for this behaviour would be investigated. The first that was done with the results, was to find a way to compare the different results. Since the whole rig had been taken out between each experiment, the start positions between them were not the same and could not initially be compared. The way of doing this was finding a zero point in the axial direction. The procedure chosen was to set the smallest value of x to zero. Then subtract the same amount from each x-position, then the results were actually shifted to start in x = 0. The specific distance between each point remained the same as originally. Then data from all four experiments were

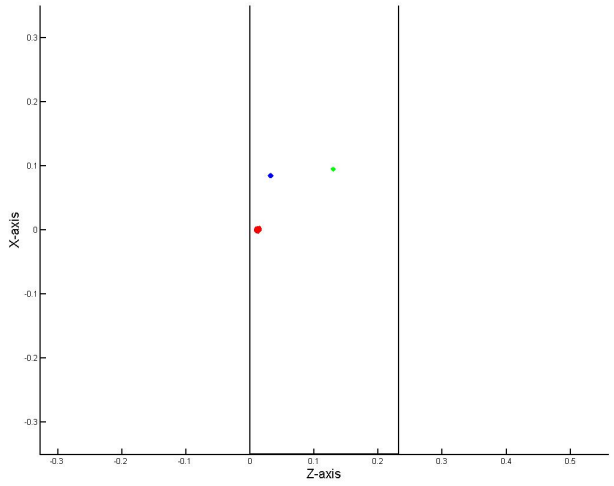

Figure 6.8: A z-y position of the particle when calculating standard deviation in PET. Black is V1, Red - V2, Blue - V3 and Green - V4.

inserted in the same plot, see Figure 6.10.

Figure 6.10 gives a presentation of the initial position to the particle in the x-y plan the first 7 cm. Here it is clear that the particles do not have the same trajectory, however there is some relation. For simplicity a point A is marked where all the particles are at a top, from the inlet and to point A. Experiment 6 had four top rotations, while experiment 5 only had three. It can also be observed that experiment 4 had many rotations before it starts going downward.

The point of interest in this stage of research is the point where the particle turns, and to figure out if there is some relation between the different experiment. Some of the turning points seems to be approximately in the same place, see Figure 6.11. So is there some uneven mechanical deviation that the particle hits so it changes direction, and follows the secondary vortex upward. Or is it because of some specific tangential velocity?

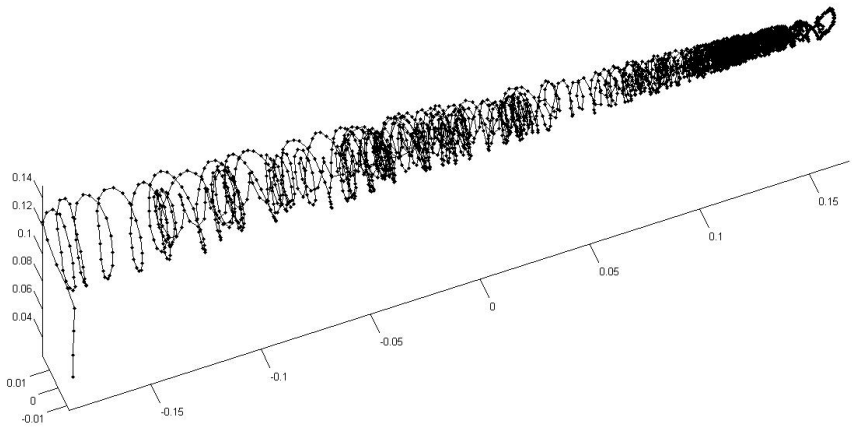

Figure 6.9: The trajectory of a particle through a hydrocyclone with closed underflow.

The axial velocity was calculated to find the position where the particle changed direction. The axial velocity (Va) [m/s] is calculated by the difference in x-position [m] with respect to time [s]. Then the axial velocities at each point in time were plotted against axial position. This gives a negative axial velocity in the point where the particle changes direction from downward to upward. The x-axis was further divided in smaller sections and each section was investigated manually, comparing the axial velocity and position between the different experiments, see example Figure 6.12.

In Figure 6.12 it can be seen that experiment 5 and 6 goes straight through the section. Experiment 4 has some periods of negative axial velocity. In x-position 0.095 both experiment 3 and 4 has a negative axial velocity. Experiment 4 has probably just some extra rotations, with a short periode of negative axial velocity. While experiment 3, is in the beginning of sever upward trajectory. Figure 6.13 shows experiment 3 with the first turn upwards in x = 0.095, before turning down again after some time. It turns one more time upwards around 0.095, it follows the upward trajectory, before the particle

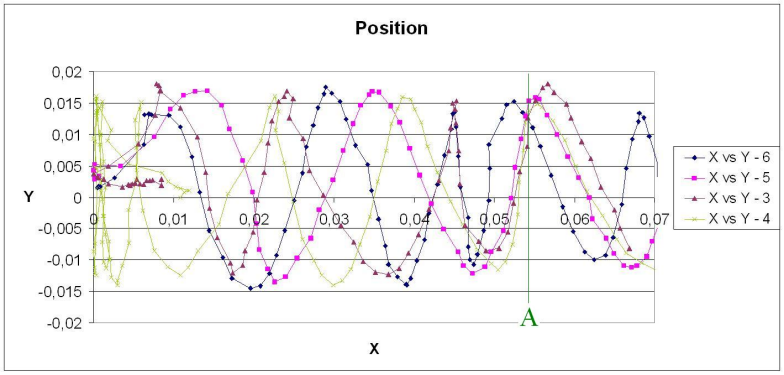

Figure 6.10: x-y trajectory to several experiments in the upper part of the hydrocyclone.

again turns and follows the primary vortex downwards and out of the section of interest.

It is important to notice that in this thesis the only position that is taken into consideration is where the particle first turns. The reason for why it turns back from the secondary upwards vortex may be related to the particle size, turbulence, speed, different directions of eddies, this has to be further investigated.

6.5 Tangential velocity

Very important information can be retrieved from calculating the tangential velocity and finding out if it is some relation to the turning of the particle. Figure 6.12 and Figure 6.13 are examples of plots where the particle turns and follows the secondary vortex upward. The same manual procedure is followed through the whole axial direction, and several critical points of interest are found. The definition of these critical points are positions were two experiments turns in the same area. In these positions the tangential velocity (V_t) has been calculated in the rotation before the particle turn.

$$V_t = r \times V_{ang} \tag{6.1}$$

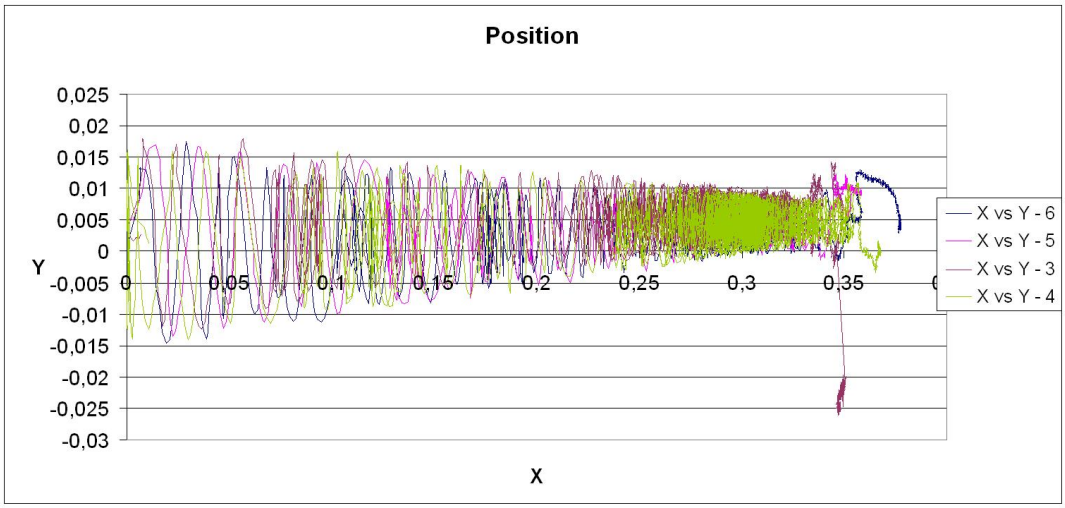

Figure 6.11: The x-y trajectory for several experiments in the whole length of the hydrocyclone.

$$V_{ang} = 2 \times Pi \times f \times r \tag{6.2}$$

r is radii and V_{ang} is angular velocity. f is frequency, and frequency is radiations pr sec.

This is done by finding the nearest "good" rotation before the particle turns, this is done in a similar way as shown in Figure 6.10. By plotting the x vs y positions in the area that is found of interest in negative axial velocity. Finding two similar tops or bottoms in a "good" rotation, and from them calculate the time for one rotation, further find the difference in top and bottom position to calculate the radii.

f = 1000 / (milliseconds pr rotation) [rad/sec] $r = (x - y)/2$ [m]

It should be mentioned that all point after axial position x = 0.276 is not taken into concern in the present work. The reason for this is the highly turbulent flow, and it does not appear to follow a primary vortex flow after this point. This is a visual observation that has been stated for all the experimental results, a more in-depth investigation of

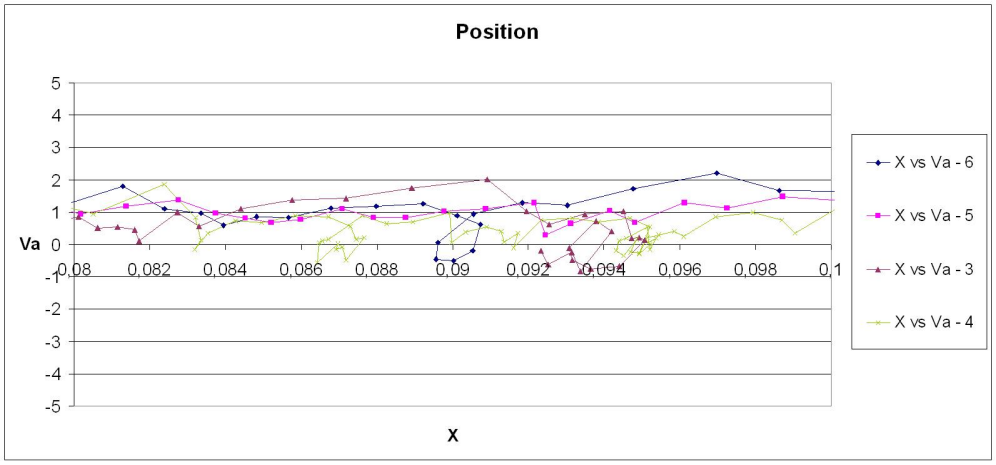

Figure 6.12: x vs axial velocity to several experiments in a restrained section of the hydrocyclone.

this will be needed.

The calculated tangential velocities are shown in Figure 6.14, the velocity is plotted against axial position. That is because it has been tried to find out if there is some pattern between the different critical points.

These results were interesting, because in comparison with known theory, see section 2.5.1 the tangential velocity should increase with decreasing radii. As can be seen here the tangential velocity decreases with decreasing radii.

For getting more information about the tangential velocity when the particle turns, more positions are investigated. A more extensive manual review was made by going through all negative axial velocity that had not been investigated above. Further calculating the tangential velocity in the same manner as explained above, the results are plotted in Figure 6.15.

The tangential velocity against position is in the same area as the once of critical points. A reduction in tangential velocity with decreasing radii. To figure out if there is

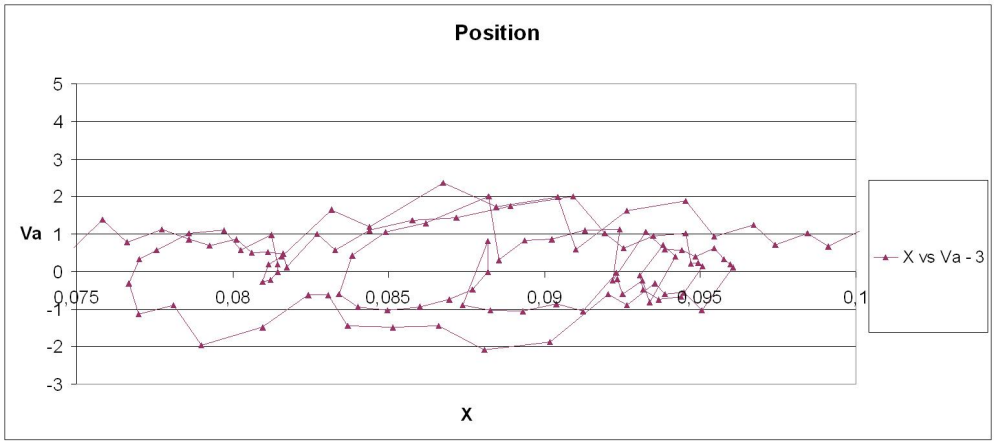

Figure 6.13: x vs axial velocity to a particle, when it changes direction several times, in a restrained section of the hydrocyclone.

something unusual with that, since the same appears in all positions where the particle turns, a new calculation is done. The same method as above was used to calculate the tangential velocity at places where the particle followed the primary vortex downwards without any interruption, these positions are referred to as "random".

In Figure 6.16 the positions that was calculated from just before the particle turns, are plotted against the random primary vortex rotations. As seen from Figure 6.16 there has not been possible to find any significant relation between particles turning and tangential velocity. Generally the tangential velocity decreases with decreasing radii, when the particles turns and when it goes smoothly downwards. According to the known theory referred to in section 2.5.1 the tangential velocity should increase with decreasing radii. That is not the case in these experiments. The reason that it does not follow the theory, might be because the conical section is so long. Therefore the friction forces from the wall are of greater magnitude.

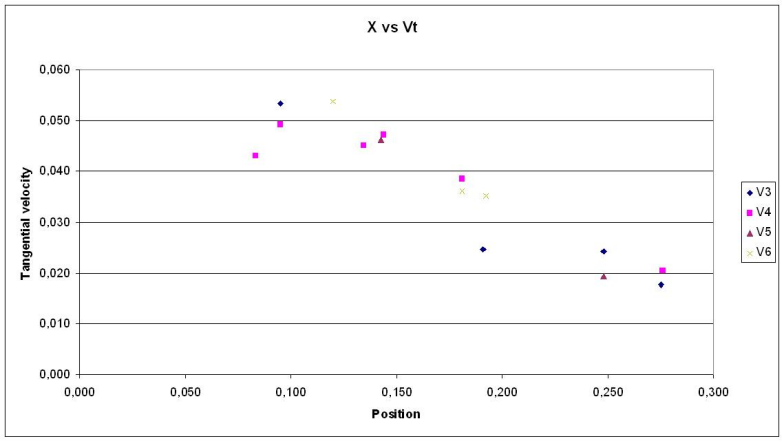

Figure 6.14: Axial position against tangential velocity at critical points.

6.6 Impacting on the wall

Since there was not found any relation between the tangential velocity and the position where the particle turns, another procedure was tried to find out why the particle changes direction. The most obvious would be that the particle actually hits the surface of the cyclone walls. Maybe something that was not mechanically done properly in the machine work. The idea was to go through the critical points that first where found of interest, where something happened in several experiments at about the same places. The hope was to find something like indicated in Figure 6.17, where it is clear that it changed direction.

An example is given in Figure 6.18, this is a plot from experiment 4. Here it can be seen that the particle goes inward, and at some points starts going more against the center. But there is nothing that states that the particle hits something, the trajectory seems relatively smooth all the way.

Because of lack of time there has only been investigated six critical positions in experiment 4. It could only be found one point where the particle might have hit something,

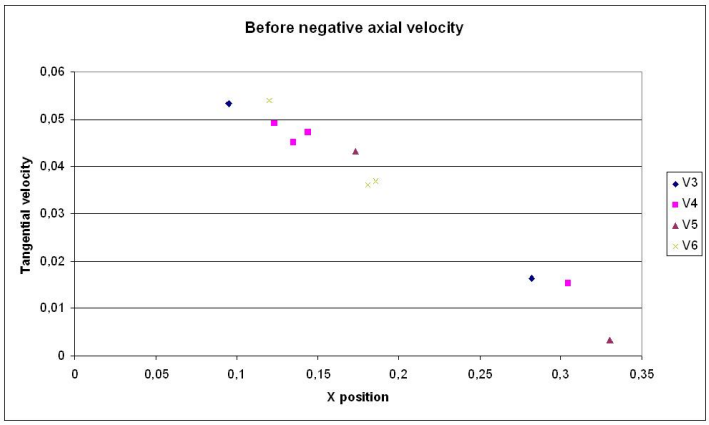

Figure 6.15: Axial position against tangential velocity, just before negative axial velocity.

see Figure 6.19. Looking at the spatial resolution on the rest of the nearby trajectory, it is too soon to say anything about what actually happens here. It might only be the high velocity of the particle that makes this sharp bended output. This position has to be taken into consideration and compared with the others and further results. The problem with this procedure, is that at this stage in the research the wall of the cyclone is not accurately known. This is a very important element that has to be figured out in the work to come.

6.7 Residence time

Another important element in the investigation of flow pattern through a hydrocyclone, is the residence time. The residence time is a specification of how long time the particle stays inside the hydrocyclone. The residence time were divided in two, first a calculation of the residence time down the rather straight downward conical section to x position 0.283. The second residence time calculation was the real residence time from the top to the outlet of the cyclone, at the point the particle entered the particle box. As can be seen from Table 6.2 the difference in time between the different experiments are considerable.

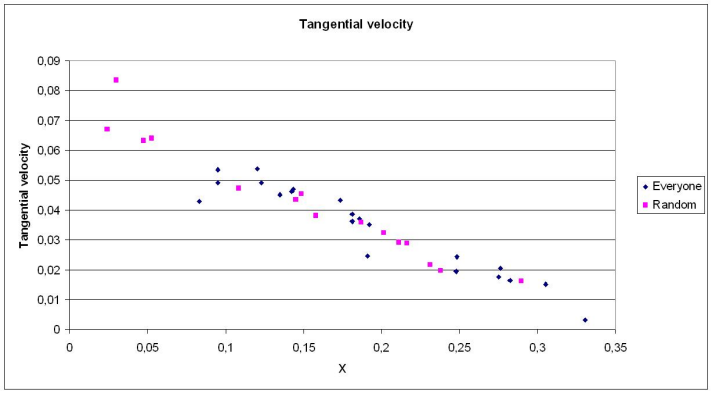

Figure 6.16: Axial position against Tangential velocity at random and all points where the particle turns.

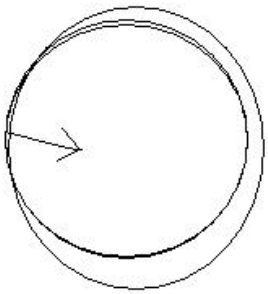

Figure 6.17: Drawing of possible z-y trajectory.

Figure 6.20 and Figure 6.21 shows experiment 3 and 5. Where the considerably higher activity of particle retention time can be seen in the lower part of experiment 3.

6.8 Source of error

There is several possible reasons that has to be taken into consideration regarding the results in this thesis.

- Only one pressure tapping was in use, on the inlet. The pressure was about 0.6

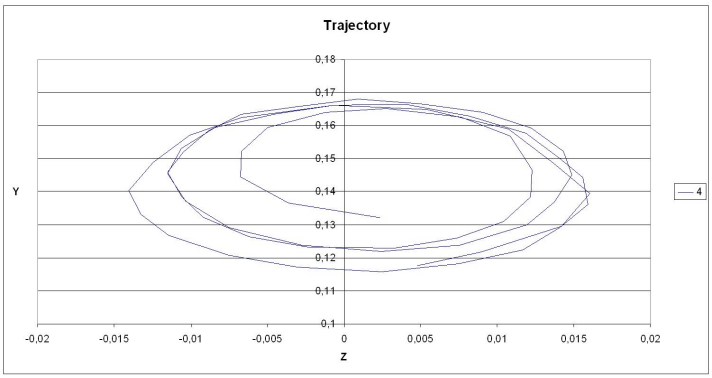

Figure 6.18: z-y smooth inwards trajectory.

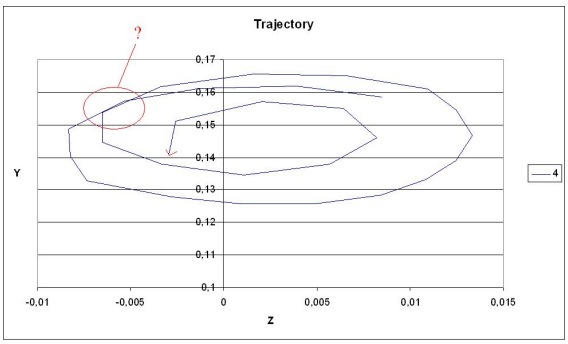

Figure 6.19: z-y inwards trajectory.

bar, referring to the design criteria where the minimum should be 0.7 bar.

- The measurement results out from FORTRAN program has to be more adjusted and are not to reflect the precise physical measurements of the camera. This gives the deviation between the apparent height and the actual height.
- The reason for the difference in end point between cyclones may be related to several reasons that have to be further investigated.
  - For instance the way to calculate the "zero point" is probably not accurate enough; it does not take where the particle enters the cyclone into considera-

Experiment	X = 0.283 [ms]	End [ms]
3	431	4746
4	613	4723
5	410	743
6	470	1482

Table 6.2: Residence time.

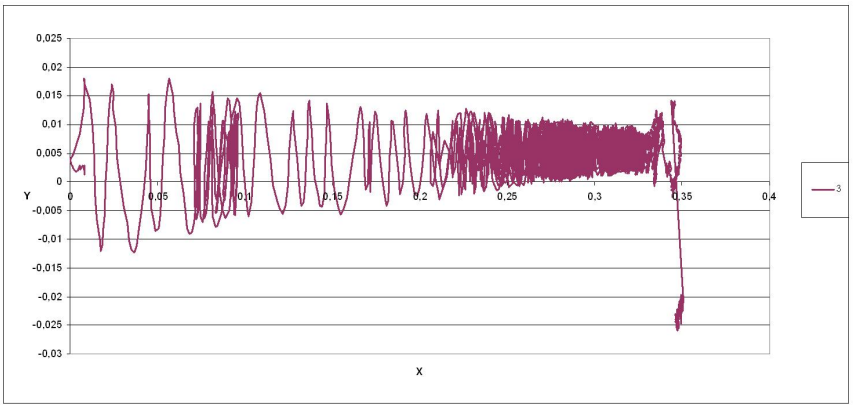

Figure 6.20: x-y plot of experiment 3.

tion. The inlet hole is 29 mm high, now it is assumed that the particle goes to the top of the hydrocyclone before going down.

– The position of the hydrocyclone inside the scanner, if it is not totally parallel with the direction of the scanner there will be some deviation both in length and axial velocity.

- The tangential velocity at the specific point where the particle turns may deviate from the point that has been calculated, which is for the whole rotation before it turns.

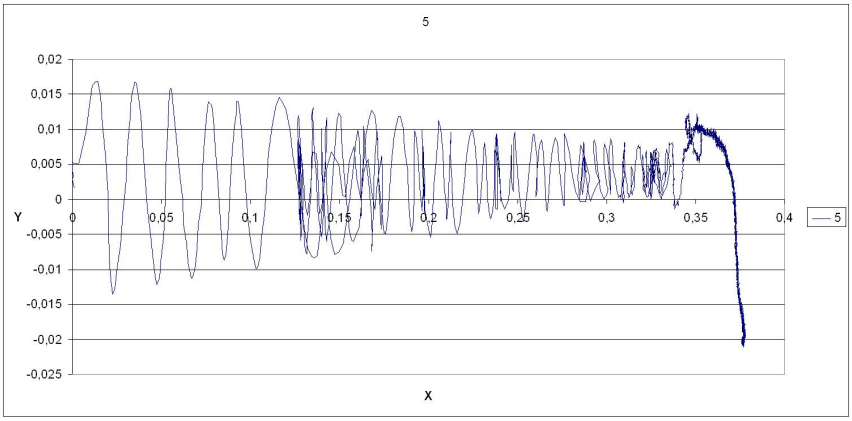

Figure 6.21: x-y plot of experiment 5.

- The size of the underflow opening, this was closed between each experiment, and it is not sure that it was opened to the same amount.
- The difference in starting time of pump related to injection of particle, there maybe that some other flow pattern forms, depending on time.
- Size of particle, has to be further investigated and taken into concern.
- Vibration from the pump that stood on the same table as the hydrocyclone. This is now improved for the further work, by dividing hydrocyclone and pump, and flexible hoses to connect.

Chapter 7

Conclusion

The present work has shown distinguished results that probably will lead to improved design of hydrocyclone. This will be very important in many industries. The first part of this thesis has been very interesting work. An extensive literature survey has given the knowledge to use and understand positron emission tomography scanner in the best way. The hydrocyclone literature survey has given much information about today's methods of designing and understanding hydrocyclones, this gives a better understanding of the importance of this present work. After some experiments with particles, sufficient activity in or on the surface was successful. That the number of effective cut-points of LORS does not drop, and the scatter does not increase in time shows that the radioactivity does not leach off the particle during the hydrocyclone operation. The most important for the feasibility of this project was to get access to the right list mode files and algorithms. This present work has used a technique to precisely follow a fast-moving particle in a hydrocyclone. Following the particle motion reveals phenomena which are difficult or impossible to discover by other measurement techniques.

The conclusion of the second part is a conclusion of the experimental results. To make a definite conclusion regarding particle trajectory is not possible at this time in

the present work. The foundation of experimental results are too fragile, and not in the region of giving specific results. The result from this second part of conclusion has to be seen as an introduction to the work to come. In work and conclusion there has been taken several assumption which are listed in Source of error. These has to be taken into consideration in the further work.

The accuracy of the results is far better than anything that has been found in the literature for state-of-the-art liquid-solid hydrocyclones. Because of the accuracy of PET scanner and the magnitude of results, PET will probably be much more used in the future. The standard deviation is regarded as very good, an accuracy of about 0.24 mm in x direction, 0.32 in y and 0.3 in z direction in the middle of the scanner. From the results that is available at this time in the present work, it was clear that the particles had sever difference in trajectory. There was some points of interest were the particles turned in the approximately same area, it has been tried to figure out the reason for this. From the calculation of tangential velocity there was not possible to see anything that indicated a relation between tangential velocity and particle turning. The stable primary flow had the same tangential velocity profile. The tangential velocity decreases with decreasing radii. This is opposed to the known theory. The reason for why it does not follow the theory, might have relation to the length of the hydrocylone. With a long hydrocyclone the influence from the friction forces from the wall may be considerable. To see if the particle actually hits the wall or hits something physical on the surface of the hydrocyclone has been looked at, but it was not possible to see anything specific. One point that might be of interest was found, and this has to be taken into consideration with the results to come. The residence time has a very large difference between them, this is very interesting to see because of its importance. A high residence time will result in more particles in the hydrocyclone at the same time, and make the potential for clogging higher. The residence time needs to be wider examined because of its importance.

This is a point where information related to the stability of the flow and particle size has to be further investigated. The present work provides the opportunities for directly studying the instability in hydrocyclones of various geometries and under various operating conditions. At this point it is not possible to conclude if the trajectory is random or specific.

Chapter 8

The way forward

The present work has shown results for how to detect the position of the particle with an very high accuracy. The way forward would be to use this present information to further understand the reason for this trajectory. In that manner it is need for much more experimental results to figure out what exactly happens inside the hydrocyclone. This thesis has only given an introduction to what happens. The further work has to take the "Source of error" into consideration and improve the mentioned points. In the experimental results in this thesis it was not installed any venturi pressure tapping's, so it was not any measurement of the velocity. The future work will hopefully have great advantage of this information in the further investigation. The pressure tapping's on the underflow outlet and vortex finder outlet has to be installed, so the crucial pressure drop over the hydrocyclone can be taken into consideration. In addition to the higher amount of experiments needed, more information regarding the particle size in the experiments has to be taken into consideration. Further the exact position of the walls has to be determined to figure out if the particle actually hits the wall or if there is some deviation in the smooth conical wall. The lower part of the hydrocyclone has been very superficially investigated and more work has to be done there. Some visual observations has been

made about this trajectory, it might be related to "End of vortex" or "Induced flow".

Bibliography

[1] *[Section 59 "Discharge of cuttings, sand and solid particles" , REGULATIONS RELATING TO CONDUCT OF ACTIVITIES IN THE PETROLEUM ACTIVITIES (THE ACTIVITIES REGULATIONS)]*, These regulations enter into force on 01.01.2002.

[2] A. C. Hoffmann, C. Dechsiri, F. van de Wiel, and H. G. Dehling. Pet investigation of a fluidized particle: spatial and temporal resolution and short term motion. *Measurement Science and Technology*, pages 851–858, 2005.

[3] Health System University of Virginia. Radiology - positron emission tomography (pet), 12 2007.

[4] Peter E. Valk, D. L. Bailey, D. W. Townsend, and M. N. Maisey. *Positron emission tomography: basic science and clinical practice*. Springer, London, 2003.

[5] J. Thibaud. L'annihilation des positrons au contact de la matiere et la radiation qiu en resulte. *C R Acad Sci*, 197:1629 – 1632, 1933.

[6] F. Joliot. Preuve experimentale de l'annihilation des electrons positifs. *C R Acad Sci*, 197:1622 –5, 1933. Paris.

[7] NA. Dynson, P. Hugh-Jones, GR. Newbury, and JB West. The preparation and use og oxygen-15 with particular reference to its value in the study of pulmonary

malfunction. *Peaceful Uses of Atomic Energy*, pages p. 103 – 115, 1958. Geneva: Pergamon Press.

[8] SIEMENS medical. Biograph truepoint pet-ct: Smaller, faster, better, jan 2010.

[9] USA Knickerbocker Company. Separation purposes for removing dust from air streams, 1885.

[10] Knickerbocker Company. Separation purposes for removing dust from air streams., 1885.

[11] Bretney. Air cyclone to liquid streams, 1891.

[12] MBA Polymers. Development of hydrocyclones for use in plastics recycling - 1914. Summary report, A Summary Report of Research Sponsored by the American Plastics Council., Richmond, July 1998. Submitted by MBA Polymers, Richmond, July, 1998 Copyright 1998, American Plastics Council, Inc.

[13] Z. Stegowski and E. Nowak. Radiotracer experiments and cfd simulation for industrial hydrocyclone performance. *Nukleonika*, 52(3):115–123–, 2007.

[14] International Atomic Energy Agency. Radiotracer applications in industry Ů a guidebook. Technical Reports SeriEs No.423 423, INTERNATIONAL ATOMIC ENERGY AGENCY VIENNA, 2004, 2004.

[15] Ladislav Svarovsky. *Solid-liquid separation processes and technology*, volume 5 of *HANDBOOK OF POWDER TECHNOLOGY*. Elsevier, Amsterdam, 1985.

[16] A. Rushton, A. S. Ward, and R. G. Holdich. *Solid-liquid filtration and separation technology*. Wiley-VCH, Weinheim, 2000.

[17] Coleman and Thew. Chemical engineering research & design. pages pp. 233–239–, 1983.

[18] J. P. Beeby and S. K. Nicol. Concentration of oil-in-water emulsion using the air-sparged hydrocyclone. *Filtration and Separation*, 30(2):pp. 141–146–, 1993.

[19] L. Svarovsky. Errors in measurement of efficiency of particle-fluid separators. *Powder Technology*, 17(1):139–143–, 1977.

[20] D. F. Kelsall. *The theory and applications of the hydrocyclones*. H.M.S.O. LONDON, 1966.

[21] F. W. Mayer. *Zement -Kalk-Gips*, 6:259–268, 1966.

[22] H.J. Van Ebbenhorst Tengbergen and K. Rietema. *Efficiency of Phase Separations*. Cyclones in Industry. Elsevier, Amsterdam, 1961.

[23] Michaluk and Mubarak. Recent advances in the treatment of produced water for reinjection and disposal. Technical report, Serck Backer.

[24] Alfa Laval. Theory of separation in disc stack separators and decanter centrifuges. Technical report.

[25] Kjell. Lohne. Behandling av produsert vann (treatment of produced water). Technical report, Statoil, Div. for Driftsteknologi.

[26] Ladislav Svarovsky. *Solid-liquid separation*. Butterworth-Heinemann, Oxford, 2000.

[27] Jun. Huang, Lian-suo An, and Zhi-quan. Wu. Study on application and operation optimization of hydrocyclone for solid-liquid separation in power plant. volume 1, San Francisco, USA, October 20-22 2009. WCECS 2009.

[28] L. Svarovsky. A critical review of hydrocyclone models. pages p.17–30–, 1996.

[29] Alaina G. Levine. Carl anderson - discovery of the positron. American Physical Society Sites, 2009.

[30] Carl D. Anderson. Şthe positive electronŤ. *The Physical Review*, 43(Number 6):491–49.

[31] Rachel A. Powsner and Edward R. Powsner. *Essential Nuclear Medicine Physics*. Blackwell Publishing, 2006.

[32] Peter E. Valk, Dale L. Bailey, David W. Townsend, and Michael N. Edit. Maisey. *Positron emission tomography. Basic science*. Springer, 2005.

[33] www.wikipedia.com.

[34] Tjibbe Jan de Groot. *SYNTHESIS AND EVALUATION OF [18F]FLUOROPROGESTINS AND [18F]FLUOROMETOPROLOL*. PhD thesis, RIJKSUNIVERSITEIT GRONINGEN, 1993.

[35] LE. Adam, H. Zaers, H. Ostertag, H. Trojan, ME. Bellemann, and G. Brix. Performance evaluation of the whole-body pet scanner ecat exact hr + following the iec standard. *IEEE Trans Nucl Sci*, 44:1172 – 9, 1997.

[36] D. F. Kelsall. A study of the motion of solid particles in a hydraulic cyclone. *Transactions of Chemical Engineering Science*, 30:87–, 1952.

[37] A.B. Holland-Batt. A bulk model for separation in hydrocyclones. *Transactions (Institution of Mining and Metallurgy). Section C, Mineral processing and extractive metallurgy*, pages C21– 25–, 1982.

[38] L. Svarovsky. *Hydrocyclones*. Holt, Rinehart and Winston, London, 1984.

[39] M. Bloor. Solid-liquid separation practice iii. In *Symposium series*, volume 113, pages pp. 1–16–, Rugby, 1989. The Institution. Bidrag fra kongress holdt ved University of Bradford, 29.til 28. september 1989.

[40] J. J. Derksen. Separation performance predictions of a stairmand highefficiency cyclone. *AIChE Journal*, 49:1359Ű1371, 2003.

[41] J. J. Derksen. Simulations of confined turbulent vortex flow. *Computers & Fluids*, 34:301Ű318, 2005.

[42] J. J. Derksen, S. Sundaresan, and H. E. A. van den Akker. Simulation of massloading effects in gas-solid cyclone separators. *Powder Technology*, 163:59Ű68, 2006.

[43] F. Concha, A. Barrientos, L. Munoz, O. Bustamante, and O. Castro. A phenomenological model of a hydrocyclone. *Hydrocyclones '96*, pages –, 1996.

[44] A. J. Lynch and T. C. Rao. Studies on operating characteristics of hydrocyclone classifiers. *11. Int Miner Process Congr, Cagliari, Italy*, 6(4):106–&–, 1968.

[45] A. J. Lynch, T. C. Rao, and K.A. Prisbrey. The influence of hydrocyclone diameter on reduced-efficiency curves. *International Journal of Mineral Processing*, 1(2):p. 173 – 181–, 1974.

[46] A. J. Lynch and T. C. rao. Modelling and scale-up of hydrocyclone classifiers. *Indian Journal of Technology*, (paper 9):245– 269–, 1975.

[47] L. R. Plitt. Mathematical-model of hydrocyclone classifier. *Cim Bulletin*, 69(776):114–123–, 1976.

[48] R.A. Medronho and L. Svarovsky. *Tests to verify hydrocyclone scale-up procedure*. BHRA, The Fluid Engineering Centre, Cranfield, 1984.

[49] D. Bradley and D. J. Pulling. Flow patterns in the hydraulic cyclone and their interpretaition in term of performance. *Transactions of Chemical Engineering Science*, 51:263–, 1959.

[50] K. Rietema. Performance and design of hydrocyclones, part i to iv, 1961.

[51] M. I. G. Bloor and D. B. Ingham. Theoretical investigation of flow in a conical hydrocyclone. *Transactions of the Institution of Chemical Engineers*, 51(1):36–41–, 1973.

[52] M. I. G. Bloor and D. B. Ingham. Turbulent spin in a cyclone. *Transactions of the Institution of Chemical Engineers*, 53(1):1–6–, 1975.

[53] M. I. G. Bloor and D. B. Ingham. Boundary-layer flows on side walls of conical cyclones. *Transactions of the Institution of Chemical Engineers*, 54(4):276–280–, 1976.

[54] M. I. G. Bloor and D. B. Ingham. The flow in industrial cyclones. *Journal of Fluid Mechanics*, 178:507–519–, 1987.

[55] M.D. Brayshaw. A numerical model for inviscid flow of fluid in a hydrocyclone. Technical report, University of Potchestroom, Dpt. of Metallurgical Engineering, Vanderbijlparck 1900, South Africa, 1978.

[56] K. R. Upadrashta, V. J. Ketcham, and J. D. Miller. Tangential velocity profile for pseudoplastic power-law fluids in the hydrocyclone - a theoretical derivation. *International Journal of Mineral Processing*, 20(3-4):309–318–, 1987.

[57] H. Schubert. Wet classification and wet screening of fine particles. *Particulate Science and Technology*, pages 393 – 407–, 1983.

[58] H. Schubert and T. Nesse. A hydrocyclone separation model in consideration of the turbulent multi-phase flow. In G. Priestley and H. S. Stephens, editors, *Papers presented at an International Conference on Hydrocyclones held at Churchill College, Cambridge, U.K., October 1980*, pages 23–26–, Cranfield, 1980. BHRA Fluid Engineering.

[59] K. T. Hsieh. *Phenomenological model of hydrocyclone*. PhD thesis, University of Utah, Utah, 1988.

[60] K. T. Hsieh and K. Rajamani. Phenomenological model of the hydrocyclone - model development and verification for single-phase flow. *International Journal of Mineral Processing*, 22(1-4):223–237–, 1988.

[61] M. Frachon and J. J. Cilliers. A general model for hydrocyclone partition curves. *Chemical Engineering Journal*, 73(1):53–59–, 1999.

[62] W. Kraipech, W. Chen, F. J. Parma, and T. Dyakowski. Modelling the fish-hook effect of the flow within hydrocyclones. *International Journal of Mineral Processing*, 66(1-4):49–65–, 2002.

[63] G. Q. Dai, W. M. Chen, J. M. Li, and L. Y. Chu. Experimental study of solid-liquid two-phase flow in a hydrocyclone. *Chemical Engineering Journal*, 74(3):211–216–, 1999.

[64] B. Chine and F. Concha. Flow patterns in conical and cylindrical hydrocyclones. *Chemical Engineering Journal*, 80(1-3):267–273–, 2000.

[65] M. J. Fisher and R. D. Flack. Velocity distributions in a hydrocyclone separator. *Experiments in Fluids*, 32(3):302–312–, 2002.

[66] T. Dyakowski, L. F. C. Jeanmeure, and A. J. Jaworski. Applications of electrical tomography for gas-solids and liquid-solids flows - a review. *Powder Technology*, 112(3):174–192–, 2000.

[67] M. A. Bennett and R. A. Williams. Monitoring the operation of an oil/water separator using impedance tomography. *Minerals Engineering*, 17(5):605–614–, 2004.

[68] H. I. Schlaberg, F. J. W. Podd, and B. S. Hoyle. Ultrasound process tomography system for hydrocyclones. *Ultrasonics*, 38(1-8):813–816–, 2000.

[69] J. C. Cullivan, R. A. Williams, T. Dyakowski, and C. R. Cross. New understanding of a hydrocyclone flow field and separation mechanism from computational fluid dynamics. *Minerals Engineering*, 17(5):651–660–, 2004.

[70] A. F. Nowakowski, J. C. Cullivan, R. A. Williams, and T. Dyakowski. Application of cfd to modelling of the flow in hydrocyclones. is this a realizable option or still a research challenge? *Minerals Engineering*, 17(5):661–669–, 2004.

[71] T. J. Olson and R. Van Ommen. Optimizing hydrocyclone design using advanced cfd model. *Minerals Engineering*, 17(5):713–720–, 2004.

[72] M. D. Slack, S. Del Porte, and M. S. Engelman. Designing automated computational fluid dynamics modelling tools for hydrocyclone design. *Minerals Engineering*, 17(5):705–711–, 2004.

[73] I. H. Yang, C. B. Shin, T. H. Kim, and S. Kim. A three-dimensional simulation of a hydrocyclone for the sludge separation in water purifying plants and comparison with experimental data. *Minerals Engineering*, 17(5):637–641–, 2004.

[74] K. Vavro, P. Hodur, and F. Dizianik. An analytical model for the prediction of solid-liquid hydrocyclone performance. *Hydrocyclone '96*, 1:105 – 119–, 1996.

[75] R.A. Medronho. PhD thesis, University of Bredford, 1984.

[76] K. Nageswararao, D. M. Wiseman, and T. J. Napier-Munn. Two empirical hydrocyclone models revisited. *Minerals Engineering*, 17(5):671–687–, 2004.

[77] Z. Stegowski and J. P. Leclerc. Determination of the solid separation and residence time distributions in an industrial hydrocyclone using radioisotope tracer experiments. *International Journal of Mineral Processing*, 66(1-4):67–77–, 2002.

[78] S. Bhusarapu, M. Al-Dahhan, and M. P. Dudukovic. Quantification of solids flow in a gas-solid riser: single radioactive particle tracking. *Chemical Engineering Science*, 59(22-23):5381–5386–, 2004.

[79] A. C. Hoffmann, C. Dechsiri, F. van de Wiel, A. Ghione, H. G. Dehling, and A.M.J. Paans. Tracking individual particles in a fluidized bed using a medical pet-camera. 2003.

[80] F. Depypere, J.G. Pieters, and K. Dewettinck. Pept visualisation of particle motion in a tapered fluidised bed coater. *Journal of Food Engineering*, 93:324Ű336, 2009.

[81] P.W. Cox, S. Bakalis, H. Ismail, R Forster, D.J Parker, and P.J. Fryer. Visualisation of three-dimensional flows in rotating cans using positron emission particle tracking (pept). *Journal of Food Engineering*, 60:229Ű240, January 2003.

[82] Z. Yang, X. Fan, S. Bakalis, D.J. Parker, and P.J. Fryer. Impact of solids fraction and fluid viscosity on solids flow in rotating cans. *Food Research International*, 41:658Ű666, 2008.

[83] J. Bridgwatera, S. Forresta, and D.J. Parker. Pept for agglomeration? *Powder Technology*, 140:187Ű 193, 2004.

[84] B.H. Ng, C.C. Kwan, Y.L. Ding, M. Ghadiri, and X.F. Fan. Solids motion of calcium carbonate particles in a high shear mixer granulator: A comparison between dry and wet conditions. *Powder Technology*, 177:1–11, 2007.

[85] SIEMENS medical. Lso hi-rez pet vs. conventional pet: Specification details, May 2010.

[86] Norwegian Radiation Protection Authority. Stråledoser og grenseverdier, jan 2006.

[87] S.A Qaim. Recent developments in the production of 18f, 75/76/77br and 123 i. *Appl. Radiat. Isot.*, 37:803, 1986.

[88] D. W. Townsend. Physical principles and technology og clinical pet imaging. *THEME PAPERS*, 33(2), March 2004.

[89] X. Fan, D.J. Parker, and M.D. Smith. Labelling a single particle for positron emission particle tracking using direct activation and ion-exchange techniques. *Nuclear instruments & methods in physics research*, Section A 562:345 – 350, March 2006.

[90] D.J. Parker and X. Fan. Positron emission particle tracking - application and labelling techniques. *Particuology*, 6:16 – 23, May 2008. School of Physics and Astronomy, the University of Birmingham.

[91] C.J. Stairmand. The design and performance of cyclone separators. *Trans. Inst. Chem. Eng.*, 29:356–383, 1951.

Appendix A

Centrifugal acceleration

Consider a limited body in circular motion around a point O with an angular velocity ω, as shown in Figure A.1. As derived in Rushton, Ward & Holdich [16], from point A to point B the velocity change, i.e. acceleration following equation A.1

$$\nu_B - \nu_A = \nu \frac{\delta\theta}{\delta t} \tag{A.1}$$

where ν_A and ν_B are the vector quantity velocity vectors at point A and B respectively. ν is the speed of travel of the point, δ represent a very small change in either angle θ or time t. If the vectors are summed by the means of a vector plot and $\delta\theta \rightarrow 0$ then the side in the vector plot between ν_B - ν_A points towards the center O of the circle. This leads to a conclusion that there is a velocity change, i.e. acceleration, and therefore a force acting *towards* the centre of the circle, which is known as centripetal force.

When approaching the limit $\delta t \rightarrow 0$:

$$\frac{\delta\theta}{\delta t} = \frac{d\theta}{dt} = \omega \tag{A.2}$$

the velocity of an object is constant but its direction changes, therefore, the acceleration a_c is:

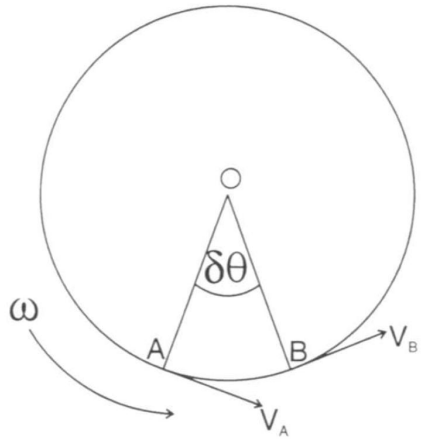

Figure A.1: An illustration of angular velocity during rotation. Reference: [16]

$$a_c = \nu \frac{d\theta}{dt} = \nu\omega \tag{A.3}$$

Also, using the result that:

$$\nu = r\omega \tag{A.4}$$

the centrifugal acceleration is:

$$a_c = r(\omega)^2 \tag{A.5}$$

Which acts toward the center of a circle for a restrained object.

Appendix B

Product Data Sheet: Amberlyst A 26

AMBERLYST® A26 OH

Industrial Grade Strongly Basic Polymeric Resin

PRODUCT DATA SHEET

AMBERLYST A26 OH is a bead form, strongly basic, anionic, macroreticular, polymeric resin. Its porous structure makes it a good choice for use in non aqueous and aqueous media. AMBERLYST A26 OH is virtually inert in strong acids, concentrated alkalies, aliphatic and aromatic hydrocarbons, alcohols, ethers and other common solvents.

AMBERLYST A26 OH is used to catalyze reactions such as aldol condensation where a strongly basic catalyst is required.
It is also used to remove anionic transition metal complexes and mercaptans from hydrocarbons, in addition to removing acids from hydrocarbons and other non-polar solvents, remove oleic acid from chlorinated hydrocarbons and deacidify phenol-acetone solutions.

PROPERTIES

Physical form	Tan opaque spherical beads
Ionic form as shipped	Hydroxide (OH)
Concentration of active sites [1]	≥ 0.80 eq/L
Moisture holding capacity [1]	66 to 75 % (OH form)
Shipping weight	675 g/L (42.1 lbs/ft^3)
Particle size	
Uniformity coefficient	≤ 1.45
Harmonic mean size	0.560 to 0.700 mm
Surface area	30 m^2/g
Average pore diameter	400 Å

[1] *Contractual value*

Test methods are available on request.

SUGGESTED OPERATING CONDITIONS

Maximum operating temperature	60°C (140°F)
Minimum bed depth	600 mm (24 inches)
Service flow rate	1 to 4 BV*/h
Operating flow rate	1 to 4 BV/h
Regenerant concentration	1 N NaOH
Regenerant flow rate	1 to 4 BV/h
Rinse water requirement	4 to 10 BV

** 1 BV (Bed Volume) = 1 m^3 solution per m^3 resin*

All our products are produced in ISO 9002 certified manufacturing facilities.

Rohm and Haas/Ion Exchange Resins - Philadelphia, PA - Tel. (800) RH AMBER - Fax: (215) 537-4157
Rohm and Haas/Ion Exchange Resins - 75579 Paris Cedex 12 - Tel. (33) 1 40 02 50 00 - Fax : 1 43 45 28 19

WEB SITE: http://www.rohmhaas.com/ionexchange

Ion exchange resins and polymeric adsorbents, as produced, contain by-products resulting from the manufacturing process. The user must determine the extent to which organic by-products must be removed for any particular use and establish techniques to assure that the appropriate level of purity is achieved for that use. The user must ensure compliance with all prudent safety standards and regulatory requirements governing the application. Except where specifically otherwise stated, Rohm and Haas Company does not recommend its ion exchange resins or polymeric adsorbents, as supplied, as being suitable or appropriately pure for any particular use. Consult your Rohm and Haas technical representative for further information. Acidic and basic regenerant solutions are corrosive and should be handled in a manner that will prevent eye and skin contact. Nitric acid and other strong oxidising agents can cause explosive type reactions when mixed with Ion Exchange resins. Proper design of process equipment to prevent rapid buildup of pressure is necessary if use of an oxidising agent such as nitric acid is contemplated. Before using strong oxidising agents in contact with Ion Exchange Resins, consult sources knowledgeable in the handling of these materials.

Appendix C

Volume

$$
\begin{aligned}
A &= Pi * r^2[m^2] \\
V &= A * L[m^3] \\
d = 1" = 25.4mm &=> r = 1.24 * 10^-2m \\
L &= 4m \\
V = Pi * 1.27 * 10^-2 * 4 &= 2.03 * 10^-3m^3 = 2.03litre
\end{aligned}
\tag{C.1}
$$

Appendix D

Position and time

x [m]	y [m]	z [m]	time [ms]
-0,17162	0,002201	0,06086	29877
-0,17221	0,002815	0,076002	29878
-0,17287	0,003106	0,089994	29879
-0,17299	0,003256	0,107833	29880
-0,17348	0,003763	0,122131	29881
-0,17165	0,004943	0,137742	29882
-0,16788	0,008452	0,150021	29883
-0,16583	0,012982	0,155009	29884
-0,16517	0,017092	0,160854	29885
-0,16531	0,017827	0,166354	29886
-0,16562	0,018013	0,173864	29887
-0,16523	0,016968	0,182695	29888
-0,16263	0,014307	0,190852	29889

Table D.1: Position and time